Non-Smooth Dynamics in the Stommel Model

by

Cody Griffith

B.Sc., Metropolitan State University of Denver, 2016

A THESIS SUBMITTED IN PARTIAL FULFILLMENT OF
THE REQUIREMENTS FOR THE DEGREE OF

MASTER OF SCIENCE

in

The Faculty of Graduate and Postdoctoral Studies

(Mathematics)

THE UNIVERSITY OF BRITISH COLUMBIA

(Vancouver)

May 2018

The following individuals certify that they have read, and recommend to the Faculty of Graduate and Postdoctoral Studies for acceptance, a thesis entitled:

Non-Smooth Dynamics in the Stommel Model

submitted by **Cody Griffith** in partial fulfillment of the requirements of the degree of **Master's of Science** in **Applied Mathematics**.

Examining Committee:

Rachel Kuske
Supervisor

Brian Wetton
Supervisory Committee Member

Abstract

We analyzed the non-smooth dynamics inside the two-dimensional Stommel model with additional mechanisms like slowly varying bifurcation parameters and high frequency oscillatory forcing. Our goal was to find an analytic approximation to the tipping or bifurcation induced by the new features in the model. We first analyze a simpler one-dimensional model that has similar structure to the Stommel model and gradually build in more complexity into the one-dimensional problem and study the effects on the solutions. With the one-dimensional model understood, we then apply similar methods to the Stommel model and discover the effects on the non-smooth tipping and bifurcations. With these results we have the ability to fully describe the hysteresis found in the Thermohalcine current of which the Stommel model describes.

Lay Summary

We study the behavior in the Stommel model for the Thermohalcine current responsible for driving the water flow from around the globe. Work has previously been done on this before but this focused on the behavior around the well studied smooth components. The analysis we provide is done around the second half of this model, the understudied non-smooth components. We ultimately provide a solution to the non-smooth behavior with increasingly complex additions to the original model. This allows for a better understanding of the Thermohalcine current and could help predict and prepare for sudden abrupt changes to the ocean currents that drive our climate.

Preface

This thesis is original, unpublished, independent work by the author, C. Griffith.

Table of Contents

Abstract . . . iii

Table of Contents . . . vi

List of Figures . . . viii

1 One Dimensional Model . . . 9
- 1.1 Static Bifurcations . . . 9
- 1.2 Slowly Varying Parameter . . . 11
  - 1.2.1 Stability . . . 15
- 1.3 High Frequency Oscillatory Forcing . . . 17
  - 1.3.1 Case I: $v_0(t) \leq -|A|$ . . . 21
  - 1.3.2 Case II: $|v_0(t)| < |A|$ . . . 22
  - 1.3.3 Stability . . . 26
- 1.4 Slowly Varying and Oscillatory Forcing . . . 27
  - 1.4.1 Case I: $\lambda \leq 1$ . . . 29
  - 1.4.2 Case II: $\lambda > 1$ . . . 33
  - 1.4.3 Stability . . . 38

2 Two Dimensional Model . . . 42
- 2.1 Slowly Varying Parameter . . . 43
- 2.2 High Frequency Oscillatory Forcing . . . 50
  - 2.2.1 Case I: $P_0(t) \leq -|A|$ . . . 54
  - 2.2.2 Case II: $|P_0(t)| < |A|$ . . . 55
  - 2.2.3 Stability . . . 60
- 2.3 Slow Variation with Oscillatory Forcing . . . 62
  - 2.3.1 Case I: $\lambda \leq 1$ . . . 66
  - 2.3.2 Case II: $\lambda > 1$ . . . 70
  - 2.3.3 Stability . . . 79

3 Summary and Future Work . . . 84

Appendices

A One-Dimensional 86

B Two-Dimensional 88

List of Figures

1 Vector field of a saddle-node bifurcation 1

2 The Stommel Two Box Model: Differing volume boxes with a temperature and salinity, T_i and S_i. The boxes are connected by an overflow and capillary tube that has a flow V. There is also a surface temperature and salinity for each box, $T_i{}^s$ and $S_i{}^s$. We assume that there is some stirring to give a well mixed structure. 4

3 The equilibria of the non-dimensionalized system (2). Parameters values are $\eta_1 = 4$ and $\eta_3 = .375$. We see non-smooth behavior happening in both plots when $V = 0$. The red line indicates a stable branch where the dashed dotted line is for an unstable branch. 5

4 The choice in η_3 dictates the orientation of the problem, in each plot we have fixed $\eta_1 = 4$. The case for $\eta_3 = 1$ is special due to the two bifurcations overlapping and the unstable equilibrium vanishing. 6

1.1 The one-dimensional bifurcation diagram with the upper and lower equilibrium branches as well as the unstable middle branch. The non-smooth bifurcation occurs at (0,0) with the black circle and the smooth bifurcation occurs at (1,1) with the black cross. 11

1.2 In (a) the numerical solution (black dotted line) to (1.1) is given with $A = 0$ and $\epsilon = .01$. The bifurcation plot is overlayed for convenience. In (b) a zoom in of what happens near the non-smooth bifurcation. The solid vertical lines dictate the tipping estimate (blue) and the dotted vertical line is the numerical tipping, when $x > .5$. In (c) a range of ϵ and their corresponding tipping (red stars) are compared to our estimate (solid black line) from (1.14). 15

1.3 The parameter range is shown here with Case I being to the right of the vertical green line and Case II being in between the vertical blue and green lines. For reference, the original bifurcation diagram is overlayed. 21
1.4 The non-smooth function $|y_0| = |v_0 - A\cos(T)|$ that we integrate over is shown as the solid red line. We also show an example choice of v_0 as a horizontal blue dotted line. Here the value of $|v_0| \leq |A|$, which causes kinks to appear at the roots, T_1 and T_2 respectively which are vertical black dashed dotted lines. 23
1.5 In (a) the numerical time series solutions to (1.1) are given from bottom to top with μ in Case I, Case II and after the bifurcation respectively with $A = 2$, $\Omega = 10$ and $\epsilon = 0$. In (b) we show the time series in the phase plane. In (c) a zoom in closer to the non-smooth bifurcation, where the dotted vertical lines dictate the region between Case I and Case II (green) as well as the bifurcation estimate (blue) respectively. The dotted vertical line is the numerical bifurcation, when $x > .2$. In (d) a range of inverse frequencies and their corresponding bifurcations (red stars) are compared to our prediction (black solid line). 25
1.6 Parameter values are $\epsilon = .05$, $\lambda = .8$ and $A = 1$. On the left, this is the bifurcation diagram for the 1D system with the numerical solution to (1.1) (black dotted line). The solid vertical lines dictate the region between Sub-Case I and Sub-Case II (green) as well as the tipping estimate (blue) respectively. The dotted vertical line is the numerical tipping, when $x > .2$. On the right, this is a zoom in. 36
1.7 An example of numerical tipping (red stars) as the numerical solution to (1.1) passes $x = .2$ for the last time. Parameter values are $\epsilon = .01$ and $A = 1$. The lines are the Case I tipping estimate (black solid line) and the Case II tipping estimate (blue dotted line). 37
1.8 The numerical tipping (red stars) follows the appropriate case depending on λ for $\epsilon = 0.005$. The Case I tipping estimate (black solid line) and the Case II tipping estimate (blue dotted line) are shown. 38

2.1 In (a) the numerical solution (black dotted line) to (2.1) is given with $\eta_1 = 4$, $\eta_3 = .375$, and $\epsilon = .01$. In (b) a zoom in closer to the non-smooth bifurcation region where the blue vertical line is the prediction (2.19) against the black dotted vertical line which is the numerical tipping point. 48
2.2 In (a) we have the numerical solution (black dotted) over the standard equilibrium plot for V vs. T. In (b) a zoom of the bifurcation area. 49
2.3 The numerical tipping vs the estimate with $\eta_1 = 4$ and $\eta_3 = \frac{3}{8}$. The tipping criteria is $V > .5$. 50
2.4 Here we have the parameter ranges for Case I and Case II shown as the right most green vertical line and the bifurcation at the left blue vertical line respectfully. 54
2.5 In (a) the numerical time series solutions to (2.1) is given with parameters in each qualitatively different case of η_2 with $\eta_1 = 4$, $\eta_3 = .375$, $A = 10$ and $\Omega = 10$. In (b) these same solutions are shown on the phase plane. In (c) a zoom in closer to the non-smooth bifurcation region where the blue vertical line is the prediction (2.19) against the black dotted vertical line which is the numerical bifurcation. 58
2.6 In (a) we have the numerical time series solutions for a qualitatively different cases of η_2. In (b) we plot these solutions over the standard equilibrium plot for V vs. T. In (c) a zoom of the bifurcation area. 59
2.7 The numerical tipping vs the estimate with $\eta_1 = 4$ and $\eta_3 = \frac{3}{8}$. The tipping criteria is $V > .5$. 60
2.8 Model values are $\lambda = .8$, $\epsilon = .01$ with $A = B = 2$. In (a) the numerical solution (black dotted line) to (2.1) is given with $\eta_1 = 4$, $\eta_3 = .375$. In (b) a zoom in closer to the non-smooth bifurcation region where the blue vertical line is the tipping prediction against the black dotted vertical line which is the numerical bifurcation. 74
2.9 Model values are $\lambda = .8$, $\epsilon = .01$ with $A = B = 2$. In (a) we have the numerical solution (black dotted) over the standard equilibrium plot for V vs. T. In (b) a zoom of the bifurcation area. 74

2.10 Model values are $\lambda = 1.3$, $\epsilon = .01$ with $A = B = 2$. In (a) the numerical solution (black dotted line) to (2.1) is given with $\eta_1 = 4$ and $\eta_3 = .375$. In (b) a zoom in closer to the non-smooth bifurcation region where the blue dotted vertical line is the prediction against the black solid vertical line which is the numerical bifurcation. 75
2.11 Model values are $\lambda = 1.3$, $\epsilon = .01$ with $A = B = 2$. In (a) we have the numerical solution (black dotted) over the standard equilibrium plot for V vs. T. In (b) a zoom of the bifurcation area. 76
2.12 Model values are $\lambda = 2$, $\epsilon = .01$ with $A = B = 2$. In (a) the numerical solution (black dotted line) to (2.1) is given with $\eta_1 = 4$ and $\eta_3 = .375$. In (b) a zoom in closer to the non-smooth bifurcation region where the blue vertical line is the prediction against the black dotted vertical line which is the numerical bifurcation. 77
2.13 Model values are $\lambda = 2$, $\epsilon = .01$ with $A = B = 2$. In (a) we have the numerical solution (black dotted) over the standard equilibrium plot for V vs. T. In (b) a zoom of the bifurcation area. 77
2.14 An example of numerical tipping (red stars) as the numerical solution to (1.1) passes $x = .2$ for the last time. Parameter values are $\epsilon = .01$ and $A = 1$. The lines are the Case I tipping estimate (black solid line) and the Case II tipping estimate (blue dotted line). 78
2.15 The numerical tipping (red stars) follows the appropriate case depending on λ for $\epsilon = 0.005$. The Case I tipping estimate (black solid line) and purely slow tipping estimate (blue dotted line) are shown. 79

Introduction

The main focus of studying dynamical systems is to understand the possible states an observable solution can experience and with most engineering, physics or even chemical systems, this is a cumbersome task. Often we find parameters inherent in the model for the system to play huge roles in the dynamical behavior and can be the difference between a system being capable of finding an equilibrium or not. When we find a parameter that has this effect, we call it a bifurcation parameter as there is some value that can be found that suddenly bifurcates the behavior of the system. The canonical example and one of the first to be studied was the system that contained a saddle-node bifurcation: $\dot{x} = a - x^2$.

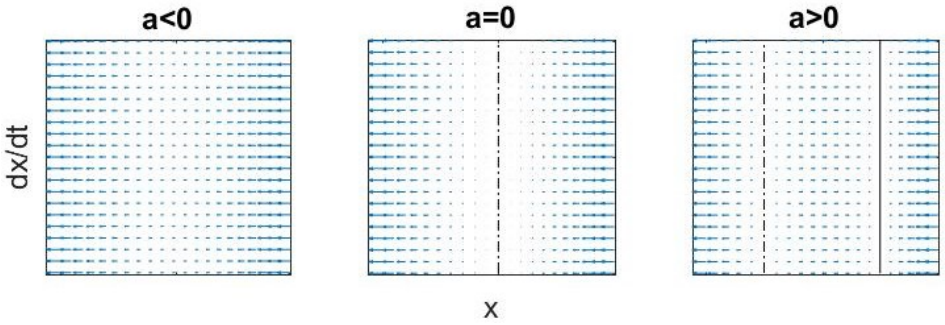

Figure 1: Vector field of a saddle-node bifurcation

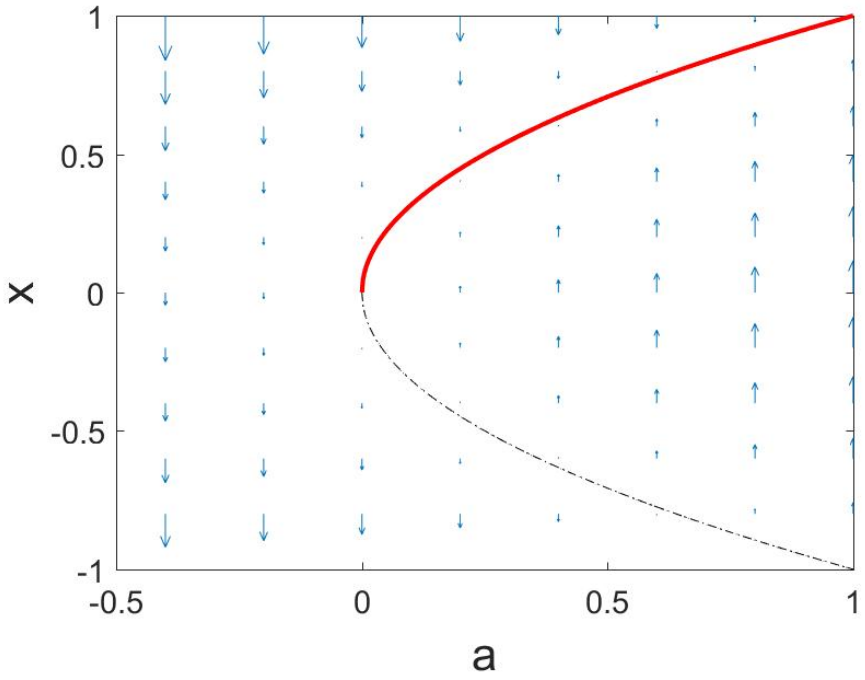

Figure 2: Phase plane of saddle-node bifurcation

In figure 1 we show the vector field of the system that contains a saddle-node bifurcation. The equilibrium of this system is $x = \pm\sqrt{a}$ for any $a > 0$ where stable equilibrium points with solid lines and unstable with dash-dotted lines. Notice that at $a = 0$ and when $a < 0$ we are no longer unable to find a stable equilibrium. This is known to be the simplest example of different qualitative behavior arising from a change in the parameter and it happens by two equilibria annihilating. In figure **??** we plot the same system against the parameter a, which we call the phase plane. Here we still see the region with two equilibrium, the bifurcation and the region of no stability. Although, there are many types of bifurcations that have arisen in different systems that each have their own key properties. Studying these properties lead to a deeper understanding of the system on both the global and local scale. Much work has been done on systems that have smooth bifurcations due to the analysis being easier to perform, but non-smooth dynamics still are present in the physical world.

Non-smooth bifurcations are a topic that arise in special systems and for how frequent they appear, they have not been studied nearly as much as

their smooth counter parts. This paper discusses the role of the non-smooth saddle-node bifurcation in a simplified one-dimensional system in chapter 1 as well as in the classic two-dimensional Stommel model for Thermohalcine current dynamics in chapter 2. But many interesting ocean and weather mechanisms may be incorporated into the Stommel model to provide more realistic predictions for weather patterns. We choose to study slowly varying bifurcation parameters and their effect on the stability of a system while contrasting this with non-autonomous oscillatory forcing. The interaction of these features create complex dynamics around the standard bifurcations and can lead to early bifurcation or delayed tipping. For the one-dimensional system, a detailed analysis of these features is done on the smooth bifurcation by Zhu & Kuske [**?**].

Stommel Model

Global circulation models have primarily focused on three different categories:

- Atmospheric- the effect of greenhouse gases have on the atmosphere,
- Oceanic- the effect of tides and interaction of temperature with salinity in the ocean,
- Sea ice and land surface components.

These categories all contribute significantly to the overall prediction of weather and climate for the planet, which has importance to just about every industry and economy. Failure to adhere to and prepare for sudden changes in the climate led to drastic situations like severe droughts or ocean acidification. Atmospheric models have been vastly studied but far less work has been done on the contribution from the ocean and the dynamics that drive the tides and current.
A key feature of oceanic contributions is when patterns form around regions of bi-stability of temperature and salinity. An example of this is the thermohaline circulation (THC) which experience abrupt qualitative changes at certain points, see Alley [**?**], Marotzke [**?**], or Rahmstorf [**?**] and [**?**]. Even of more importance, just earlier this year Rahmstorf was able to find evidence of weakening occurring around these abrupt changes in a system of ocean patterns known as the Atlantic meridional overturning circulation (AMOC) [**?**]. This is the first evidence of ocean dynamics responding to temperature change on the surface and can help further predict the future of the system.

It is imperative that appropriate action is taken to prepare for the future of these type of systems as they are outside our realm of control.
To study these phenomenon we create parametric models to replicate the dynamics we observe. Initially, Henry Stommel proposed the two box model in 1961 to understand the physics of the THC, shown in figure 2. In Stommel [**?**], it is suggested that there are actually two different stability regimes which even overlap in the system that is proposed and concluded that oceanic dynamics behave very similarly about these equilibria. These type of systems have since been a heavily studied area for both climatology due to the wide ranging applications and dynamical systems for its generalization into dual stability.

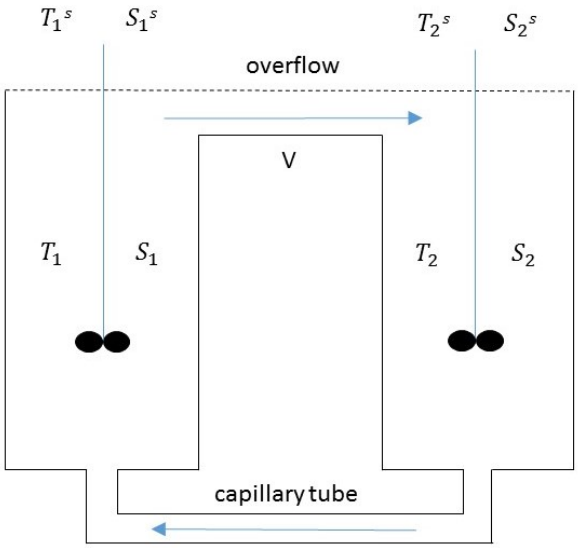

Figure 3: The Stommel Two Box Model: Differing volume boxes with a temperature and salinity, T_i and S_i. The boxes are connected by an overflow and capillary tube that has a flow V. There is also a surface temperature and salinity for each box, $T_i{}^s$ and $S_i{}^s$. We assume that there is some stirring to give a well mixed structure.

With emphasis on mathematics, the focus of this paper is on developing an effective approach to problems with bi-stability and additional mechanisms and thus the physical quantities are brushed aside in favor of their

non-dimensional alternatives. The non-dimensionalized Stommel Model is represented with the system

$$\begin{aligned} \dot{T} &= \eta_1 - T(1 + |T - S|), \\ \dot{S} &= \eta_2 - S(\eta_3 + |T - S|). \end{aligned} \tag{1}$$

The variables T and S are the temperature and salinity respectively, the parameters η_1, η_2, and η_3 are all dimensionless quantities that all have physical interpretation to the relaxation times and volumes of the box. Where η_1 is thought of as the thermal variation, η_2 as the saline variation otherwise known as the freshwater flux, and η_3 as the ratio of relaxation times of temperature and salinity. Here η_1 is a positive quantity that takes any value whereas η_3 is also positive but has the property to determine the orientation of the equilibria. A standard orientation will be when $\eta_3 < 1$, $\eta_3 = 1$ is a special case and $\eta_3 > 1$ will have reverse orientation, this is seen in figure 4. This is due to the nature of the parameter, when $\eta_3 = 1$, the relaxation rates for both the thermal and salinity variables are the same and hence we lose the dual stability.

The parameter η_2 is the most interesting as different values cause major qualitative and quantitative changes in the dynamics of the system. These changes have been discovered at two different points in the system, each being called either a smooth or a non-smooth saddle-node bifurcation.

It is convenient to view this system in terms of the variable $V = T - S$, which leads to the system

$$\begin{aligned} \dot{T} &= \eta_1 - T(1 + |V|), \\ \dot{V} &= (\eta_1 - \eta_2) - V|V| - T + \eta_3(T - V). \end{aligned} \tag{2}$$

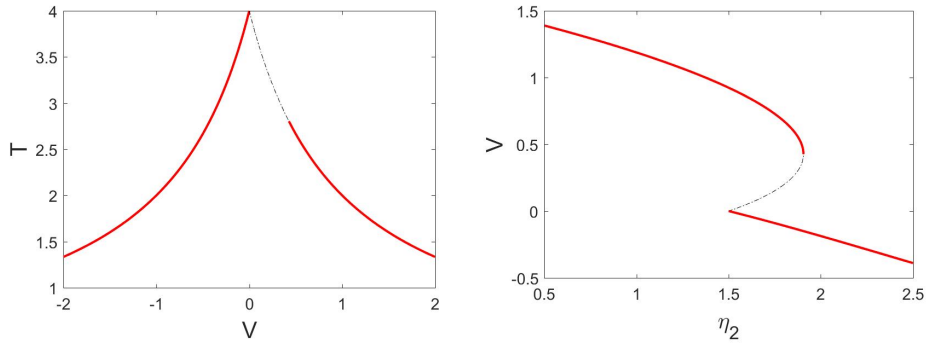

(a) V vs. T (b) η_2 vs. V

Figure 4: The equilibria of the non-dimensionalized system (2). Parameters values are $\eta_1 = 4$ and $\eta_3 = .375$. We see non-smooth behavior happening in both plots when $V = 0$. The red line indicates a stable branch where the dashed dotted line is for an unstable branch.

As shown in figure 3, the equilibrium curves reveal much about the dynamics. In (a) the graph of the equilibria for V vs. T shows non-smooth behavior occurring at $V = 0$ and in (b) the two types of bifurcation appear clearly in the graph of equilibria for η_2 vs. V. In this plot, both the upper and lower branches of the equilibrium are stable with the middle branch being unstable. The stable branches relate to which variable is dominate. For the lower branch, we call this the halcine branch, and the upper branch the thermal branch. The location of the non-smooth bifurcation is found analytically, $\eta_2 = \eta_1\eta_3$, and the smooth bifurcation is the only real solution to a cubic polynomial. The smoothness of each bifurcation is apparent and arise from the absolute value term in the defining dynamics of (2), which is non-smooth only at $V = 0$.

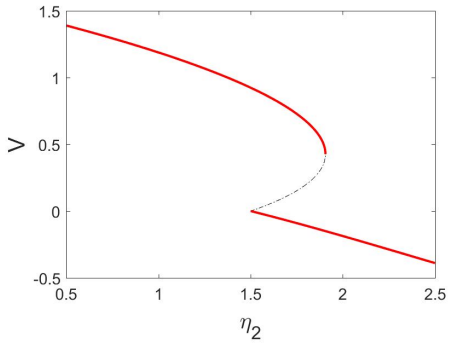

(a) $\eta_3 = .375$

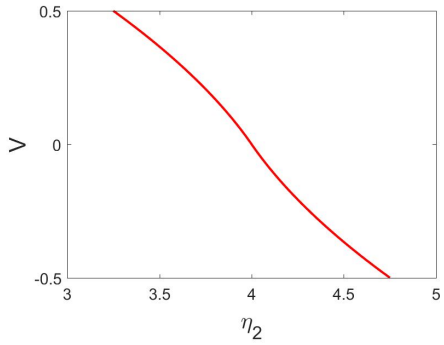

(b) $\eta_3 = 1$

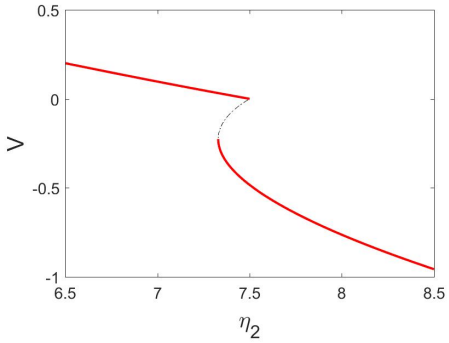

(c) $\eta_3 = 1.875$

Figure 5: The choice in η_3 dictates the orientation of the problem, in each plot we have fixed $\eta_1 = 4$. The case for $\eta_3 = 1$ is special due to the two bifurcations overlapping and the unstable equilibrium vanishing.

Much is known about the Stommel model in the case where η_2 is fixed to be a constant value throughout the analysis but realistically this is not the case. In Rahmstorf [**?**], this parameter is described as the influx of freshwater into the Atlantic and the changing nature of η_2 is justified by a positive feedback loop for salinity that drives the THC to move high-salinity water towards deep oceans. This loop causes the abrupt smooth bifurcation but then afterwards, a salinity deficit causes the parameter to decrease back towards the non-smooth bifurcation.
This type of behavior is known as hysteresis, where there is some bi-stability region that the solution cycles through and hits both states of the equilibria. A similar analysis to the Stommel model's hysteresis can be found in Roberts [**?**]. The phenomenon of hysteresis appears in many physical systems, for

example Jung [**?**], Hohl [**?**] or Joshi [**?**]. The smooth component of the hysteresis curve has been studied in a reduced one dimensional model, see Zhu & Kuske [**?**], we provide the other half of the analysis for the non-smooth component here.

Slowly Varying Tipping

A system with a parameter known to cause a bifurcation will no longer admit a bifurcation in the standard sense when there is slow variation. Instead, these conditions give rise to a smooth but rapid change in the system's equilibria and where this occurs is called a tipping point.
A tipping point is a point that causes an abrupt smooth transition in dynamical behavior as the system moves into a qualitatively different state. The idea being that some positive feedback pushes change towards a different state once a critical point has been passed, for example with biological systems seen in Angeli [**?**]. These are known to be caused by small changes in one or more parameters in the system. An analysis that lays the theoretic backing of slow varying tipping with algebraic bifurcations is found in Haberman [**?**].
Tipping points have been discovered to occur in a wide variety of systems and have become a big staple in the study of areas like catastrophe theory and dynamical systems. They aid in predicting the future of a system and even could be a warning for irreversible change like in the case of the Stommel model. A tipping point thus shares similar characteristics of a bifurcation and typically occurs close to the standard bifurcation location.
An important paper that we extend the results of is Zhu & Kuske [**?**] where work was done on the system

$$\begin{aligned} \dot{x} =& Da + k_0 + k_1 x + k_2 x^2, \\ \dot{a} =& -\mu, \end{aligned} \tag{3}$$

where $\mu \ll 1$. This system is a slowly varying quadratic differential equation containing a smooth saddle-node bifurcation and appears in many physical problems like Erneux [**?**]. A major result from Zhu & Kuske is that the tipping point for (3) has the form

$$a_{\text{tip}} = (D|k_2|)^{-1/3} a_{\text{Airy}} - \frac{a_s}{D} \quad \text{for} \quad a_s = k_0 + \frac{k_1^2}{4|k_2|}, \tag{4}$$

with $a_{\text{Airy}} = \epsilon^{2/3} \cdot (-2.33810\ldots)$ corresponding to the first zero of the Airy function. The tipping found in (4) is a recurring tool for the work presented

in this paper, even though we deal with a version of (3) that has a non-smooth bifurcation.

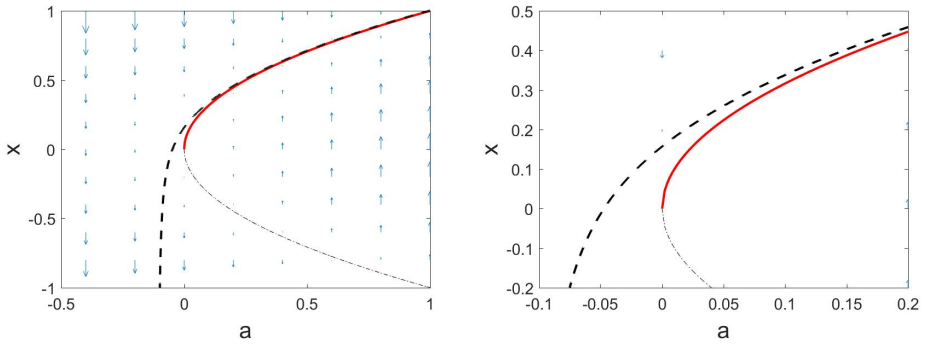

(a) (b)

Figure 6: An example of tipping occurring in the saddle-node around the saddle-node bifurcation.

In figure **??** we show a numerical solution to the simple saddle-node system with tipping (3). Here we have $D = 1$, $k_0 = k_1 = 0$ and $k_2 = -1$ which is the same system we saw earlier. The solution follows closely to the stable branch even after the bifurcation would have occurred, which is indicative of this delayed-typed behavior.
The task of finding where tipping occurs depends on the situation, but in general the approach is to search for when a solution to a problem fails or becomes uncontrollable. This happens, for example, when the interior of a square root becomes negative or when an exponential grows too quickly, both of which we see throughout this paper.

Chapter 1

One Dimensional Model

We consider a simpler system to give insight into the more complex two dimensional Stommel model, here we choose to look at a one-dimensional model with

$$\begin{aligned} \dot{x} &= -\mu + 2|x| - x|x| + A\sin(\Omega t), \\ \dot{\mu} &= -\epsilon, \quad \epsilon \ll 1, \end{aligned} \tag{1.1}$$

$$x(0) = x^0, \quad \mu(0) = \mu^0,$$

where the constants are the slow variation rate ϵ, the amplitude of oscillation A and the frequency of oscillation Ω. We also assume the initial conditions to be $x^0 = 1 - \sqrt{1+\mu^0}$ and $\mu^0 > 0$ while focuses our calculations on the lower equilibrium branch where $x < 0$ and search for nearby behavior.
The system (1.1) is generalized from a basic model that contains both a smooth and non-smooth saddle-node bifurcation. This structure gives the similarity to the Stommel model and hence a good place to test generalizations like slow variation or oscillatory forcing. In each case, emphasis is put on the non-smooth component of the model to study the non-smooth bifurcation and it's role in the hysteresis curve we anticipate in the Stommel model.

1.1 Static Bifurcations

The foundation to our understanding comes from the simplest structure lying within the canonical system (1.1) which is the bifurcation structure. This means finding the general form for the equilibria in (1.1) with $A = 0$ and $\epsilon = 0$, which is our basic model with a static μ and no forcing. As we have a fixed parameter value, we search for a point or set of points that the solution relaxes to with sufficiently long time. We call these points the equilibrium points and depending on their sensitivity, are either stable or unstable equilibria. But as we are considering all possible μ, we want all of the equilibrium points for each μ. We call these the equilibrium branches.

To find all equilibrium branches, we search for when the solution has come to a rest, which is equivalent to setting the derivative of x is zero. Thus we set (1.1) to zero with

$$0 = -\mu + 2|x| - x|x|. \tag{1.2}$$

Solving (1.2) results in 3 solutions, the stability of each depends on if small perturbations to the equilibrium result in growth or decay. We denote the stable equilibria as x_l and x_u for lower and upper respectfully, and a single unstable middle branch, x_m,

$$x_l = 1 - \sqrt{1+\mu}, \quad x_u = 1 + \sqrt{1-\mu}, \quad x_m = 1 - \sqrt{1-\mu}.$$

Where x_l is valid for $\mu \geq 0$ and both x_u, x_m for $\mu \leq 1$. Thus this system has a stable equilibrium for every choice in the parameter, but has a region of bi-stability for $0 \leq \mu \leq 1$. This indicates that the boundary of this region are bifurcations with $\mu = 0$ and $\mu = 1$. These are the points $(\mu, x) = (0, 0)$ and $(\mu, x) = (1, 1)$ which are the non-smooth and smooth saddle-node bifurcations respectfully. Both are of saddle-node type due to pairs of equilibria annihilating at these locations. This all is shown in figure 1.1.

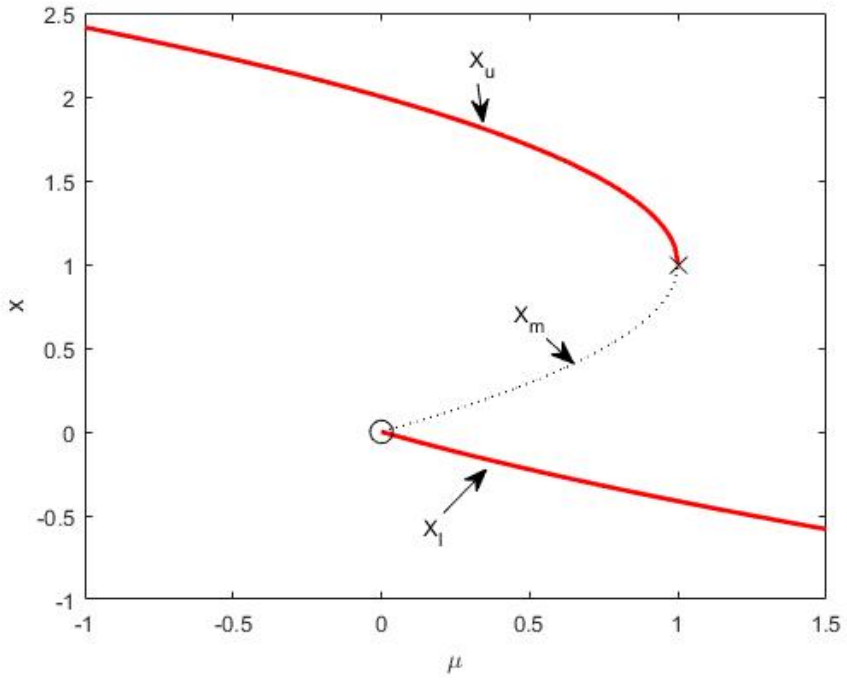

Figure 1.1: The one-dimensional bifurcation diagram with the upper and lower equilibrium branches as well as the unstable middle branch. The non-smooth bifurcation occurs at (0,0) with the black circle and the smooth bifurcation occurs at (1,1) with the black cross.

1.2 Slowly Varying Parameter

To develop a method for the slowly varying Stommel model, let us consider (1.1) with $\epsilon \ll 1$ and $A = 0$. Under these conditions, $\mu(t)$ is a function of time and thus a bifurcation no longer occurs. Instead, it is expected that a tipping point occurs nearby the previous bifurcation points as long as ϵ is small. The smooth case is well understood, see Zhu & Kuske [**?**], so let us consider the behavior of the non-smooth bifurcation with $x < 0$. Since the parameter $\mu(t)$ is slowly varying in time, it makes sense to rescale using this as our 'slow' time, $\tau = \epsilon t$. Applying both $x < 0$ and this 'slow' time approach to the system (1.1) then gives

$$\begin{aligned} \epsilon x_\tau &= -\mu(\tau) - 2x + x^2, \\ \mu_\tau &= -1. \end{aligned} \tag{1.3}$$

A standard approach to extracting information out of complicated models is to try to find reduced equations by separating the behavior at each order. This approach is known as using an asymptotic expansion and further details can be found in Murray's *Asymptotic Analysis* [**?**]. With ϵ being the small quantity that dictates our 'slow' time, we choose to use an asymptotic expansion of x with

$$x(\tau) \sim x_0(\tau) + \epsilon x_1(\tau) + \epsilon^2 x_2(\tau) + O(\epsilon^3). \tag{1.4}$$

This approach captures the slowly varying behavior of the solution in terms of this small quantity ϵ and aims to relate the slow variation to the solution. We substitute the expansion (1.4) into the scaled system (1.3) to get

$$\epsilon x_{0\tau} + \epsilon^2 x_{1\tau} + \ldots = -\mu(\tau) - 2x_0 + x_0^2 + \epsilon(-2x_1 + 2x_1 x_0) + \epsilon^2(-2x_1 + 2x_2 x_0 + x_1^2) + \ldots$$

Once we separate the equations at each order, we find the following system of equations

$$O(1): \quad 0 = -\mu(t) - 2x_0 + x_0^2, \tag{1.5}$$
$$O(\epsilon): \quad x_{0\tau} = -2x_1 + 2x_1 x_0, \tag{1.6}$$
$$O(\epsilon^2): \quad x_{1\tau} = -2x_2 + 2x_2 x_0 + x_1^2. \tag{1.7}$$

We then solve each equation (1.5)-(1.7) progressively **** Should the work for this be shown in the appendix? Its only algebra **** to find the terms of our asymptotic expansion (1.4) as

$$x(t) \sim 1 - \sqrt{1+\mu(t)} + \frac{\epsilon}{4(1+\mu(t))} - \frac{3\epsilon^2}{32(1+\mu(t))^{5/2}} + O(\epsilon^3). \tag{1.8}$$

We call (1.8) the outer solution as it approximates the solution well for large values of $x(t)$. But since the dynamics of the system (1.1) change at $x = 0$ due to the non-smoothness of the problem, this solution is valid only for $x < 0$ and $\mu > 0$. This gives rise to a critical point at $(\mu_c, x_c) = (0, 0)$ which is the non-smooth bifurcation, and a local analysis about $x = 0$ is necessary. It is a key assumption of an asymptotic expansion that the terms in are clearly separated by order of ϵ. To perform the inner analysis, we search for a scaling of μ and x for which (1.8) is no longer valid under this assumption of order separation, here occurring when $x_0 \sim \epsilon x_1$. We suspect that $\mu \sim$

$O(\epsilon)$ causes the expansion to fail, but we conduct a simple scale analysis to determine the appropriate scaling for the local region about $x = 0$. We consider the general scales

$$x = \epsilon^{\alpha} y, \quad \mu = \epsilon^{\beta} m,$$

with α and β being some positive number to be an inner scaling. We apply this scaling in (1.1) to give the system

$$\begin{aligned} \epsilon^{\alpha}\dot{y} &= -\epsilon^{\beta} m + \epsilon^{\alpha} 2|y| - \epsilon^{2\alpha} y|y|, \\ \epsilon^{\beta}\dot{m} &= -\epsilon. \end{aligned} \tag{1.9}$$

We balance the leading order terms $\epsilon^{\alpha}\dot{y}$ with $\epsilon^{\beta} m$ to give that $\alpha = \beta$. But the equation for m gives that $\beta = 1$, thus we have the scaling for the local analysis

$$x = \epsilon y, \quad \mu = \epsilon m. \tag{1.10}$$

Now, we have found that the scalings in (1.10) apply to all x and thus we consider the region of $x > 0$. Substituting the scales into (1.1) we find the following inner system for the region of $x > 0$

$$\begin{aligned} \dot{y} &= -m(t) + 2y - \epsilon y^2, \\ \dot{m} &= -1. \end{aligned} \tag{1.11}$$

We recall that we are searching for a link between y and m, it is then convenient to change the differentiation on y to be with respect to the parameter m. This incorporates the behavior of $m(t)$ directly into the equation we solve and gives us a direct method for finding the tipping. Then the leading order is

$$y_m = m - 2y. \tag{1.12}$$

Where the leading order solution to (1.12) is found explicitly as follows

$$y(m) = Ce^{-2m} + \frac{m}{2} - \frac{1}{4} + O(\epsilon).$$

With the inner solution found in terms of the parameter, we write this in terms of the original coordinates with

$$x(t) \sim \epsilon Ce^{-2\mu(t)/\epsilon} + \frac{\mu(t)}{2} + O(\epsilon). \tag{1.13}$$

Since the solution (1.13) behaves exponentially, the tipping point occurs when the exponential term begins to grow rapidly, here we consider this to be $O(1/\epsilon)$. This behavior occurs when

$$\mu_{\text{slow}} = \frac{1}{2}\epsilon \log(\epsilon). \tag{1.14}$$

Thus we have the tipping point for the purely smooth one-dimensional model. Notice that for small values of ϵ, the slowly varying parameter causes tipping to occur when $\mu(t) < 0$; which is after the non-smooth bifurcation and is consistent with considering the inner equation (1.11) for the region $x > 0$ as we found in the analysis. Thus we find that a slow varying parameter causes a delay in the non-smooth bifurcating behavior for this problem and we expect the solution to remain in a state of bi-stability for longer than the static problem. In terms of hysteresis, then slow variation allows for a longer period before the states switch from the lower branch to the upper.

In figure 1.2 (a,b), an example of the tipping occurring is given for a choice in ϵ along with the standard bifurcation diagram where (c) demonstrates the tipping approximation across a range of ϵ. The concavities match as well as clear agreement in the estimation and bifurcation as ϵ goes to 0.

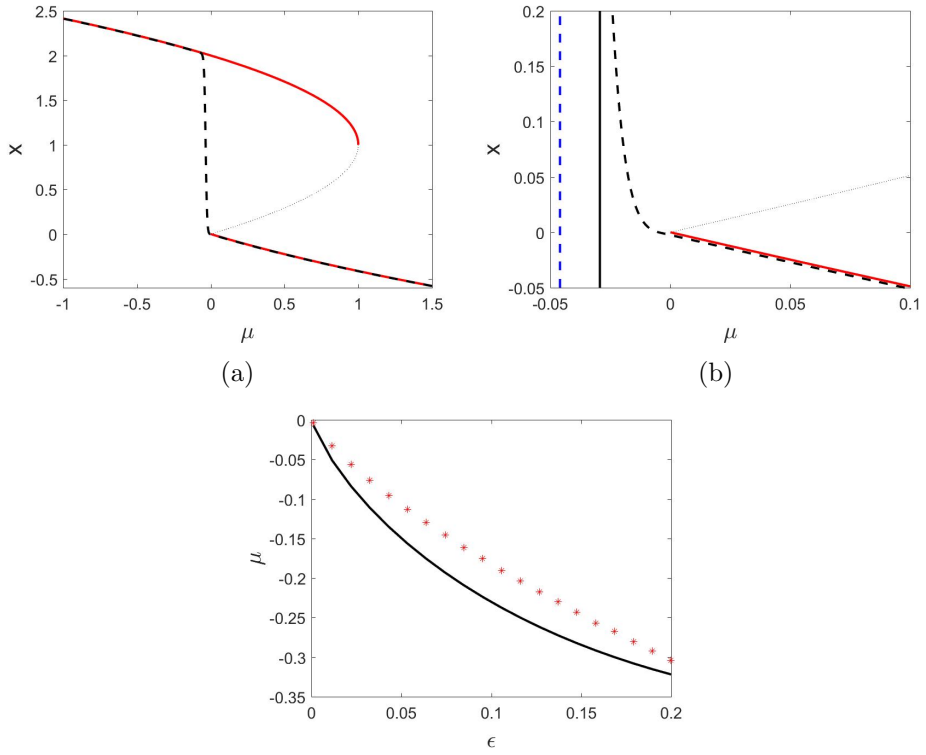

Figure 1.2: In (a) the numerical solution (black dotted line) to (1.1) is given with $A = 0$ and $\epsilon = .01$. The bifurcation plot is overlayed for convenience. In (b) a zoom in of what happens near the non-smooth bifurcation. The solid vertical lines dictate the tipping estimate (blue) and the dotted vertical line is the numerical tipping, when $x > .5$. In (c) a range of ϵ and their corresponding tipping (red stars) are compared to our estimate (solid black line) from (1.14).

1.2.1 Stability

From the basic model we know our outer solution (1.8) to be stable, but to verify the inner solution (1.13) we found is stable, we use a simple linear perturbation on the inner system. Typically to do this, an analysis would be performed about an equilibrium to see if perturbations would grow or decay. But as this problem has a parameter that is allowed to vary, we instead must be careful to note the analysis must be done on the pseudo-

equilibrium instead. In the first region of interest, $m(t) \geq 0$, the following inner equation and pseudo-equilibrium hold below the axis

$$\dot{y} = -m(t) - 2y = f(t, y), \quad z^0(t) = -\frac{m(t)}{2}. \tag{1.15}$$

We then consider simple perturbations about the pseudo-equilibrium in (1.15) with

$$y(t) = z^0(t) + u(t), \quad \|u(t)\| \ll 1.$$

Here we must treat the pseudo-equilibrium with care, normally a Taylor expansion would result in expressing the perturbations with their own equation that we could use to determine stability. Since $z^0(t)$ isn't fixed here, we must consider its contribution to the derivative in this region of the parameter space (i.e $m(t) \geq 0$). Thus we find

$$\begin{aligned} \dot{y} =& \dot{z^0} + \dot{u}, \\ \dot{z^0} =& \begin{cases} \frac{1}{2} & m(t) > 0, \\ 0 & m(t) = 0. \end{cases} \end{aligned} \tag{1.16}$$

Now we apply the standard Taylor expansion to see the behavior of perturbations, with (1.16), (1.15) becomes

$$\begin{aligned} \dot{y} =& f(t, z^0) + f_y(t, z^0)(y - z^0) = \quad f_y(t, z^0)u, \\ \dot{u} =& \begin{cases} -\frac{1}{2} - 2u, & m(t) > 0, \\ -2u, & m(t) = 0. \end{cases} \end{aligned} \tag{1.17}$$

If this were the fixed parameter problem, we would always have the second case in (1.17), which is always stable due to the sign. But since we allow for a varying parameter, we learn that the solution is attracted to just below the pseudo-equilibrium $z^0(t)$. But as this system always experiences the critical point $m_c = 0$ due to the smooth decrease in $m(t)$, the slowly varying parameter eventually acts like the fixed parameter in section 1.1. Hence we have that for $x < 0$, the pseudo-equilibrium is hyperbolic and asymptotically stable. But as we had noticed from our analysis, there is a critical point $(\mu_c, x_c) = (0, 0)$ which corresponds to a non-hyperbolic equilibrium point. Generally, non-hyperbolic behavior signals equilibrium structure to be changing. Here, this signals a transition in behavior for $x > 0$ and helps identify that the tipping occurs here.

For the second region of interest, $m(t) < 0$, we found a solution that had the following inner equation which has the pseudo-equilibrium above the axis with

$$\dot{y} = -m(t) + 2y, \quad z^0(t) = \frac{m(t)}{2}. \tag{1.18}$$

But we find a contradiction with (1.18), here $m(t) < 0$ yet and the solution of this region is supposed to be above the axis. Thus we may conclude that this inner equation has no equilibrium in this region and further verifies that the critical point (μ_c, x_c) was non-hyperbolic and tipping occurs for $m(t) < 0$.

1.3 High Frequency Oscillatory Forcing

To understand the oscillatory forcing in the Stommel model, consider the canonical system (1.1) with $A \sim O(1)$, $\Omega \gg 1$ and $\epsilon = 0$, which gives purely high frequency oscillatory forcing in the system. Under these conditions, we are back to seeing fixed parameter values but we have equilibrium points for each parameter value but with the oscillatory forcing there are oscillations about this point. Thus we should expect to find a regular bifurcation influenced by oscillations occurring under these conditions. Thus, we develop a method to find the equilibrium up to the oscillations to determine what the effect of oscillatory forcing has on the bifurcation of (1.1). Where section 1.2 focused only on the slowly varying dynamics, here we have both a 'slow' time scale t and a 'fast' time scale $T = \Omega t$. This naturally suggests a multiple scales approach where we search for a solution that is dependent on both of these scales, $x(t) = x(t, T)$. This method is commonly used in problems that have behavior observable on multiple scalings, and we use it here to find a way to accurately analyze each scale and effectively combine their behavior into a single unifying solution. Further discussion on this method can be found in Sanchez [**?**].
Recall that our focus is on the non-smooth behavior and hence we restrict the solution to follow along the lower stable equilibrium branch where $x < 0$. Using this multiple scales approach, our canonical system (1.1) has the following form

$$x_T + \Omega^{-1} x_t = \Omega^{-1} \left(-\mu - 2x + x^2 + A \sin(T) \right). \tag{1.19}$$

From (1.19), we see the small quantity Ω^{-1} appearing which suggests an

asymptotic expansion in powers of this quantity

$$x(t,T) \sim x_0(t,T) + \Omega^{-1}x_1(t,T) + \Omega^{-2}x_2(t,T) + O(\Omega^{-3}). \tag{1.20}$$

Substituting (1.20) in our multiple scales system (1.19), we find

$$x_{0T}+\Omega^{-1}x_{0t}+\Omega^{-1}x_{1T}+\ldots = \Omega^{-1}(-\mu-2x_0+x_0^2+A\sin(T))+\Omega^{-2}(-2x_1+2x_1x_0)+\ldots$$

Where we separate the reduced equations at order of Ω to get

$$O(1): \quad x_{0T} = 0, \tag{1.21}$$

$$O(\Omega^{-1}): \quad x_{1T} + x_{0t} = -\mu - 2x_0 + x_0^2 + A\sin(T), \tag{1.22}$$

$$O(\Omega^{-2}): \quad x_{2T} + x_{1t} = -2x_1 + 2x_0x_1. \tag{1.23}$$

With an equation at each order, we must able to solve each to proceed to the next but we must also further restrict our solution from having resonant or linearly growing terms to prevent any multiplicity or exponential growth. This assures that the terms in the asymptotic expansion are compatible with one another and we find a robust solution. A common method to guarantee compatible solutions at each order are found with less than linearly growing terms is the Fredholm alternative. This provides a solvability condition for each equation of the form $x_{iT} = R_i(t,T)$ with

$$\lim_{T\to\infty} \frac{1}{T}\int_0^T R_i(t,u)\,du = 0,$$

which for this system we consider the periodic form of the Fredholm alternative

$$\frac{1}{2\pi}\int_0^{2\pi} R_i(t,T)\,dT = 0. \tag{1.24}$$

Both the general and periodic form of the Fredholm alternative have been well studied, a more theoretic approach to the periodic version is discussed in Bensoussan's *Asymptotic analysis for periodic structures* [**?**]. From (1.21), we learn the leading order term is only dependent on the 'slow' time, $x_0 = x_0(t)$. Applying the Fredholm alternative (1.24) to (1.22) gives

$$\begin{aligned} 0 =& \frac{1}{2\pi}\int_0^{2\pi} -x_{0t}(t) - \mu - 2x_0(t) + x_0(t)^2 + A\sin(T)\,dT, \\ x_{0t} =& -\mu - 2x_0 + x_0^2, \\ x_{1T} =& A\sin(T). \end{aligned} \tag{1.25}$$

Searching for the equilibrium solution of (1.25) leads to the leading order solution, x_0 but also allows us to partially solve the first correction term x_1 with

$$\begin{aligned} x_0 =& 1 - \sqrt{1+\mu}, \\ x_1(t,T) =& v_1(t) - A\cos(T). \end{aligned}$$

Repeating this procedure with (1.23), the work for this is found in Appendix A, results in the terms of the expansion (1.20) with original coordinates

$$x \sim 1 - \sqrt{1+\mu} - \Omega^{-1} A\cos(\Omega t) + O(\Omega^{-2}). \tag{1.26}$$

Once again, the explicit outer solution (1.26) performs well for large x, we search for when the assumptions of the asymptotic series fail to see where an inner analysis is needed. This occurs when $x_0 \sim \epsilon x_1$ which we suspect happens for $\mu \sim O(\Omega^{-1})$.
We consider a general scaling for $x = \Omega^{-\alpha} y$ and $\mu = \Omega^{-\beta} m$ where since we are searching for an inner equation, we anticipate $\alpha > 0$ and $\beta > 0$. Applying these scalings to (1.1) results in

$$\dot{y} = -\Omega^{\alpha-\beta} m + 2|y| - \Omega^{-\alpha} y|y| + \Omega^{\alpha} A\sin(\Omega t) \tag{1.27}$$

Since the parameter is fixed for this section, we are still able to use the same scales, $t = t$ and $T = \Omega t$, with the assumption that $y(t) = y(t,T)$, and hence a similar multiple scales argument in (1.27) leads to

$$y_T + \Omega^{-1} y_t = -\Omega^{\alpha-\beta-1} m + \Omega^{-1} 2|y| - \Omega^{\alpha-1} y|y| + \Omega^{-\alpha-1} A\sin(T). \tag{1.28}$$

With a standard balancing argument between the leading order terms in (1.28),y_T and $\Omega^{\alpha-1} A\sin(T)$, we see that $\alpha = 1$. But we also want to see the terms $\Omega^{\alpha-\beta-1} m$ communicating with $\Omega^{-1} 2|y|$, which gives us that $\beta = 1$ as well. This results in the inner equation

$$y_T + \Omega^{-1} y_t = \Omega^{-1}\left(-m + 2|y|\right) - \Omega^{-2} y|y| + A\sin(T). \tag{1.29}$$

Similarly to the outer equation, we have a need for the asymptotic expansion in terms of Ω^{-1} with

$$y(t,T) \sim y_0(t,T) + \Omega^{-1} y_1(t,T) + O(\Omega^{-2}). \tag{1.30}$$

Substituting the expansion (1.30) into the inner multiple scales system (1.29) we find

$$y_{0T}+\Omega^{-1}y_{0t}+\Omega^{-1}y_{1T}+\ldots = \Omega^{-1}(-m+2|y_0+\Omega^{-1}y_1+\ldots|)+A\sin(T) \\ +\Omega^{-2}(y_0+\Omega^{-1}y_1+\ldots)|y_0+\Omega^{-1}y_1+\ldots|$$

Where we then find the following reduced equations at each order of Ω^{-1} with the system

$$O(1): \quad y_{0T} = A\sin(T), \tag{1.31}$$

$$O(\Omega^{-1}): \quad y_{1T}+y_{0t} = -m+2|y_0|. \tag{1.32}$$

Solving the leading order equation gives that the leading order term has the form, $y_0(t,T) = v_0(t) - A\cos(T)$. But applying the Fredholm alternative (1.24) on (1.32) leads to

$$v_{0t}(t) = -m + \frac{1}{\pi}\int_0^{2\pi} |v_0(t) - A\cos(T)|\, dT. \tag{1.33}$$

Here we must consider two cases of $v_0(t)$ that determine the difficulty of this integrand, Case I: if $v_0(t)$ is large enough to keep the interior from ever changing signs and Case II: if $v_0(t)$ is too small and the interior changes sign. In figure 1.3 we see the behavior of each case where the solution on the right is following under Case I, the first vertical line defining the parameter range between the cases, the middle region following under Case II and the second vertical line giving the bifurcation.

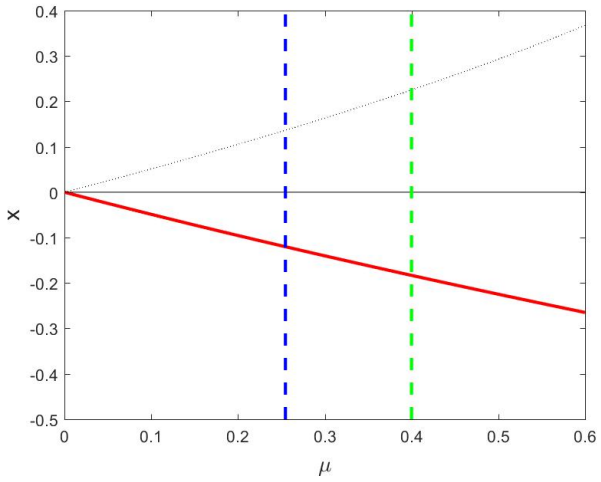

Figure 1.3: The parameter range is shown here with Case I being to the right of the vertical green line and Case II being in between the vertical blue and green lines. For reference, the original bifurcation diagram is overlayed.

1.3.1 Case I: $v_0(t) \leq -|A|$

We call this the entirely below axis case, the solution stays far from the axis $x = 0$ for most of it's oscillation and thus the behavior is consistent and controllable. We don't expect to see the bifurcation occur under these conditions but instead we find the parameter range for the cases. Here the integral equation (1.33) simplifies nicely to a simple equation that we can find the equilibrium of

$$v_{0t}(t) = -m - 2v_0(t), \quad v_0(t) = -\frac{m}{2}.$$

Which gives the leading order equilibrium solution with oscillations to our inner equation for this case which we write in original coordinates

$$\begin{aligned} y(t,T) &\sim -\frac{m}{2} - A\cos(T) + O(\Omega^{-1}), \\ x(t) &\sim -\frac{\mu}{2} - \Omega^{-1}A\cos(\Omega t) + O(\Omega^{-2}). \end{aligned} \tag{1.34}$$

The condition $v_0(t) \leq -|A|$ combined with the equilibrium allows us to establish when (1.34) holds

$$\mu \geq \frac{2|A|}{\Omega}. \tag{1.35}$$

Following the equilibrium to (1.35) leads us to Case II where we see the oscillations crossing the axis and the assumptions of this case no longer hold.

1.3.2 Case II: $|v_0(t)| < |A|$

We call this the crossing case; here the equilibrium is small enough that the oscillations can now push the equilibrium above the axis. Under these conditions, the solution spends most of its time near the axis $x = 0$ and thus experiences much of the non-smooth influence. As the crossing continues, the solution is gradually becoming more and more uncontrollable and thus we expect to find the bifurcation here. From (1.35), we have a range of μ for when this case applies, $\mu < \frac{2|A|}{\Omega}$. But the integrand in (1.33) is non-trivial when $|v_0(t)| < |A|$. In order to deal with the irregular sign changing inside the integral, we break the integration into regions based on sign. Recall that we are searching for equilibrium behavior, and so we may make the assumption that we are dealing with a fixed value of v_0 such that $|v_0| \leq |A|$. In figure 1.4 we observe the function that we are integrating over.

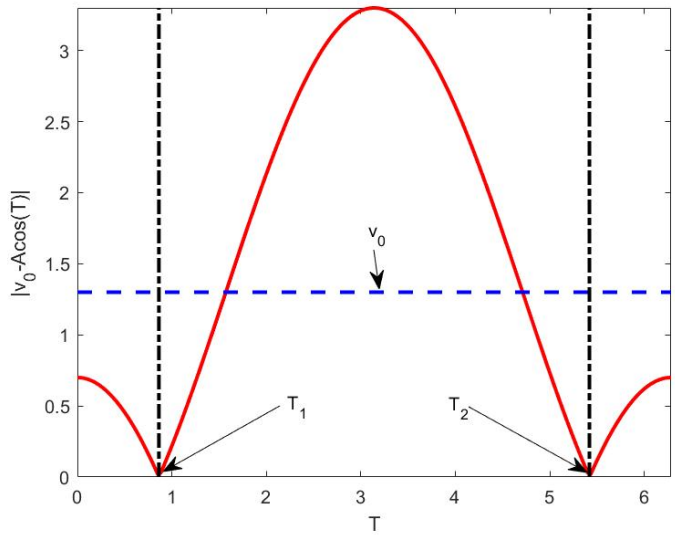

Figure 1.4: The non-smooth function $|y_0| = |v_0 - A\cos(T)|$ that we integrate over is shown as the solid red line. We also show an example choice of v_0 as a horizontal blue dotted line. Here the value of $|v_0| \leq |A|$, which causes kinks to appear at the roots, T_1 and T_2 respectively which are vertical black dashed dotted lines.

We now consider the following roots of the integrand with

$$T_1 = \arccos(v_0/A), \qquad T_2 = 2\pi - \arccos(v_0/A).$$

Where we notice $0 < T_1 < T_2 < 2\pi$ and that the sign of the integrand stays the same on each interval. We only assume that the first interval is following the solution while the center is still negative, thus the integrand will also be negative. From this, we expand the integral as

$$\int_0^{2\pi} |v_0 - A\cos(T)|\, dT = -\int_0^{T_1} v_0 - A\cos(T)\, dT + \int_{T_1}^{T_2} v_0 - A\cos(T)\, dT - \int_{T_2}^{2\pi} v_0 - A\cos(T)\, dT. \tag{1.36}$$

Evaluating (1.36) and using a trig identity, $\sin(\arccos(x)) = \sqrt{1-x^2}$, we find the integral to be

$$\int_0^{2\pi} |v_0 - A\cos(T)\, dT = \frac{2}{\pi}\left(\arcsin(v_0/A)v_0 + \sqrt{A^2 - v_0^2}\right).$$

Now, we notice that our argument above is simple for v_0 in equilibrium, but we may even take advantage of our 'fast' time with $t \ll T$ implying that $v_0(t)$ is approximately fixed over $T \in [0, 2\pi]$. This holds true due to having a high frequency Ω and otherwise would not be a valid approximation. Thus we can evaluate (1.33) to find the inner equation

$$v_{0t} = -m + \frac{4}{\pi}\left(\arcsin(v_0/A)v_0 + \sqrt{A^2 - v_0^2}\right). \tag{1.37}$$

But in its current form, (1.37) restricts any analytic insight due to its difficulty, so we use a quadratic Taylor approximation to be able to solve this equation explicitly

$$v_{0t} \approx -m + \frac{4|A|}{\pi} + \frac{2}{\pi|A|}v_0^2, \tag{1.38}$$

which has the following equilibrium with positive constant C

$$v_0 = -C\sqrt{m - \frac{4|A|}{\pi}}. \tag{1.39}$$

Thus we have the leading order inner equilibrium solution (1.39), we translate back into the original coordinates,

$$\begin{aligned} y &\sim -C\sqrt{m - \frac{4|A|}{\pi}} - A\cos(T) + O(\Omega^{-1}), \\ x(t) &\sim -C\sqrt{\Omega^{-1}\left(\mu - \frac{4|A|}{\pi\Omega}\right)} - \Omega^{-1}A\cos(\Omega t) + O(\Omega^{-2}). \end{aligned} \tag{1.40}$$

It then is clear that the bifurcation happens when (1.40) fails, here being when the square root no longer makes sense

$$\mu_{\text{osc}} = \frac{4|A|}{\pi\Omega}. \tag{1.41}$$

From the result (1.41), we gather that the oscillatory forcing in the system causes the bifurcation to occur sooner and that this is controlled by the size of A and Ω. This should be expected as we are causing the model to experience the non-smooth behavior sooner with the oscillations as opposed to later with the slow variation. This effect is opposite that of the slow variation where the solution experienced a delayed tipping, it now experiences an

accelerated bifurcation. This also indicated that the region of bi-stability is shrunk with oscillatory forcing and thus can be used to eliminate the region entirely with A and Ω chosen properly. We now compare our estimate to numerical results for varying sizes of Ω^{-1}.

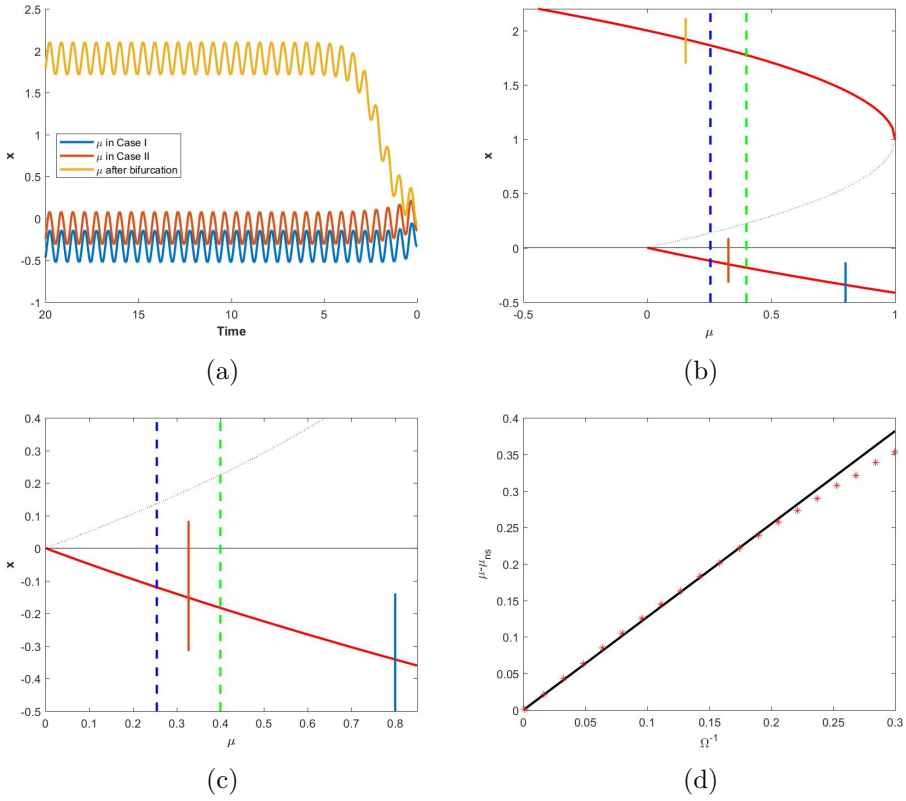

Figure 1.5: In (a) the numerical time series solutions to (1.1) are given from bottom to top with μ in Case I, Case II and after the bifurcation respectively with $A = 2$, $\Omega = 10$ and $\epsilon = 0$. In (b) we show the time series in the phase plane. In (c) a zoom in closer to the non-smooth bifurcation, where the dotted vertical lines dictate the region between Case I and Case II (green) as well as the bifurcation estimate (blue) respectively. The dotted vertical line is the numerical bifurcation, when $x > .2$. In (d) a range of inverse frequencies and their corresponding bifurcations (red stars) are compared to our prediction (black solid line).

In figure 1.5 an example is given of the effect oscillatory forcing has for

a choice of A and Ω with (a), (b) and (c), but (c) shows the bifurcation approximation across a range of Ω^{-1}. There is an allowed range of Ω from our assumption of $\Omega \gg 1$, which in this region we see agreement. The concavity is well represented and the behavior as $\Omega^{-1} \to 0$ converges to the standard bifurcation. This shows that our methodology will work well in the Stommel problem.

1.3.3 Stability

Once more, we have that the outer solution (1.26) is stable from the basic model. In this section, we have two regions of interest and care to establish their stabilities agree with our analysis. Each region has a particular version of the same inner equation dictating their solution's behavior

$$v_{0t}(t) = -m + \frac{1}{\pi}\int_0^{2\pi} |v_0(t) - A\cos(T)|\, dT = f(v_0(t)). \tag{1.42}$$

Case I: $v_0(t) < -|A|$

In this region we didn't find any bifurcating behavior and (1.42) simplifies and has the inner equation and equilibrium as follows

$$v_{0t}(t) = -m - 2v_0(t) = f(v_0), \quad z^0 = -\frac{m}{2}.$$

Similarly to section 1.2, we have a fixed parameter equation that we have shown to cause perturbations to decay exponentially and hence we find the equilibrium to be hyperbolic and asymptotically stable in the paramter range found in the analysis (1.35)

$$\mu \geq \frac{2|A|}{\Omega}.$$

Case II: $|v_0(t)| < |A|$

For this region we did find the bifurcating behavior to occur and we found the Taylor approximation (1.38) for the inner equation and equilibrium to be

$$v_{0t}(t) = -m + \frac{4|A|}{\pi} + \frac{2}{\pi|A|}v_0(t)^2, \quad z^0 = -C\sqrt{m - \frac{4|A|}{\pi}}. \tag{1.43}$$

We consider a simple linear perturbation of (1.43), $v_0(t) = z^0 + u(t)$ with $\|u(t)\| \ll 1$. Applying the standard Taylor expansion to determine the equation for the perturbations, we find

$$\begin{aligned} v_{0t}(t) =& f(z^0) + f_{v_0}(z^0)(v_0(t) - z^0) + O(\|v_0(t) - z^0\|^2), \\ u_t(t) =& f(z^0) + f_{v_0}(z^0)u(t) + O(\|u(t)\|^2), \\ u_t(t) =& -2\sqrt{m - \frac{4|A|}{\pi}}u(t). \end{aligned} \tag{1.44}$$

From (1.44), the sign gives that the perturbations decay exponentially and hence the equilibrium is hyperbolic and asymptotically stable as long as $m > \frac{4|A|}{\pi}$ or $\mu > \frac{4|A|}{\pi\Omega}$. We find that once μ reaches the value in (1.41), then the stability of (1.44) is non-hyperbolic. When the stability switches like this, we expect a bifurcation, thus we have further evidence to support that (1.41) is the oscillatory bifurcation we seek.

1.4 Slowly Varying and Oscillatory Forcing

Since we have established an approach for each feature of the problem individually, we combine them in the full one-dimensional model (1.1) with $\epsilon \ll 1$ and $A \sim O(1)$. Once again, due to the slow variation in μ, we wont see a bifurcation occurring for under these conditions but rather a tipping point. Hence we must find the behavior of the solution and search for when it becomes uncontrollable. We also seek a relationship between the slow drift and the high frequency, so we consider a generic $\Omega = \epsilon^{-\lambda}$ with strength parameter $\lambda > 0$ to determine this relationship. With a general λ, we classify regions of behavior with ranges of λ and will be able to find the boundaries of high frequency with respects to the slow variation. With both mechanisms in effect, we again choose to use a multiple scales approach that captures both slow behavior and fast oscillations. But now, we truly have 'slow' time, the slowly varying parameter $\mu(t)$, as well as 'fast' time, the rapid oscillations $\sin(\Omega t)$. The choice in scales would then be $\tau = \epsilon t$ and $T = \epsilon^{-\lambda} t$, which leads to the system

$$\begin{aligned} x_T + \epsilon^{\lambda+1} x_\tau =& \epsilon^\lambda(-\mu(\tau) + 2|x| - x|x| + A\sin(T)), \\ \mu_\tau(\tau) =& -1. \end{aligned}$$

Once again, we begin in the region $x < 0$ before any crossing occurs to find

the outer solution of the non-smooth behavior. Thus we have the system

$$\begin{aligned} x_T + \epsilon^{\lambda+1} x_\tau =& \epsilon^\lambda(-\mu(\tau) - 2x + x^2 + A\sin(T)), \\ \mu_\tau(\tau) =& -1. \end{aligned} \tag{1.45}$$

We consider an asymptotic expansion in terms of the small quantity ϵ^λ which is in terms of the generic frequency relationship

$$x(\tau, T) \sim x_0(\tau, T) + \epsilon^\lambda x_1(\tau, T) + O(\epsilon^{1+\lambda}, \epsilon^{2\lambda}). \tag{1.46}$$

Depending on the value of λ, $O(\epsilon^{\lambda+1})$ may be the next order before $O(\epsilon^{2\lambda})$, although both produce the same equation at their respective order and hence our choice in λ doesn't change the calculations up to this correction term. Introducing the expansion (1.46) into the outer multi-scaled equation (1.45) gives

$$x_{0T}+\epsilon^{\lambda+1}x_{0\tau}+\epsilon^\lambda x_{1T}+\ldots = \epsilon^\lambda(-\mu(\tau)-2x_0+x_0^2+A\sin(T))+\epsilon^{2\lambda}(-2x_1+x_1x_0)+\ldots \tag{1.47}$$

Where we separate (1.47) to find equations at each order of ϵ^λ, but we consider the system with $O(\epsilon^{2\lambda})$ here

$$O(1): \quad x_{0T} = 0, \tag{1.48}$$

$$O(\epsilon^\lambda): \quad x_{1T} = -\mu(\tau) - 2x_0 + x_0^2 + A\sin(T), \tag{1.49}$$

$$O(\epsilon^{2\lambda}): \quad x_{2T} + \epsilon^{1-\lambda} x_{0\tau} = -2x_1 + 2x_0x_1. \tag{1.50}$$

Each equation reveals more about the behavior of each order of the solution; (1.48) indicates that the leading order term is purely slow dependent, $x_0 = x_0(\tau)$. In Appendix A we apply the Fredholm alternative (1.24) to (1.49) and (1.50) to find the first few terms of our expansion (1.46) explicitly, the resulting solution is

$$x \sim 1 - \sqrt{1+\mu(t)} - \frac{\epsilon}{4(1+\mu(t))} - \epsilon^\lambda A\cos(\Omega t) + O(\epsilon^{1+\lambda}, \epsilon^{2\lambda}). \tag{1.51}$$

With the outer solution (1.51), we search for when the terms violate the assumptions of the expansion to find where we need to form an inner equation. This happens either when $x_0 \sim O(\epsilon)$ or when $x_0 \sim O(\epsilon^\lambda)$ where we suspect is once $\mu \sim O(\epsilon)$ or $\mu \sim O(\epsilon^\lambda)$ respectively, the occurrence of which depends on λ.

To find an inner equation we chose a general scaling for both x and μ given the ambiguity of choice in μ with

$$x = \epsilon^{\alpha} y, \quad \mu(t) = \epsilon^{\beta} m(t), \tag{1.52}$$

where we anticipate $\alpha > 0$ and $\beta > 0$. Applying the scaling (1.52) to the canonical equation (1.1) gives

$$\begin{aligned} \epsilon^{\alpha}\dot{y} &= -\epsilon^{\beta} m(t) + \epsilon^{\alpha} 2|y| - \epsilon^{2\alpha} y|y| + A\sin\Big(\epsilon^{-\lambda} t\Big), \\ \dot{m}(t) &= -\epsilon^{1-\beta}. \end{aligned} \tag{1.53}$$

From (1.53) we find the 'fast' time still appears but the 'slow' time has multiple choices depending on λ. For convenience we choose to take a multiple scales approach with scales t and $T = \epsilon^{-\lambda} t$ in (1.53) to find

$$\begin{aligned} \epsilon^{\alpha-\lambda} y_T + \epsilon^{\alpha} y_t &= -\epsilon^{\beta} m(t) + \epsilon^{\alpha} 2|y| - \epsilon^{2\alpha} y|y| + A\sin(T), \\ m_t(t) &= -\epsilon^{1-\beta}. \end{aligned} \tag{1.54}$$

To determine the correct scalings in (1.52), we balance the leading order terms on both sides of (1.54) $\epsilon^{\alpha-\lambda} y_T$ and $A\sin(T)$, which gives us that $\alpha = \lambda$. This suggests the oscillatory term will persist in the inner asymptotic expansion of (1.1) regardless of choice in λ.
We now consider the same scales t and $T = \epsilon^{-\lambda} t$ on the canonical system (1.1)

$$\begin{aligned} x_T + \epsilon^{\lambda} x_t &= -\epsilon^{\lambda+\beta} m(t) + \epsilon^{\lambda} 2|x| - \epsilon^{\lambda} x|x| + \epsilon^{\lambda} A\sin(T), \\ m_t(t) &= -\epsilon^{1-\beta}. \end{aligned} \tag{1.55}$$

Where we use the expansion

$$x(t,T) = \epsilon^{\lambda} y_0(t,T) + \dots$$

that has the next terms of this expansion depending on whether $\lambda \leq 1$ or if $\lambda > 1$. We consider these ranges as Case I and Case II respectively.

1.4.1 Case I: $\lambda \leq 1$

We call this the mixed effects case due to both slow variation and oscillatory forcing causing noticeable effects on the solution for this range of λ. We consider the expansion

$$x(t,T) \sim \epsilon^{\lambda} y_0(t,T) + \epsilon^{q} y_1(t,T) + \dots \tag{1.56}$$

with $q > \lambda$ to be consistent with our findings thus far. Substituting (1.56) into (1.55) gives

$$\begin{aligned} y_{0T} + \epsilon^{\lambda} y_{0t} + \epsilon^{q-\lambda} y_{1T} + \epsilon^{q} y_{1t} + \ldots = & -\epsilon^{\beta} m(t) + \epsilon^{\lambda} 2|y_0 + \epsilon^{q-\lambda} y_1 + \ldots| + A\sin(T) \\ & + \epsilon^{2\lambda}(y_0 + \epsilon^{q-\lambda} y_1 + \ldots)|y_0 + \epsilon^{q-\lambda} y_1 + \ldots| \end{aligned}$$

Separation by distinct orders of ϵ then gives the following equations at each order

$$O(1) : y_{0T} = A\sin(T), \tag{1.57}$$

$$O(\epsilon^{\lambda}) : \epsilon^{q-2\lambda} y_{1T} + y_{0t} = -\epsilon^{\beta-\lambda} m(s) + 2|y_0|. \tag{1.58}$$

We learn from (1.58) that the appropriate next term in the expansion (1.56) is with $q = 2\lambda$, which implies that $\lambda > \frac{1}{2}$ for an expansion to be found without including the quadratic terms, as with the quadratic terms the equations become inseparable and unsolvable. We also have the choice between $\beta = \lambda$ or $\beta = 1$ and each has a particular appeal. With $\beta = \lambda$, the form of (1.58) is simple, but small coefficients appear further in the analysis. We choose to allow $\beta = 1$ for convenience and track the small coefficient on $m(t)$ now in exchange for having a simple equation for $m(t)$. Using (1.57) gives the appropriate separation in slow and fast scales, $y_0(t, T) = v_0(t) - A\cos(T)$. We then apply the Fredholm alternative (1.24) to (1.58) we find a similar equation to the integral (1.33) in section 1.3 with

$$v_{0t} = -\epsilon^{1-\lambda} m(t) + \frac{1}{\pi}\int_0^{2\pi} |v_0(t) - A\cos(T)|\, dT. \tag{1.59}$$

The approach developed in section 1.3 is applied here to (1.59), where we separate the difficulty of the integral based on the relative size of $v_0(t)$. We have the following situations, Sub-Case I: $v_0(t) \leq -|A|$ and Sub-Case II: $|v_0(t)| < |A|$.

Sub-Case I: $v_0(t) \leq -|A|$

Once more, we call this the entirely below axis sub-case; We don't expect that tipping to occur under these conditions since the solution is entirely negative and far from the axis most of the time. Under these conditions, (1.59) gives the simple inner equation

$$v_{0t} = -\epsilon^{1-\lambda} m(t) - 2v_0. \tag{1.60}$$

Solving (1.60) can be done under our assumptions much like in subsection 1.3.1 but instead we focus on how the solution evolves via the equilibrium. This choice results in finding the effective parameter range for μ which distinguishes these sub-cases, which helps to determine when the solution will enter the region we do expect tipping to occur. Since $m(t)$ is allowed to vary, this must be thought of more as a pseudo-equilibrium and we are only interested in when the pseudo-equilibrium violates the assumptions of this case. Finding the pseudo-equilibrium of (1.60) gives

$$v_0 = -\epsilon^{1-\lambda}\frac{m(t)}{2}.$$

Using the condition $v_0(t) \leq -|A|$ gives that $m(t) \geq \epsilon^{\lambda-1}2|A|$ for Sub-Case I to be effective. Writing this result in original coordinates gives us the parameter range for Sub-Case I

$$\mu(t) \geq \frac{2|A|}{\Omega}, \tag{1.61}$$

which agrees with the range from (1.35) in section 1.3. Following the pseudo-equilibrium to the boundary (1.61), we eventually reach Sub-Case II where we see the oscillations crossing the axis.

Sub-Case II: $|v_0(t)| < |A|$

Again, we call this the crossing sub-case; here the behavior of the solution depends strongly on the sign of the solution similarly to section 1.3, but we seek the relationship between slow variation and oscillatory forcing. As the pseudo-equilibrium get closer to the axis, the solution spends more time above the axis and more complicated contributions from the flipping signs appears. With this increasingly erratic behavior, we expect tipping to happen under these conditions.
The methodology of solving this integral (1.71) holds identically to that of subsection 1.3.2 and thus we evaluate by separating the sign of the integrand and then approximate with a quadratic Taylor expansion to find

$$v_{0t} = -\epsilon^{1-\lambda}m(t) + \frac{4|A|}{\pi} + \frac{2}{\pi|A|}v_0^2. \tag{1.62}$$

But as (1.62) is in terms of 'slow' time, it restricts any analytical approaches to the effects of the varying parameter. Instead we switch the differentiation

onto the parameter m with

$$v_{0m} = \epsilon^{1-\lambda} m - \frac{4|A|}{\pi} - \frac{2}{\pi|A|} v_0^2. \tag{1.63}$$

It is here we take advantage of the form of (1.63) with the result from Zhu & Kuske (4) to solve, this results in

$$v_0(m) \sim \epsilon^{(1-\lambda)/3} \left(\frac{\pi|A|}{2}\right)^{2/3} \frac{Ai'\left(\epsilon^{2(\lambda-1)/3}\left(\frac{2}{\pi|A|}\right)^{1/3}(\epsilon^{1-\lambda}m - \frac{4|A|}{\pi})\right)}{Ai\left(\epsilon^{2(\lambda-1)/3}\left(\frac{2}{\pi|A|}\right)^{1/3}(\epsilon^{1-\lambda}m - \frac{4|A|}{\pi})\right)}.$$

With the solution to (1.56) we rewrite back into the original coordinates

$$\begin{aligned}
y_0(t,T) \sim & \epsilon^{(1-\lambda)/3}\left(\frac{\pi|A|}{2}\right)^{2/3} \frac{Ai'\left(\epsilon^{2(\lambda-1)/3}\left(\frac{2}{\pi|A|}\right)^{1/3}(\epsilon^{1-\lambda}m(t) - \frac{4|A|}{\pi})\right)}{Ai\left(\epsilon^{2(\lambda-1)/3}\left(\frac{2}{\pi|A|}\right)^{1/3}(m(t) - \frac{4|A|}{\pi})\right)} - \epsilon^{\lambda} A\cos(T) + \ldots, \\
x(t) \sim & \epsilon^{(2\lambda-1)/3}\left(\frac{\pi|A|}{2}\right)^{2/3} \frac{Ai'\left(\left(\frac{\Omega}{\epsilon^2}\right)^{1/3}\left(\frac{2}{\pi|A|}\right)^{1/3}(\mu(t) - \frac{4|A|}{\pi\Omega})\right)}{Ai\left(\left(\frac{\Omega}{\epsilon^2}\right)^{1/3}\left(\frac{2}{\pi|A|}\right)^{1/3}(\mu(t) - \frac{4|A|}{\pi\Omega})\right)} - \epsilon^{\lambda} A\cos(\Omega t) + \ldots.
\end{aligned} \tag{1.64}$$

With the inner solution (1.64) we search for the singularity of this solution in order to identify tipping. Recall from (4) that the singularity relates to the first root of the Airy equation, which is when the argument is $-2.33811\ldots$. We find the tipping to be

$$\mu_{\text{mixed}} = \left(\frac{\epsilon^2}{\Omega}\right)^{1/3}\left(\frac{\pi|A|}{2}\right)^{1/3}(-2.33811\ldots) + \frac{4|A|}{\pi\Omega}. \tag{1.65}$$

This value of μ that causes this singularity in turn is our tipping point, where we rewrite (1.65) to show the interaction between slow variation on the parameter and the oscillatory forcing

$$\mu_{\text{mixed}} = \left(\frac{1}{\epsilon\Omega}\right)^{1/3}\left(\frac{\pi|A|}{2}\right)^{1/3}\mu_{\text{smooth}} + \mu_{\text{osc}}, \tag{1.66}$$

with $\mu_{\text{smooth}} = \epsilon\,(-2.33811\ldots)$, similarly to the smooth problem from Zhu & Kuske [**?**], and μ_{osc} from (1.41) respectively.

The resulting tipping approximation (1.66) indicates that the size of the amplitude A will determine whether the tipping occurs early or late in reference to the bifurcation, naturally we see a larger cause more contribution from the oscillations and hence an earlier tipping. On the other hand, larger values in ϵ will cause this tipping to occur later. So these effects have opposite pulls on the tipping and can effectively cancel one another out under the proper conditions. It would even be possible to break the hysteresis cycle by eliminating the region of bi-stability of this problem with sufficiently large amplitude and small ϵ. This tipping holds for any $\lambda \in (\frac{1}{2}, 1]$ and we see different behavior for larger λ.

1.4.2 Case II: $\lambda > 1$

We call this the slowly dominate case as this is when we begin to see the oscillations contribute less than the slow variation. For this range of λ the scaling for μ is simple, $\mu = \epsilon m$ and thus we expect to see integer powers along with λ powers so we choose the expansion

$$x(t,T) \sim \epsilon^{\lambda} y_0(t,T) + \epsilon y_1(t,T) + \epsilon^q y_2(t,T) + \dots \tag{1.67}$$

Substituting (1.67) into (1.55) gives

$$\begin{aligned}\epsilon y_{0T} + \epsilon^{\lambda+1} y_{0t} + \epsilon^{\lambda} y_{1T} + \epsilon^{2\lambda} y_{1t} + \epsilon^q y_{2T} + \dots = &-\epsilon^{\lambda+1} m(t) + \epsilon^{\lambda+1} 2|y_0 + \epsilon^{\lambda-1} y_1 + \dots| \\ &+ \epsilon^{\lambda+2}(y_0 + \epsilon^{\lambda-1} y_1 + \dots)|y_0 + \epsilon^{\lambda-1} y_1 + \dots| \\ &+ \epsilon^{\lambda} A \sin(T)\end{aligned}$$

Where we separate out each order of ϵ to find the equations at each order

$$O(\epsilon) : y_{0T} = 0, \tag{1.68}$$

$$O(\epsilon^{\lambda}) : y_{1T} = A\sin(T), \tag{1.69}$$

$$O(\epsilon^{\lambda+1}) : \epsilon^{q-\lambda-1} y_{2T} + y_{0t} = -m(t) + 2|y_0 + \epsilon^{\lambda-1} y_1|. \tag{1.70}$$

We learn in (1.70) that $q = \lambda + 1$ to keep terms from becoming trivial or unbalanced. Where (1.68) tells us that the dominate behavior for this case is purely slow, $y_0 = y_0(t)$. We find the oscillatory behavior in y_1 with (1.69) which gives $y_1(t,T) = v_1(t) - A\cos(T)$. But as we have y_1 as a

correction to y_0, we may absorb it's slow behavior into y_0. Thus we treat $y_0(t) = y_0(t) + \epsilon^{\lambda+1} v_1(t) \approx y_0(t)$. Applying Fredholm to (1.70) gives

$$y_{0t} = -m(t) + \frac{1}{\pi}\int_0^{2\pi} |y_0(t) - \epsilon^{\lambda-1} A\cos(T)|\, dT. \tag{1.71}$$

With λ being slightly larger than 1, we still see nearly identical behavior in (1.71) as that of what we explored in subsection 1.4.1 as long as the amplitude of oscillations here behave similarly to those of Case I, $\epsilon^{\lambda-1}A \sim O(1)$. To see this, we follow the same approach as to integrate (1.71) with $T_1 = \arccos\big(y_0/\epsilon^{\lambda-1}A\big)$ and $T_2 = 2\pi - \arccos\big(y_0/\epsilon^{\lambda-1}A\big)$ then apply the same quadratic Taylor approximation to find

$$y_{0t} = -m(t) + \epsilon^{\lambda-1}\frac{2|A|}{\pi} + \epsilon^{1-\lambda}\frac{2}{\pi|A|}y_0^2. \tag{1.72}$$

We use the result from Zhu & Kuske (4) to find the tipping, which we then write into original coordinates

$$\begin{aligned} m_{\text{mixed}} =& \epsilon^{(\lambda-1)/3}\left(\frac{\pi|A|}{2}\right)^{1/3}(-2.33811\ldots) + \epsilon^{\lambda-1}\frac{4|A|}{\pi}, \\ \mu_{\text{mixed}} =& \left(\frac{1}{\epsilon\Omega}\right)^{1/3}\left(\frac{\pi|A|}{2}\right)^{1/3}\mu_{\text{smooth}} + \mu_{\text{osc}}. \end{aligned} \tag{1.73}$$

We conclude that there is a natural transition into Case II from Case I with almost the same behavior and identical tipping as in (1.66). As λ continues to grow, the oscillations in (1.71) begin to die off. This allows us to say that the integral is approaching

$$y_{0t} = -m(t) + 2|y_0|. \tag{1.74}$$

But (1.74) has the same form as in section 1.2 allowing us to use the results there to find the solution, where we put this back in terms of the original coordinates

$$\begin{aligned} y_0(t,T) \sim& Ce^{-2m(t)} + \frac{m(t)}{2} - 1/4 + \epsilon^{\lambda} A\cos(T), \\ x(t) \sim& \epsilon Ce^{-2\mu(t)/\epsilon} + \frac{\mu(t)}{2} - \epsilon^{\lambda} A\cos(\Omega t) + O(\epsilon^{2\lambda}). \end{aligned} \tag{1.75}$$

Which also leads to the same tipping from the slow case with

$$\mu_{\text{slow}} = \frac{1}{2}\epsilon\log\epsilon.$$

Thus we find that in this case that even as λ grows past 1, the same μ_{mixed} tipping as in (1.66) occurs from subsection 1.4.1. But as λ continues to grow, the oscillations continue to have less of an impact until the solution tips entirely like μ_{slow} as in (1.14) from section 1.2. For convenience, this is summarized in the following table.

One-Dimensional Tipping	
Slow:	$\mu_{\text{slow}} = \epsilon \ln(\epsilon)/2$
High Freq. Osc:	$\mu_{\text{osc}} = \frac{4\|A\|}{\pi\Omega}$
Slowly Oscillatory $\lambda \leq 1$:	$\mu_{\text{mixed}} = \epsilon^{(\lambda-1)/3} \left(\frac{\pi\|A\|}{2}\right)^{1/3} \mu_{smooth} + \mu_{osc}$
Slowly Oscillatory $\lambda \leq 1$ and $\lambda \approx 1$:	$\mu_{\text{mixed}} = \epsilon^{(\lambda-1)/3} \left(\frac{\pi\|A\|}{2}\right)^{1/3} \mu_{smooth} + \mu_{osc}$
Slowly Oscillatory $\lambda > 1$:	$\mu_{\text{slow}} = \epsilon \ln(\epsilon)/2$

Table 1.1: The tipping of the one-dimensional model for each mechanism and case.

In figure 1.6, we see an example of the numerical solution to the canonical system (1.1) with slow variation and oscillatory forcing. This example has tipping occurring in Case I due to $\lambda \in (\frac{1}{2}, 1]$ allowing the slow variation and oscillatory forcing to produce a mixed effect on the tipping. Although we see noticeable contributions from the slow varying parameter the tipping still is occurring in the region near the oscillatory bifurcation. This tells us that for these choices in the values the strongest effect is the oscillatory forcing. It is now possible here find values of ϵ, A and λ that will cause the non-smooth tipping to occur at the same place as the smooth bifurcation. This in theory, would eliminate the region of bi-stability and destroy the hysteresis curve entirely for this model.

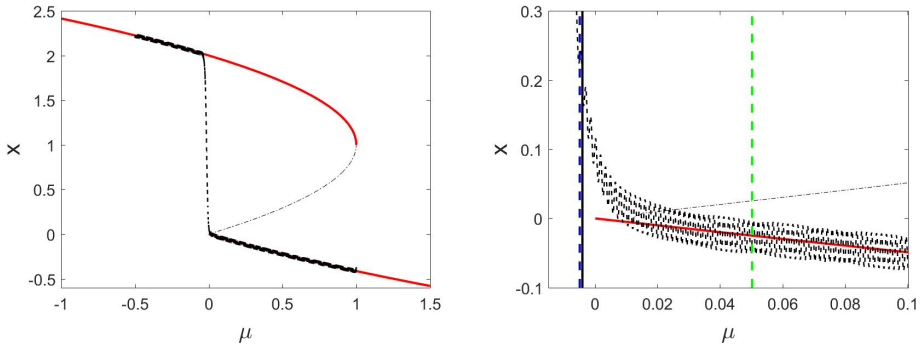

(a) (b)

Figure 1.6: Parameter values are $\epsilon = .05$, $\lambda = .8$ and $A = 1$. On the left, this is the bifurcation diagram for the 1D system with the numerical solution to (1.1) (black dotted line). The solid vertical lines dictate the region between Sub-Case I and Sub-Case II (green) as well as the tipping estimate (blue) respectively. The dotted vertical line is the numerical tipping, when $x > .2$. On the right, this is a zoom in.

In figure **??**, we see an example of λ falling into Case II but is close enough to 1 that we see mixed behavior in the tipping still. Here the slow variation is now dominant and the oscillations are only noticeable in the zoom in.

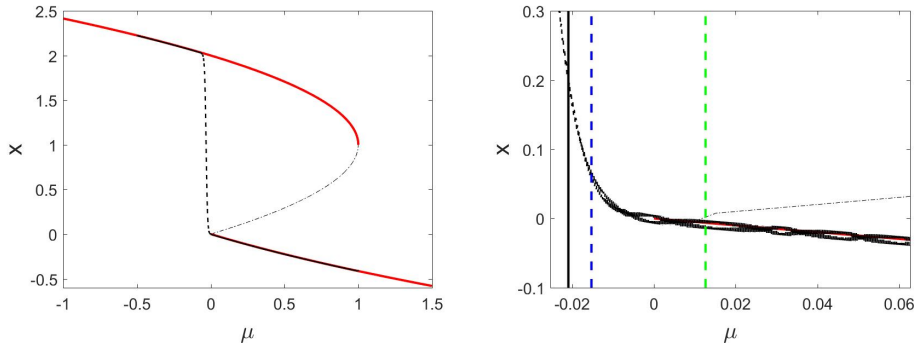

(a) (b)

Figure 1.7: Parameter values are $\epsilon = .05$, $\lambda = 1.1$ and $A = 1$. On the left, this is the bifurcation diagram for the 1D system with the numerical solution to (1.1) (black dotted line). The solid vertical lines dictate the region between Sub-Case I and Sub-Case II (green) as well as the tipping estimate (blue) respectively. The dotted vertical line is the numerical tipping, when $x > .2$. On the right, this is a zoom in.

In figure **??**, we see an example of λ falling into Case II but is far enough from 1 that we see almost entirely slow behavior in the tipping. Even upon closer inspection there its hardly noticeable that oscillations are present in the model.

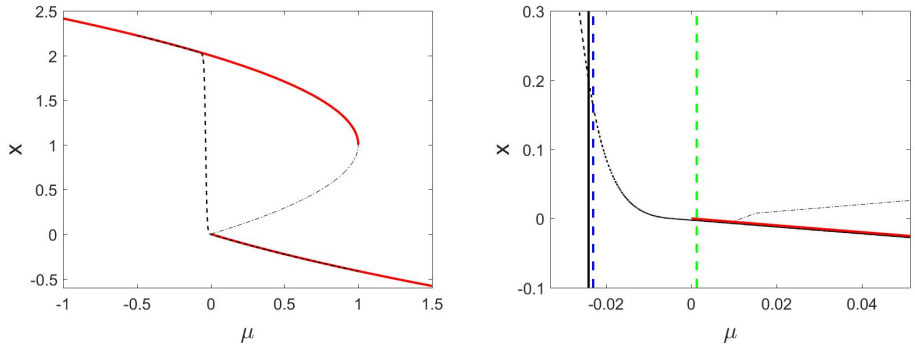

(a) (b)

Figure 1.8: Parameter values are $\epsilon = .05$, $\lambda = 1.6$ and $A = 1$. On the left, this is the bifurcation diagram for the 1D system with the numerical solution to (1.1) (black dotted line). The solid vertical lines dictate the region between Sub-Case I and Sub-Case II (green) as well as the tipping estimate (blue) respectively. The dotted vertical line is the numerical tipping, when $x > .2$. On the right, this is a zoom in.

In figure 1.7 we compare the tipping between Case I and Case II with the numerical tipping. For smaller λ, the frequency Ω gets smaller and the Case I tipping becomes more predominant. But for the analysis performed in this section, $\Omega \gg 1$ and for $\lambda \leq \frac{1}{2}$ we have $\Omega \sim O(1)$. We will not consider low frequency corresponding to $\lambda \leq \frac{1}{2}$ in this section. The larger λ becomes, the less effect we see from the oscillatory forcing until it is negligible for some $\lambda > 1$. Further intuition behind this is in the asymptotic solution for each case, (1.51), (1.64), and (1.75). The oscillatory component of the term has a ϵ^{λ} coefficient and will shrink the effects as λ grows.

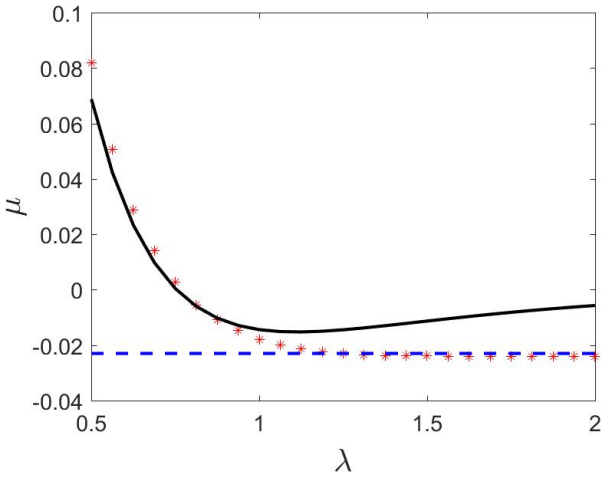

Figure 1.9: An example of numerical tipping (red stars) as the numerical solution to (1.1) passes $x = .2$ for the last time. Parameter values are $\epsilon = .01$ and $A = 1$. The lines are the Case I tipping estimate (black solid line) and the Case II tipping estimate (blue dotted line).

The performance of our estimates are seen in figure 1.8. For Case I tipping, the range of appropriate ϵ is highly dependent on the choice in λ. Often, the range is very small to get accurate estimates. Once this range is left, there are interesting phase effects for the tipping which causes oscillations in the numeric tipping points. For Case II tipping, we see very accurate estimates over a larger window, similarly to section 1.2

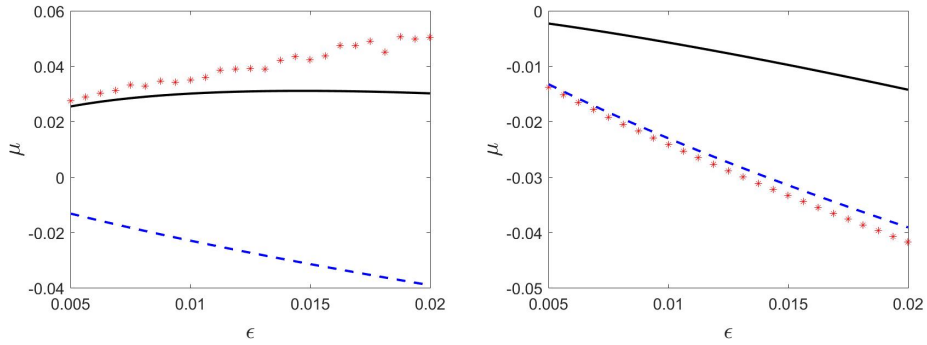

(a) $\lambda = .8$ (b) $\lambda = 1.3$

Figure 1.10: The numerical tipping (red stars) follows the appropriate case depending on λ for $\epsilon = 0.005$. The Case I tipping estimate (black solid line) and the Case II tipping estimate (blue dotted line) are shown.

1.4.3 Stability

Similarly to section 1.3, there are two ranges for λ of interest that will govern the stability of solutions found in our analysis, $\lambda \leq 1$ and $\lambda > 1$.

Case I: $\lambda \leq 1$

Recall for this case, we must have $\lambda \in (\frac{1}{2}, 1]$ and for this range, we found the inner equation

$$v_{0t} = -\epsilon^{1-\lambda} m(t) + \frac{1}{\pi} \int_0^{2\pi} |v_0(t) - A\cos(T)|\, dT = f(t, v_0). \tag{1.76}$$

Like in our analysis, we consider two regions in the solution $v_0(t)$ for this integral, Sub-Case I: $v_0(t) \leq -|A|$ and Sub-Case II: $|v_0(t)| \leq |A|$ where these sub-cases deal with the respective size of $v_0(t)$ to the oscillations and their resulting stability.

Sub-Case I: $v_0(t) \leq -|A|$

Recall from the analysis that the equation (1.76) simplifies in this region of $v_0(t)$ and has the following inner equation and pseudo-equilibrium

$$v_{0t} = -\epsilon^{1-\lambda} m(t) - 2v_0 = f(t, v_0), \quad z^0(t) = -\epsilon^{1-\lambda} \frac{m(t)}{2}. \tag{1.77}$$

As we saw in section 1.2, special treatment of the pseudo-equilibrium stability analysis is needed with linear perturbations $v_0(t) = z^0(t) + u(t)$ where $\|u(t)\| \ll 1$ and $z_t^0 = -\epsilon^{1-\lambda}\frac{m_t}{2} = \frac{\epsilon^{1-\lambda}}{2}$. The resulting Taylor expansion is thus

$$\begin{aligned} v_{0t} =& f(t, z^0) + f_{v_0}(t, v_0)(v_0(t) - z^0(t)) + O(\|v_0(t) - z^0(t)\|^2), \\ u_t + z_t^0 =& -2u(t) + O(\|u(t)\|^2), \\ u_t =& -\frac{\epsilon^{1-\lambda}}{2} - 2u(t). \end{aligned}$$

Which leads to the conclusion that equation (1.77) causes perturbations to decay exponentially to a nearby equilibrium. Hence we find the pseudo-equilibrium to be hyperbolic and asymptotically stable.

Sub-Case II: $v_0(t) \leq |A|$

With the Taylor approximation from the analysis (1.62), we have the following inner equation and pseudo-equilibrium

$$v_{0t} = -\epsilon^{1-\lambda}m(t) + \frac{4|A|}{\pi} + \frac{2}{\pi|A|}v_0^2 = f(t, v_0), \quad z^0(t) = -C\sqrt{\epsilon^{1-\lambda}m(t) - \frac{4|A|}{\pi}} \tag{1.78}$$

We consider simple linear perturbations to this pseudo-equilibrium (1.78), $v_0(t) = z^0(t) + u(t)$ with $\|u(t)\| \ll 1$. Treating the pseudo-equilibrium carefully, we find that the slowly varying component of the equilibrium contributes to the derivative. Thus we have

$$\begin{aligned} v_{0t} =& z_t^0(t) + u_t, \\ z_t^0(t) =& \begin{cases} \frac{\epsilon^{1-\lambda}}{2C\sqrt{\epsilon^{1-\lambda}m(t) - \frac{4|A|}{\pi}}} & \epsilon^{1-\lambda}m(t) > \frac{4|A|}{\pi}, \\ 0 & \epsilon^{1-\lambda}m(t) = \frac{4|A|}{\pi}. \end{cases} \end{aligned} \tag{1.79}$$

Now applying a Taylor expansion, we find the following behavior of perturbations

$$\begin{aligned} v_{0t} =& f(t, z^0) + f_{v_0}(t, z^0)(v_0 - z^0(t)) + O(\|v_0(t) - z^0(t)\|), \\ u_t =& \begin{cases} -\frac{\epsilon^{1-\lambda}}{2C\sqrt{\epsilon^{1-\lambda}m(t) - \frac{4|A|}{\pi}}} - 2\sqrt{\epsilon^{1-\lambda}m(t) - \frac{4|A|}{\pi}}u & \epsilon^{1-\lambda}m(t) > \frac{4|A|}{\pi}, \\ 0 & \epsilon^{1-\lambda}m(t) = \frac{4|A|}{\pi}. \end{cases} \end{aligned} \tag{1.80}$$

From (1.80), we find that the perturbations decay to a fixed negative quantity. This indicates, much like section 1.2, that there is an attracting equilibrium below the pseudo-equilibrium. The negative sign describes exponential decay and hence this equilibrium is hyperbolic and asymptotically stable for $\epsilon^{1-\lambda}m(t) > \frac{4|A|}{\pi}$ or $\mu(t) > \frac{4|A|}{\pi\Omega}$. But for $\epsilon^{1-\lambda}m(t) = \frac{4|A|}{\pi}$ or $\mu(t) = \frac{4|A|}{\pi\Omega}$, the stability of (1.80) suddenly becomes hyperbolic. This tells us that we lose stability at the oscillatory bifurcation but tipping will occur afterwards, which agrees with the conclusion in the tipping approximation from (1.66).

Case II: $\lambda > 1$

From the analysis, we discovered that for as long as $\epsilon^{\lambda-1}A \sim O(1)$, then we have the no different behavior in the tipping. With the Taylor approximation from the analysis (1.71), the inner equation and pseudo-equilibrium is

$$\begin{aligned} y_0 =& - m(t) + \epsilon^{\lambda-1}\frac{2|A|}{\pi} + \epsilon^{1-\lambda}\frac{2}{\pi|A|}y_0^2 = f(t,y), \\ z^0(t) =& - \epsilon^{\lambda-1}C\sqrt{m(t) - \epsilon^{\lambda-1}\frac{4|A|}{\pi}}. \end{aligned} \tag{1.81}$$

Similarly to Case I, we consider simple linear perturbations to this pseudo-equilibrium (1.84), $y_0(t) = z^0(t) + u(t)$ with $\|u(t)\| \ll 1$. Treating the pseudo-equilibrium carefully, we find that the slowly varying component of the equilibrium contributes to the derivative. Thus we have

$$\begin{aligned} y_{0t} =& z_t^0(t) + u_t, \\ z_t^0(t) =& \begin{cases} \frac{\epsilon^{\lambda-1}}{2C\sqrt{m(t)-\epsilon^{\lambda-1}\frac{4|A|}{\pi}}} & m(t) > \epsilon^{\lambda-1}\frac{4|A|}{\pi}, \\ 0 & m(t) = \epsilon^{\lambda-1}\frac{4|A|}{\pi}. \end{cases} \end{aligned} \tag{1.82}$$

Now applying a Taylor expansion, we find the following behavior of perturbations

$$\begin{aligned} y_{0t} =& f(t,z^0) + f_{y_0}(t,z^0)(y_0 - z^0(t)) + O(\|y_0 - z^0(t)\|^2), \\ u_t =& \begin{cases} -\frac{\epsilon^{\lambda-1}}{2C\sqrt{m(t)-\epsilon^{\lambda-1}\frac{4|A|}{\pi}}} - 2\sqrt{m(t) - \epsilon^{\lambda-1}\frac{4|A|}{\pi}}u & m(t) > \epsilon^{\lambda-1}\frac{4|A|}{\pi}, \\ 0 & m(t) = \epsilon^{\lambda-1}\frac{4|A|}{\pi}. \end{cases} \end{aligned} \tag{1.83}$$

But the conclusions from Case I still apply to (1.83) and thus we still have stability up until $\mu(t) = \frac{4|A|}{\pi\Omega}$ and expect to see tipping occurring after the

oscillatory bifurcation which is consistent with our tipping approximation for this case.
On the other hand, for large λ, the integral (1.71) approaches

$$y_{0t} = -m(t) + 2|y_0|. \tag{1.84}$$

But this is the same type of behavior from section 1.2, where we found that for $m(t) \geq 0$ our pseudo-equilibrium was stable and for $m(t) < 0$ that searching for the pseudo-equilibrium causes a contradiction. Thus, we conclude that the tipping will occur in the region of $m(t) < 0$ which agrees with (1.14).

Chapter 2

Two Dimensional Model

With the methods and approaches developed in chapter 1 for the one-dimensional model, we have an expectation of the behavior of the two-dimensional Stommel model around the non-smooth bifurcation under similar conditions. With the bifurcation structure we explored in **??**, we consider a generalization with the canonical model

$$\begin{aligned} \dot{V} &= \eta_1 - \eta_2 + \eta_3(T - V) - T - V|V| + A\sin(\Omega t), \\ \dot{T} &= \eta_1 - T(1 + |V|) + B\sin(\Omega t), \\ \dot{\eta_2} &= -\epsilon \\ T(0) = T_i, \quad V(0) &= V_i, \quad \eta_2(0) = \eta_{2i} > \eta_1\eta_3, \end{aligned} \tag{2.1}$$

with slow variation $\epsilon \ll 1$, high frequency $\Omega \gg 1$, amplitudes of oscillation A and B, and model parameters η_1 and η_3 to be fixed positive constants. This is the generalized two-dimensional Stommel model with two additional features. First, we allow for slow variation in the bifurcation parameter, this has been shown to be realistic as the η_2 is related to the freshwater flux and therefore not a fixed parameter; the same assumption is made in Roberts [**?**]. Second, we consider periodic forcing in the additive parameters (η_1, η_2) to account for oscillations in the observed behavior in Huybers [**?**]. To fully understand the effects of each component on the model, we build them individually before putting them together.

For the remainder of this paper, we make two assumptions: first that $\eta_3 < 1$ which causes (2.1) to admit the smooth bifurcation in the positive V region. The value η_3 describes the relative strength of the temperature relaxation to that of salinity, and it is frequently assumed that salinity's is much longer, giving $\eta_3 < 1$. Although not necessary, this will align our focus and give a case to analyze in depth, the case of $\eta_3 > 1$ follows similarly. The second assumption we make is that even though we have a two-dimensional model, the variable V is leading the dynamics of the system with it's nonlinear behavior. This assumption makes it clear that we will want to understand the non-smooth behavior in V where T follows in response to the effects of V. Again, also not necessary as the opposite situation may be considered,

there is evidence to show that changes in temperature respond to changes in salinity and this assumption allows for better physical agreement. With this we have the ability to solve behavior of T in terms of V to find equations in only one variable.

2.1 Slowly Varying Parameter

We consider only the slow variation mechanism to understand it's effects on the canonical system (2.1) with $\epsilon > 0$ and $A = B = 0$, where we allow the bifurcating parameter to slowly vary but no oscillatory forcing. With the parameter η_2 slowly varying, we expect to find a tipping point in the neighborhood of the aforementioned non-smooth bifurcation. With the choice of $\eta_3 < 1$, the lower branch with $V < 0$ is the branch we focus on in order to approach the non-smooth behavior, thus (2.1) becomes

$$\begin{aligned} \dot{V} &= \eta_1 - \eta_2(t) + \eta_3(T - V) - T + V^2, \\ \dot{T} &= \eta_1 - T(1 - V), \\ \dot{\eta_2} &= -\epsilon. \end{aligned} \tag{2.2}$$

From section 1.2, we learned that the one-dimensional model had a solution that began to act differently on a smaller scale. It was this approach that gave insight into the tipping. Here we search for an outer solution to (2.2) that helps us understand the behavior of system. Since we have slow variation in the parameter, we choose to scale the system (2.2) with the 'slow' time $\tau = \epsilon t$

$$\begin{aligned} \epsilon V_\tau =& \eta_1 - \eta_2(\tau) + \eta_3(T - V) - T + V^2, \\ \epsilon T_\tau =& \eta_1 - T(1 - V), \\ \eta_{2\tau} =& -1. \end{aligned} \tag{2.3}$$

We also form an asymptotic expansions in terms of the small quantity ϵ to get an expression that separates the dynamics by their contribution to the solution. Here we choose

$$\begin{aligned} V(\tau) \sim& V_0(\tau) + \epsilon V_1(\tau) + \epsilon^2 V_2 + \dots \\ T(\tau) \sim& T_0(\tau) + \epsilon T_1(\tau) + \epsilon^2 T_2(\tau) + \dots \end{aligned} \tag{2.4}$$

and substitute (2.4) into (2.3) to find

$$\begin{aligned}\epsilon V_{0\tau} + \epsilon^2 V_{1\tau} + \ldots =& \eta_1 - \eta_2(\tau) + \eta_3(T_0 - V_0) - T_0 + V_0^2 \\ &+ \epsilon(\eta_3(T_1 - V_1) - T_1 - 2V_1V_0) + \ldots \\ \epsilon T_{0\tau} + \epsilon^2 T_{1\tau} + \ldots =& \eta_1 - T_0(1 - V_0) + \epsilon(-T_1(1 - V_0) + V_1T_0) + \ldots\end{aligned}$$

Which once we separate at each order of ϵ we find the equations

$$O(1): \quad \begin{cases} 0 = & \eta_1 - \eta_2(\tau) + \eta_3(T_0 - V_0) - T_0 + V_0^2, \\ 0 = & \eta_1 - T_0(1 - V_0), \end{cases} \tag{2.5}$$

$$O(\Omega^{-1}): \quad \begin{cases} V_{0\tau} = & \eta_3(T_1 - V_1) - T_1 + 2V_1V_0, \\ T_{0\tau} = & -T_1(1 - V_0) + V_1T_0, \end{cases} \tag{2.6}$$

Where we solve (2.5) simultaneously for the pseudo-equilibria and we choose to solve T_0 in terms of V_0 from our assumption that T responds to V and thus we find the equation for V_0 with

$$\begin{aligned} T_0(V_0) =& \frac{\eta_1}{1 - V_0}, \\ 0 =& \eta_1 - \eta_2(\tau) - T_0(V_0) + \eta_3(T_0(V_0) - V_0) + V_0^2. \end{aligned} \tag{2.7}$$

With T_0 and V_0 found, we use (2.6) to search for the solution to T_1 and V_1 but first we note that with $\eta_\tau = -1$ we have

$$\begin{aligned} T_{0\tau}(V_{0\tau}) =& \frac{V_{0\tau}T_0(V_0)}{1 - V_0}, \\ V_{0\tau} =& \frac{(1 - V_0)}{(\eta_3 - 2V_0)(1 - V_0) + (1 - \eta_3)T_0(V_0)}. \end{aligned}$$

Thus we can solve (2.6) for T_1 in terms of V_1 with the same assumption as before and this results in

$$\begin{aligned} T_1(V_1) =& \frac{T_{0\tau} - T_0(V_0)V_1}{1 - V_0}, \\ V_1 =& \frac{-(1 - V_0)V_{0\tau} + (1 - \eta_3)T_{0\tau}(V_{0\tau})}{(1 - \eta_3)T_0(V_0) + (\eta_3 - 2V_0)(1 - V_0)}. \end{aligned} \tag{2.8}$$

Which we have the first few terms of the asymptotic expansion (2.4) with (2.7) and (2.8), although the method of using an asymptotic expansion to find when the inner dynamics form isn't as feasible in the two-dimensional problem as even the leading order term is complex. But the method of

scaling the system to find an inner equation from the one-dimensional model in should hold just the same here in the two-dimensional case.
We perform a separate analysis analogous to section 1.2 to determine the appropriate scaling, and since we know our non-smooth bifurcation to occur at $\eta_2 = \eta_1\eta_3$ when $V = 0$ and $T = \eta_1$, it makes the most sense to rescale (2.1) around these values. This results in the scalings

$$\begin{aligned} \eta_2 =& \eta_1\eta_3 + \epsilon n, \\ V =& \epsilon X, \\ T =& \eta_1 + \epsilon Y. \end{aligned} \tag{2.9}$$

We introduce these scalings (2.9) into the canonical system (2.1) to find the following inner system

$$\begin{aligned} \dot{X} &= -n(t) - \eta_3 X - (1-\eta_3)Y - \epsilon X|X|, \\ \dot{Y} &= -\eta_1|X| - Y - \epsilon|X|Y, \\ \dot{n} &= -1. \end{aligned} \tag{2.10}$$

Generally speaking, the parameters η_1 and η_3 have quite an effect on the behavior of a solution. We already determined from the introduction that η_3 will determine the orientation of the problem, but here we find a relationship between the parameters η_1 and η_3 by viewing (2.17) as a 2×2 system of spatial coordinates

$$\begin{pmatrix} \dot{X} \\ \dot{Y} \end{pmatrix} = \begin{pmatrix} -\eta_3 & -(1-\eta_3) \\ -\eta_1 \mathrm{sgn}(X) & -1 \end{pmatrix} \begin{pmatrix} X \\ Y \end{pmatrix} - \begin{pmatrix} n(t) + \epsilon X|X| \\ \epsilon|X|Y \end{pmatrix}. \tag{2.11}$$

Where the system (2.11) has eigenvalues that are either real or complex depending on the choice in η_1 and η_3 dictated by

$$\lambda_{1,2} = -\frac{\eta_3 + 1}{2} \pm \frac{1}{2}\sqrt{(\eta_3+1)^2 - 4(\eta_3 - \eta_1(1-\eta_3)\mathrm{sgn}(X))}. \tag{2.12}$$

It is important to notice that there is non-smooth behavior in the discriminant of (2.12), telling us that there is different behavior for these eigenvalues for the respective sign of X. If we consider $X < 0$ like in section 1.2, then the parameters η_1 and η_3 must adhere to

$$0 < \eta_3 \leq 1 - 4\eta_1, \quad 0 < \eta_1 < \frac{1}{4} \tag{2.13}$$

to admit real eigenvalues. Under the conditions in (2.13), the discriminant in (2.12) is positive and less than $(\eta + 1)^2$ which causes both eigenvalues to be

negative. Thus we have that the solutions in this region decay exponentially and hence stable. If the conditions of (2.13) are not met, we see qualitatively different behavior with complex eigenvalues but from (2.12) we see the real component is still negative and the exponential decay is still present where stability arises from this. The eigenvalues in (2.12) describe the type of behavior we see near the non-smooth bifurcation, when $V < 0$ and for real eigenvalues we see pure decay where complex eigenvalues will result in decaying spiral behavior around the equilibrium. In both cases, no erratic behavior and no sign of tipping occur up to leading order.
In section 1.2 we found that the non-smooth bifurcation was a critical point and that the region immediately after contained the tipping. For our two-dimensional model, this critical point is $(\eta_2, V, T) = (\eta_1\eta_3, 0, \eta_1)$, which results in the eigenvalues from (2.12) as $\lambda_{1,2} = \{-1, -\eta_3\}$, which are both negative real valued and hence we still have stability. Thus we expect our tipping to occur just after the standard non-smooth bifurcation here as well. We now consider $V > 0$ and with (2.11) we find the inner system

$$\begin{aligned} \dot{X} &= -n(t) - \eta_3 X - (1-\eta_3)Y - \epsilon X^2, \\ \dot{Y} &= -\eta_1 X - Y - \epsilon XY, \\ \dot{n} &= -1. \end{aligned} \tag{2.14}$$

Following the approach from section 1.2, we relate the solution directly to the parameter to find their relationship. Thus we swap the respective differentiation onto n; for convenience we write this as a 2×2 system

$$\begin{pmatrix} X_n \\ Y_n \end{pmatrix} = \begin{pmatrix} \eta_3 & 1-\eta_3 \\ \eta_1 & 1 \end{pmatrix} \begin{pmatrix} X \\ Y \end{pmatrix} + \begin{pmatrix} n + \epsilon X^2 \\ \epsilon XY \end{pmatrix}.$$

We seek a leading order solution in this region, thus we are permitted to drop the ϵ order terms to give

$$\begin{pmatrix} X_n \\ Y_n \end{pmatrix} = \begin{pmatrix} \eta_3 & 1-\eta_3 \\ \eta_1 & 1 \end{pmatrix} \begin{pmatrix} X \\ Y \end{pmatrix} + \begin{pmatrix} n \\ 0 \end{pmatrix}. \tag{2.15}$$

For the system (2.15), we find the following eigenvalues using (2.12)

$$\lambda_{1,2} = \frac{\eta_3 + 1}{2} \pm \frac{1}{2}\sqrt{(1+\eta_3)^2 + 4(\eta_1(1-\eta_3) - \eta_3)}. \tag{2.16}$$

These eigenvalues in (2.16) must be real as $\eta_3 < 1$ guarantees the discriminant is always positive. But the stability can also be determined here, as $\lambda_1 < 0 < \lambda_2$ causes the solution to be unstable, which confirms tipping to occur in the region $V > 0$. With real eigenvalues, the solution in the $V > 0$

region takes the following exponential form with constants $K_{i,j}$ being the jth component of the corresponding ith eigenvector

$$\begin{aligned} X(n) \sim & K_{1,1}e^{\lambda_1 n} + K_{2,1}e^{\lambda_2 n} + C_1 n + C_2, \\ Y(n) \sim & K_{1,2}e^{\lambda_1 n} + K_{2,2}e^{\lambda_2 n} + C_3 n + C_4. \end{aligned} \tag{2.17}$$

Translating both solutions in (2.17) back to our original coordinates we find

$$\begin{aligned} V(t) \sim & \eta_2(t) - \eta_1\eta_3 + \epsilon K_{1,1}e^{\lambda_1(\eta_2(t)-\eta_1\eta_3)/\epsilon} + \epsilon K_{2,1}e^{\lambda_1(\eta_2(t)-\eta_1\eta_3)/\epsilon} + O(\epsilon), \\ T(t) \sim & \eta_2(t) - \eta_1 + \epsilon K_{1,2}e^{\lambda_1(\eta_2(t)-\eta_1\eta_3)/\epsilon} + \epsilon K_{2,2}e^{\lambda_2(\eta_2(t)-\eta_1\eta_3)/\epsilon} + O(\epsilon). \end{aligned} \tag{2.18}$$

With (2.18) admitting the solution in the region $V > 0$, we determine the system to tip once one of these exponentials becomes large (i.e $O(1/\epsilon)$), which causes the system to diverge away from our lower branch towards the upper stable branch. This can be seen with

$$\eta_{2\text{slow}} = \min\{\eta_1\eta_3 - \epsilon \ln \epsilon/\lambda_i\}, \quad i = 1, 2. \tag{2.19}$$

Thus we have the tipping for this problem with (2.19) and this has a noticeably similar form to the tipping from section 1.2. As we found from (2.16), one of the eigenvalues is always negative and it is with this we find that the tipping is delayed with respect to the bifurcation. This in turn allows for the region of bi-stability to be extended and with more bi-stability, the hysteresis of the Stommel model allows the solution to spend more time around the lower branch before transitioning to the upper branch. These effects shrink as $\epsilon \to 0$ until we return to the static problem with $\epsilon = 0$,

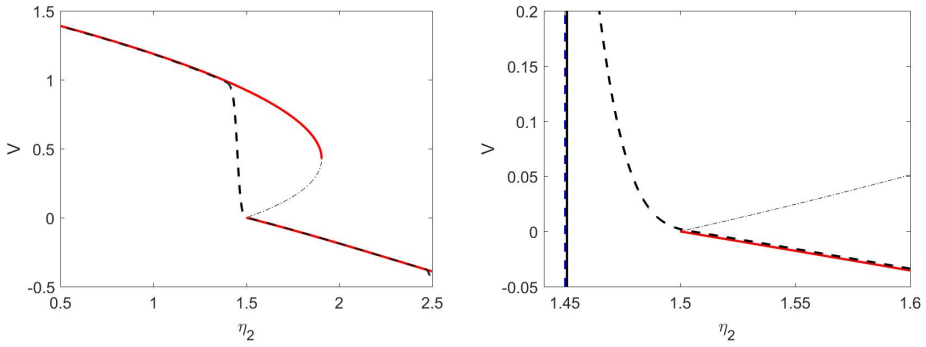

(a) (b)

Figure 2.1: In (a) the numerical solution (black dotted line) to (2.1) is given with $\eta_1 = 4$, $\eta_3 = .375$, and $\epsilon = .01$. In (b) a zoom in closer to the non-smooth bifurcation region where the blue vertical line is the prediction (2.19) against the black dotted vertical line which is the numerical tipping point.

In figure 2.1 an example of the slowly varying is given for a choice of ϵ in (a) and we zoom in around the non-smooth bifurcation in (b). Here we use the tipping criteria to be whenever $V > 0.5$, this is large enough that the solution is going towards the upper branch indefinitely and is around the point of the smooth bifurcation. The effect of seeing a delay moving towards the upper branch in the V solution causes a similar delay in T seen in figure 2.2, where the delay causes the maximum value of T to never be achieved. Here notice that after the tipping occurs, the numerical solution passes entirely over the unstable branch and even some of the upper stable branch before it resumes following closely.

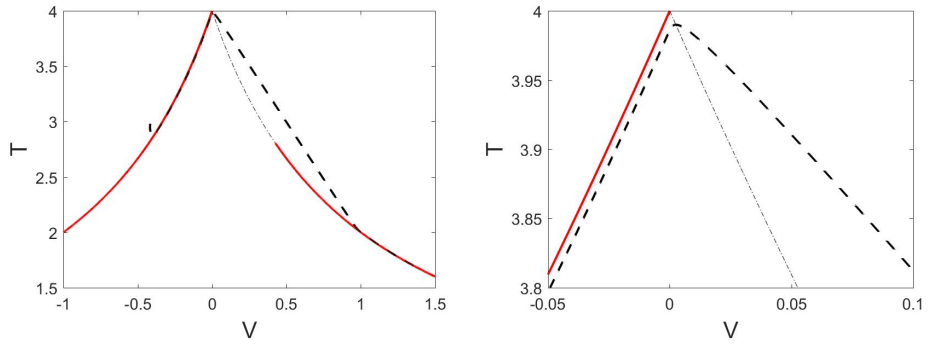

(a) (b)

Figure 2.2: In (a) we have the numerical solution (black dotted) over the standard equilibrium plot for V vs. T. In (b) a zoom of the bifurcation area.

In figure 2.3 we compare the numerical tipping to the predicted tipping in (2.19) over a range of epsilon. Here we see performance even better than in section section 1.2 as even for relatively large ϵ the prediction has small error. This is an artifact of having a higher dimensional problem, where now two exponentials in (2.18) are dominating the behavior of the solution in the $V > 0$ region. As in section 1.2, the concavity of the predicted tipping against the numerical tipping match very well and we can expect the prediction to hold for reasonably small values of ϵ.

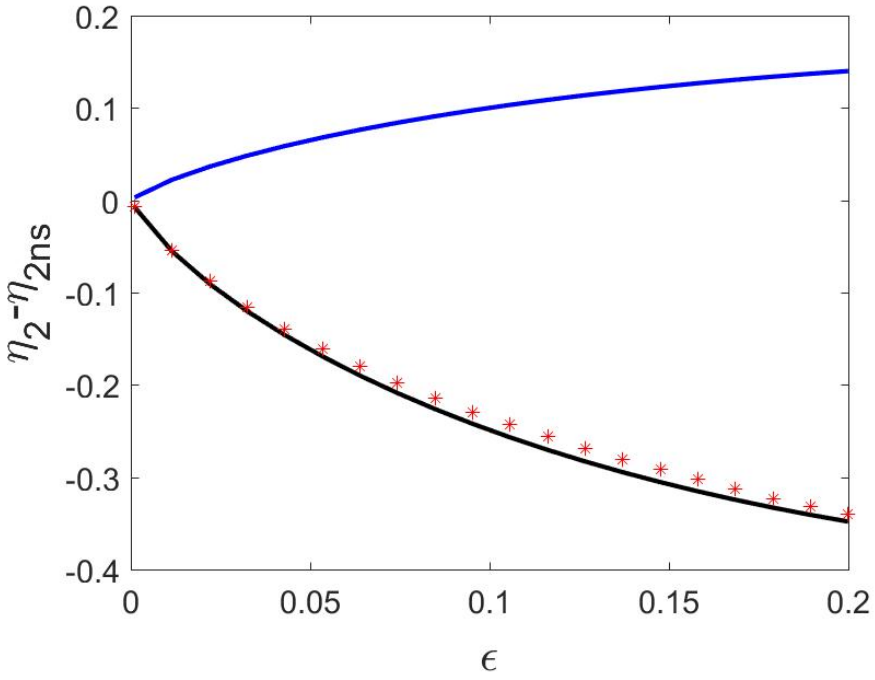

Figure 2.3: The numerical tipping vs the estimate with $\eta_1 = 4$ and $\eta_3 = \frac{3}{8}$. The tipping criteria is $V > .5$.

2.2 High Frequency Oscillatory Forcing

It is a physical behavior of the THC to see oscillations occurring in the dynamics that is not originally encompassed by the Stommel model [**?**, **?**, **?**, **?**, **?**, **?**]. We choose to allow η_1 and η_2 to exhibit oscillatory behavior to account for this. As these parameters appear in both equations for V and T, here we consider the canonical system (2.1) with $A, B \sim O(1)$, $\Omega \gg 1$ and $\epsilon = 0$ which is the purely oscillatory forcing problem. Under these conditions, we expect to find oscillations about some stable behavior; this stable behaior should act like the equilibria of a reduced inner problem. Thus our analysis must locate these equilibria for each variable up to the oscillations in order to find the bifurcation.

To begin our analysis, we note that there is behavior happening on multiple time scales, a 'slow' t and 'fast' $R = \Omega t$. Following the multiple scales method, we consider $V(t) = V(t, R)$ and $T(t) = T(t, R)$ and substituting

this into (2.1), we get the system

$$\begin{aligned} V_R + \Omega^{-1} V_t =& \Omega^{-1} \left(\eta_1 - \eta_2 + \eta_3 (T - V) - T - V|V| + A \sin(R) \right), \\ T_R + \Omega^{-1} T_t =& \Omega^{-1} \left(\eta_1 - T(1 + |V|) + B \sin(R) \right). \end{aligned} \tag{2.20}$$

As per our typical approach to the non-smooth behavior, we follow the lower branch to isolate this dynamic. Thus we consider the system (2.20) with $V < 0$

$$\begin{aligned} V_R + \Omega^{-1} V_t =& \Omega^{-1} \left(\eta_1 - \eta_2 + \eta_3 (T - V) - T + V^2 + A \sin(R) \right), \\ T_R + \Omega^{-1} T_t =& \Omega^{-1} \left(\eta_1 - T(1 - V) + B \sin(R) \right). \end{aligned} \tag{2.21}$$

From (2.21), it makes sense to consider an asymptotic expansion for both V and T in terms of the small quantity that appears, Ω^{-1}, with

$$\begin{aligned} V(t, R) &\sim V_0(t, R) + \Omega^{-1} V_1(t, R) + \Omega^{-2} V_2(t, R) + O(\Omega^{-3}), \\ T(t, R) &\sim T_0(t, R) + \Omega^{-1} T_1(t, R) + \Omega^{-2} T_2(t, R) + O(\Omega^{-3}). \end{aligned} \tag{2.22}$$

Substituting (2.22) into the system (2.21) gives

$$\begin{aligned} V_{0R} + \Omega^{-1} V_{0t} + \Omega^{-1} V_{1R} + \ldots =& \Omega^{-1} (\eta_1 - \eta_2 + \eta_3 (T_0 - V_0) - T_0 + V_0^2 + A \sin(R)) \\ & + \Omega^{-2} (\eta_3 (T_1 - V_1) - T_1 + 2 V_1 V_0) + \ldots \\ T_{0R} + \Omega^{-1} T_{0t} + \Omega^{-1} T_{1R} + \ldots =& \Omega^{-1} (\eta_1 - T_0 (1 - V_0) + B \sin(R)) \\ & + \Omega^{-2} (-T_1 (1 - V_0) + T_0 V_1) + \ldots \end{aligned}$$

Which we then find the following equations separated by order of Ω^{-1} with

$$O(1): \quad \begin{cases} V_{0R} = & 0, \\ T_{0R} = & 0, \end{cases} \tag{2.23}$$

$$O(\Omega^{-1}): \quad \begin{cases} V_{1R} + V_{0t} = & \eta_1 - \eta_2 + \eta_3 (T_0 - V_0) - T_0 + V_0^2 + A \sin(R), \\ T_{1R} + T_{0t} = & \eta_1 - T_0 (1 - V_0) + B \sin(R), \end{cases} \tag{2.24}$$

$$O(\Omega^{-2}): \quad \begin{cases} V_{2R} + V_{1t} = & \eta_3 (T_1 - V_1) - T_1 + 2 V_0 V_1, \\ T_{2R} + T_{1t} = & -T_1 (1 - V_0) + T_0 V_1. \end{cases} \tag{2.25}$$

We learn from (2.23) that both our leading order terms are purely dependent on the slow variable, $V_0 = V_0(t)$, $T_0 = T_0(t)$. But much like section 1.3, we must introduce a solvability condition on the resonant terms to be able to solve for the correction terms. This secures terms that are both consistent with one another as well as less than linear in their growth, making for a stable expansion. Here, we use the Fredholm alternative (1.24) on (2.24)-(2.25) and search for the equilibrium solutions, the work for this can be found in Appendix B. This leads to the outer solution in original coordinates

$$\begin{aligned} V \sim & V_0 - \Omega^{-1} A \cos(\Omega t) + \dots \\ T \sim & T_0 - \Omega^{-1} B \cos(\Omega t) + \dots \end{aligned} \tag{2.26}$$

Where V_0 and T_0 are the same equilibrium solutions from the static model in the introduction with

$$\begin{aligned} T_0(V_0) = & \frac{\eta_1}{1 - V_0}, \\ 0 = \eta_1 - \eta_2 + \eta_3(T_0(V_0) - V_0) - T_0(V_0) + V_0^2. & \end{aligned}$$

From the one-dimensional model in section 1.3, we discovered that in order to access the bifurcation we needed to scale both the coordinate x as well as the parameter μ and analyze the behavior occurring around axis for $x = 0$. Since we still have non-smooth behavior occurring at the axis $V = 0$, we expect this approach to hold for the two-dimensional model as well. But the outer solution (2.26) is too complex for us to search for when the assumptions of the asymptotic series break that would help find the appropriate scaling. Instead, a separate scales analysis analogous to section 1.3 leads to the following scaling

$$\begin{aligned} V = & \Omega^{-1} X, \\ T = & \eta_1 + \Omega^{-1} Y, \\ \eta_2 = & \eta_1 \eta_3 + \Omega^{-1} n. \end{aligned} \tag{2.27}$$

Substituting (2.27) into (2.1) leads to the following inner system

$$\begin{aligned} \dot{X} = & -n + \eta_3(Y - X) - Y - \Omega^{-1} X|X| + \Omega A \sin(\Omega t), \\ \dot{Y} = & -\eta_1|X| - Y - \Omega^{-1}|X|Y + \Omega A \sin(\Omega t). \end{aligned} \tag{2.28}$$

Where we still see behavior on the same time scales in (2.28), the 'slow' t and the 'fast' $R = \Omega t$. Considering both $X(t) = X(t, R)$ and $Y(t) = Y(t, R)$

gives the multiple scales inner system

$$\begin{aligned} X_R + \Omega^{-1} X_t =& \Omega^{-1}\left(-n + \eta_3(Y - X) - Y\right) - \Omega^{-2} X|X| + A\sin(R), \\ Y_R + \Omega^{-1} Y_t =& \Omega^{-1}\left(-\eta_1|X| - Y\right) - \Omega^{-2}|X|Y + B\sin(R). \end{aligned} \tag{2.29}$$

Once more, as we see the small quantity Ω^{-1} appearing in (2.29), then we choose an expansion of the form

$$\begin{aligned} X(t,R) \sim& X_0(t,R) + \Omega^{-1} X_1(t,R) + O(\Omega^{-2}), \\ Y(t,R) \sim& Y_0(t,R) + \Omega^{-1} Y_1(t,R) + O(\Omega^{-2}), \end{aligned} \tag{2.30}$$

where we then substitute (2.30) into (2.29) to give the equation containing dynamics of all orders

$$\begin{aligned} X_{0R} + \Omega^{-1} X_{0t} + \Omega^{-1} X_{1R} + \ldots =& \Omega^{-1}(-n + \eta_3(Y_0 - X_0) - Y_0) + A\sin(R) \\ & + \Omega^{-2}(X_0|X_0 + \Omega^{-1} X_1 + \ldots| + \eta_3(Y_1 - X_1) - Y_1) + \ldots \\ Y_{0R} + \Omega^{-1} Y_{0t} + \Omega^{-1} Y_{1R} + \ldots =& \Omega^{-1}(-\eta_1|X_0 + \Omega^{-1} X_1 + \ldots| - Y_0) + B\sin(R) \\ & + \Omega^{-2}(-|X_0 + \Omega^{-1} X_1 + \ldots|Y_0 - Y_1) + \ldots \end{aligned}$$

We then separate the dynamics by their respective contribution to the solution, here by order of Ω^{-1}, to find the following equations

$$O(1): \quad \begin{cases} X_{0R} = & A\sin(R), \\ Y_{0R} = & B\sin(R), \end{cases} \tag{2.31}$$

$$O(\Omega^{-1}): \quad \begin{cases} X_{1R} + X_{0t} = & -n - \eta_3 X_0 - (1 - \eta_3) Y_0, \\ Y_{1R} + Y_{0t} = & -\eta_1|X_0| - Y_0. \end{cases} \tag{2.32}$$

From (2.31) we find that the leading order terms of (2.30) have the form in terms of the time scales

$$X_0 = P_0(t) - A\cos(R), \quad Y_0 = Q_0(t) - B\cos(R). \tag{2.33}$$

Substituting (2.33) into (2.32), we apply the Fredholm alternative (1.24) to solve in terms of the separate time scales. This results in

$$\begin{aligned} P_{0t} =& -n - \eta_3 P_0 - (1 - \eta_3) Q_0, \\ Q_{0t} =& -\frac{\eta_1}{2\pi} \int_0^{2\pi} |P_0 - A\cos(R)| dR - Q_0. \end{aligned} \tag{2.34}$$

As we are concerned with finding the bifurcation, we search for the equilibrium solutions to (2.34) but we find a similar integral equation to the inner equation in section 1.3. This leads us to the similar two case argument. Case I: $|P_0(t)| \leq -|A|$ which prevents the sign of the integrand from changing, and Case II: $|P_0(t)| < |A|$ where the integrand experiences the sign flipping and the integral has a non-trivial solution. These cases can be seen in figure 2.4.

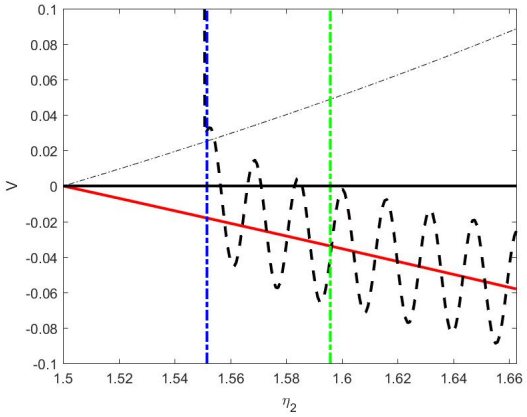

Figure 2.4: Here we have the parameter ranges for Case I and Case II shown as the right most green vertical line and the bifurcation at the left blue vertical line respectfully.

2.2.1 Case I: $P_0(t) \leq -|A|$

We call this the entirely below axis case; here with the size of the solution X_0 being far enough from the axis to see no bifurcating behavior. This case helps to simplify the integration in (2.34) but also helps us to determine when the solution begins to act differently. Here we use the equilibria to define a boundary between Case I and Case II. Under the conditions of this case, the system (2.34) simplifies to

$$\begin{aligned} P_{0t}(t) =& -n - \eta_3 P_0(t) - (1-\eta_3) Q_0(t), \\ Q_{0t}(t) =& \eta_1 P_0(t) - Q_0(t). \end{aligned} \tag{2.35}$$

Solving for the equilibria in (2.35) results in

$$Q_0(P_0) = \eta_1 P_0 \quad , P_0 = -\frac{n}{\eta_1(1-\eta_3)+\eta_3}.$$

Together with these equilibria and with the condition of the case, $P_0(t) \leq -|A|$, we find the parameter range that distinguishes between Case I and Case II in terms of our inner parameter, which we then rewrite in original coordinates with

$$\begin{aligned} n \geq & (\eta_1(1-\eta_3)+\eta_3)|A|, \\ \eta_2 \geq & \eta_1\eta_3 + \frac{(\eta_1(1-\eta_3)+\eta_3)|A|}{\Omega}. \end{aligned} \tag{2.36}$$

So for values of η_2 less that the boundary given in (2.36), we begin to see the oscillations crossing above the axis and hence use a separate case to deal with this behavior.

2.2.2 Case II: $|P_0(t)| < |A|$

We call this the crossing case; here the solution is beginning to oscillate about the axis while the center of the oscillations approach the axis. With this behavior, we expect a bifurcation to occur in this region and thus we must find the equilibria for (2.34) that will help determine the location. While this problem is two-dimensional in nature, the integral in (2.34) is nearly identical to the integral of difficulty in section 1.3. So we may use the ideas of that section here to form an approximate solution. Thus, under the assumptions of this case, we fix a value of P_0 and integrate (2.34) over the regions where the integrand take the same sign with

$$R_1 = \arccos(P_0/A), \quad R_2 = 2\pi - \arccos(P_0/A).$$

We make the same assumption in section 1.3 that the solution to (2.34) is negative for $P_0(t)$ the region $R \in [0, R_1]$ and alternates sign for the regions $R \in (R_1, R_2]$ and $R \in (R_2, 2\pi]$. With this assumption, we also follow the same procedure of integrating over each region to get the exact form for (2.34) with

$$\begin{aligned} P_{0t} = & -n - \eta_3 P_0(t) - (1-\eta_3)Q_0, \\ Q_{0t} = & -\frac{2\eta_1}{\pi}\left(\arcsin(P_0/A)P_0 + \sqrt{A^2 - P_0^2}\right) - Q_0. \end{aligned} \tag{2.37}$$

Although this is the explicit inner equation from (2.37), this is analytically too complex to find an explicit form for any bifurcating behavior and thus

we use a second order Taylor approximation to find the solvable system

$$\begin{aligned} P_{0t} =& - n - \eta_3 P_0 - (1-\eta_3)Q_0, \\ Q_{0t} =& - \frac{2\eta_1|A|}{\pi} - Q_0 - \frac{\eta_1}{\pi|A|}P_0^2. \end{aligned} \tag{2.38}$$

Recalling that the equilibria will lead to the bifurcation, we solve (2.38) to give the inner solution. For simplicity, define $a = \frac{\eta_1}{\pi|A|}$, and $c = \frac{2\eta_1|A|}{\pi}$,

$$\begin{aligned} Q_0(P_0) =& - aP_0^2 - c, \\ 0 =& -n + \frac{2\eta_1(|A|}{\pi} - \eta_3 P_0 + \frac{\eta_1}{\pi|A|}P_0^2. \end{aligned} \tag{2.39}$$

Where the equation for P_0 in (2.39) is a quadratic that would have two solutions, we recall the lower branch as being what we follow for this analysis, so we choose the negative solution with

$$P_0 = \frac{\eta_3}{2a(1-\eta_3)} - \frac{1}{2a(1-\eta_3)}\sqrt{\eta_3^2 + 4a(1-\eta_3)(n - c(1-\eta_3))}. \tag{2.40}$$

With the equilibrium for P_0 in (2.40) containing a square root, this fails once the discriminant becomes negative. It is with this sudden failure that we have the bifurcation, here occurring for

$$n_{osc} = \frac{\eta_1(1-\eta_3)|A|}{\pi}\left[2 - \left(\frac{\pi\eta_3}{2\eta_1(1-\eta_3)}\right)^2\right].$$

Where we have the inner equilibria found, we write (2.40) along with the oscillations as well as the oscillatory bifurcation in original coordinates

$$\begin{aligned} V(t) \sim& \Omega^{-1}\left(P_0 - A\cos(\Omega t)\right), \\ T(t) \sim& \eta_1 - \Omega^{-1}\left(\frac{\eta_1}{\pi|A|}P_0^2 + \frac{2\eta_1|A|}{\pi} + B\cos(\Omega t)\right), \end{aligned} \tag{2.41}$$

$$\eta_{2osc} = \eta_1\eta_3 + \frac{\eta_1(1-\eta_3)|A|}{\pi\Omega}\left[2 - \left(\frac{\pi\eta_3}{2\eta_1(1-\eta_3)}\right)^2\right]. \tag{2.42}$$

With (2.42) we have found the bifurcation induced with the addition of oscillatory forcing in the Stommel model. As we learned from the one-dimensional model in section 1.3, the effect of oscillatory forcing is early bifurcations. Our result in (2.42) agrees with this heuristic under the caveat that we restrict the parameters with

$$\eta_3 < \frac{2\sqrt{2}\eta_1}{\pi + 2\sqrt{2}\eta_1},$$

which is the condition to guarantee the second term in (2.42) is positive. This restriction is reasonable as generally the parameters have the behaviors of $\eta_3 < 1$ and $\eta_3 \ll \eta_1$ where the thermal variation is much larger in real ocean dynamics than the ratio of relaxation times.

In figure 2.5 the numerical solution to (2.1) for V and a zoom of the solution around the numerical bifurcation is shown. The static bifurcation diagram is underlayed as well for comparison. We contrast the result in (2.42) to these numerics and find the bifurcation prediction from our analysis agrees in V. Notice that there is an early bifurcation for this problem, where certain values of the lower branch are never achieved. In figure 2.6 the numerical solution to (2.1) for T and a zoom in around the bifurcation is shown. Once more, the static bifurcation diagram is underlayed and we have two interesting features to note. Due to the early bifurcation in V, the maximum value of T is never reached in (b). But due to the early bifurcation, there is a region of both the lower and the upper branch in V that is never followed and we see that range being skipped over by the numerics in (a).

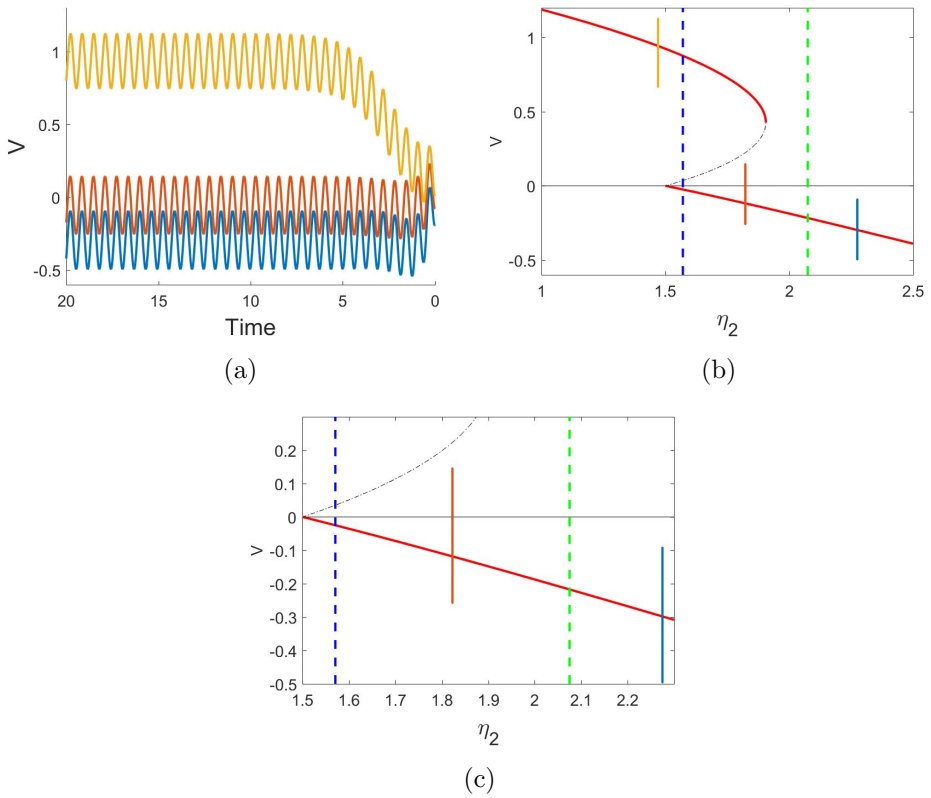

Figure 2.5: In (a) the numerical time series solutions to (2.1) is given with parameters in each qualitatively different case of η_2 with $\eta_1 = 4$, $\eta_3 = .375$, $A = 10$ and $\Omega = 10$. In (b) these same solutions are shown on the phase plane. In (c) a zoom in closer to the non-smooth bifurcation region where the blue vertical line is the prediction (2.19) against the black dotted vertical line which is the numerical bifurcation.

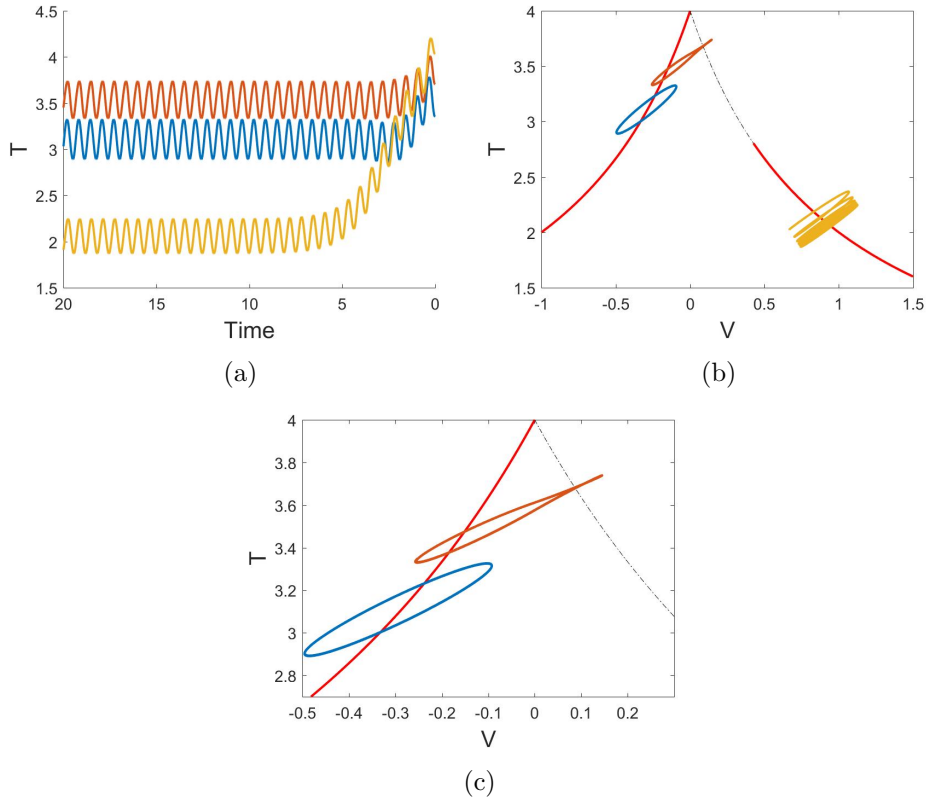

Figure 2.6: In (a) we have the numerical time series solutions for a qualitatively different cases of η_2. In (b) we plot these solutions over the standard equilibrium plot for V vs. T. In (c) a zoom of the bifurcation area.

To evaluate the performance of this prediction, we compare (2.42) to the numerical tipping criteria over a range of Ω^{-1}. In figure 2.7 we allow for this range to be $\Omega^{-1} \in (0, .5)$. For small values, the two agree very well and as we expect, they begin to diverge once the values of Ω^{-1} become too large from the assumption that $\Omega \gg 1$ and the asymptotics cannot capture the behavior for low frequency oscillations. But under our assumptions, the prediction is performing quite well and resembles the performance of section 1.3.

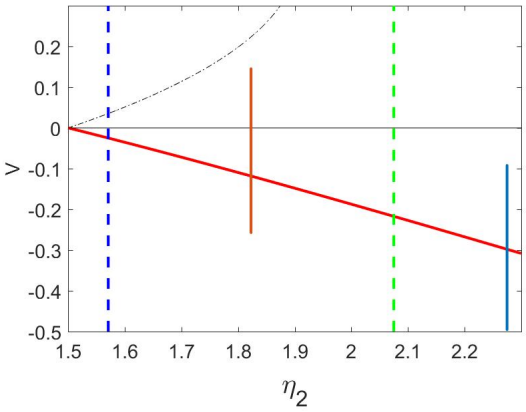

Figure 2.7: The numerical tipping vs the estimate with $\eta_1 = 4$ and $\eta_3 = \frac{3}{8}$. The tipping criteria is $V > .5$.

2.2.3 Stability

Although the eigenvalues from section 2.1 apply here, since we have a non-autonomous system when $A \neq 0$, we must approach the stability with a linearized form about the equilibria much like in section 1.3. To do this, recall from our analysis that we found the system

$$\begin{aligned} P_{0t} &= -n - \eta_3 P_0 - (1-\eta_3)Q_0, \\ Q_{0t} &= -\frac{\eta_1}{2\pi}\int_0^{2\pi} |P_0 - A\cos(R)|\, dR - Q_0. \end{aligned} \tag{2.43}$$

We must consider the stability of solutions over the relative sizes of $P_0(t)$ with Case I: $P_0(t) \leq -|A|$ and Case II: $|)_0(t)| \leq |A|$.

Case I: $v_0(t) \leq -|A|$

From the analysis, we called this case the entirely below-axis case where the solution spends most of its time away from the axis $V = 0$. We expected this case to be entirely controllable and thus we should see stability here. Under these conditions, the inner equation (2.43) simplifies to a much simpler equation

$$\begin{aligned} P_{0t} &= -m - \eta_3 P_0 - (1-\eta_3)Q_0, \\ Q_{0t} &= \eta_1 P_0 - Q_0. \end{aligned} \tag{2.44}$$

The equilibria of (2.44) is found with $Q_0(P_0) = \eta_1 P_0$, and thus we find the following one-dimensional equation and equilibrium

$$P_{0t} = -n - (\eta_3 + (1-\eta_3))Q_0 = f(P_0), \quad Z^0 = -\frac{n}{\eta_3 + \eta_1(1-\eta_3)}. \quad (2.45)$$

Now we consider a simple linear perturbation about this equilibrium with $P_0(t) = Z^0 + U(t)$ where $\|U(t)\| \ll 1$. Our standard Taylor expansion about this equilibrium results in

$$\begin{aligned} f(P_0) =& f(Z^0) + f_{P_0}(Z^0)(P_0 - Z^0) + O((P_0 - Z^0)^2), \\ U_t =& -(\eta_3 + \eta_1(1-\eta_3))U + O(\|U\|^2). \end{aligned} \quad (2.46)$$

From (2.46) we now conclude the equilibrium Z^0 is hyperbolic and asymptotically stable due to the exponential decay in perturbations. Thus we find that no tipping will occur for this case, and from the analysis, this holds true until for the parameter range of η_2 from (2.36)

$$\eta_2 \geq \eta_1\eta_3 + \frac{(\eta_3 + \eta_1(1-\eta_3))|A|}{\Omega}.$$

Case II: $|P_0(t)| < |A|$

We called this case the crossing case and here the solution experiences all of the non-smooth behavior when it crosses $V = 0$. We expect the stability to fail under these conditions and we discovered in the analysis that the crossing pattern caused the system (2.43) to behave like

$$\begin{aligned} P_{0t} =& -n - \eta_3 P_0 - (1-\eta_3)Q_0, \\ Q_{0t} =& -\frac{2\eta_1|A|}{\pi} - \frac{\eta_1}{\pi|A|}P_0^2 - Q_0. \end{aligned} \quad (2.47)$$

As we search for the equilibria of (2.47), we find the equilibrium for Q_0 in terms of P_0

$$Q_0(P_0) = -\frac{2\eta_1|A|}{\pi} - \frac{\eta_1}{\pi|A|}P_0^2$$

which then gives the following inner equation with the negatively chosen

equilibrium for P_0

$$\begin{aligned} P_{0t} =& -n + \frac{2\eta_1(|A|}{\pi} - \eta_3 P_0 + \frac{\eta_1}{\pi|A|} P_0^2 = f(P_0), \\ Z^0 =& \frac{\pi|A|}{2\eta_1(1-\eta_3)} \left(\eta_3 - \sqrt{n - n_{\text{osc}}}\right). \end{aligned} \tag{2.48}$$

For simplicity we write the argument of the square root in terms of oscillatory bifurcation we found in the analysis with (2.42). We now consider a simple linear perturbation about this equilibrium in (2.48) with $P_0(t) = Z^0 + U(t)$ where $\|U(t)\| \ll 1$. The standard Taylor expansion about the equilibrium is thus

$$\begin{aligned} f(P_0) =& f(Z^0) + f_{P_0}(Z^0)(P_0 - Z^0) + O((P_0 - Z^0)^2), \\ U_t =& \left(-\eta_3 + \frac{2\eta_1(1-\eta_3)}{\pi|A|} Z^0\right) U, \\ U_t =& -\sqrt{n - n_{\text{osc}}} U. \end{aligned} \tag{2.49}$$

Thus with (2.49) we learn that the perturbations $U(t)$ decay exponentially as long as the square-root is non-zero and makes sense. Thus we have that Z^0 is a hyperbolic and asymptotically stable equilibrium for P_0 and thus we find stability in Q_0 as well. This gives stability for this region but we lose this stability once the square-root becomes zero, here when

$$n_{osc} = \frac{\eta_1(1-\eta_3)|A|}{\pi} \left[2 - \left(\frac{\pi\eta_3}{2\eta_1(1-\eta_3)}\right)^2\right].$$

This says the equilibrium Z^0 at this point is non-hyperbolic which is indicative of a bifurcation. This is in agreement with out analysis and thus we can say that the value found in (2.42) is the bifurcation under the oscillatory forcing.

2.3 Slow Variation with Oscillatory Forcing

With the one-dimensional model solved and both the slowly varying and high oscillatory two-dimensional components analyzed, we have all of the tools needed to analyze the full system (2.1) with both $\epsilon \ll 1$ and $A, B \sim O(1)$ simultaneously. This is the most general setting we discuss in this paper where we account for both a slowly varying η_2 that leads to abrupt changes seen in [**?**, **?**, **?**] as well as oscillatory forcing in both equations in (2.1) seen in [**?**, **?**]. We care to find the interaction of mechanisms in the physical Stommel

model. Under the framework of slowly varying parameters we expect to find tipping instead of a bifurcation and hence our method for finding the tipping point follows a mixture of both section 2.1 and section 2.2. This procedure dictates that we search for inner behavior about the non-smooth bifurcation and to do so we need to solve the inner equation and estimate when this solution becomes uncontrollable. Ultimately, we provide a realistic solution for where the abrupt change from the lower stable branch to the upper occurs in the full two-dimensional Stommel model.
To begin, we take our standard approach of following the lower branch towards the non-smooth behavior with $V < 0$ in (2.1) which gives the following system

$$\begin{aligned} \dot{V} &= \eta_1 - \eta_2 - T + \eta_3(T - V) + V^2 + A\sin(\Omega t), \\ \dot{T} &= \eta_1 - T(1 - V) + B\sin(\Omega t), \\ \dot{\eta_2} &= -\epsilon. \end{aligned} \tag{2.50}$$

Much like in section 1.4, we assume there is a generic polynomial relationship between the frequency of our problem and the slow variation, $\Omega = \epsilon^{-\lambda}$ with strength parameter $\lambda > 0$. It is this assumption that helps us to find the interaction between the slowly varying parameter and fast oscillations in the tipping. We notice in (2.50) that there is behavior on a slow scale in $\eta_2(t)$ and on a fast scale in $\sin(\Omega t)$, so this suggests a multiple scales approach with 'slow' time $\tau = \epsilon t$ and 'fast' time $R = \epsilon^{-\lambda} t$. These scales cause (2.50) to take the form

$$\begin{aligned} V_R + \epsilon^{\lambda+1} V_\tau &= \epsilon^\lambda \left(\eta_1 - \eta_2 - T + \eta_3(T - V) + V^2 + A\sin(R)\right), \\ T_R + \epsilon^{\lambda+1} T_\tau &= \epsilon^\lambda \left(\eta_1 - T(1 - V) + B\sin(R)\right), \\ \eta_{2\tau} &= -1. \end{aligned} \tag{2.51}$$

From these multiple-scaled outer equations in (2.51), we find an asymptotic expansion in terms of our small recurring quantity ϵ^λ to be a good choice for separating the dynamics by order. But we must consider both multiples of λ as well as integer powers as we have not specified the range of λ and both could be significant, thus our expansion is

$$\begin{aligned} V(\tau, R) \sim& V_0(\tau, R) + \epsilon^\lambda V_1(\tau, R) + O(\epsilon^{2\lambda}, \epsilon^{\lambda+1}), \\ T(\tau, R) \sim& T_0(\tau, R) + \epsilon^\lambda T_1(\tau, R) + O(\epsilon^{2\lambda}, \epsilon^{\lambda+1}). \end{aligned} \tag{2.52}$$

Which substituting (2.52) into (2.51) results in the governing dynamics for all orders of ϵ with

$$\begin{aligned}
V_{0R} + \epsilon^{\lambda+1} V_{0\tau} + \epsilon^{\lambda} V_{1R} + \ldots =& \epsilon^{\lambda} \left(\eta_1 - \eta_2 - T + \eta_3 (T_0 - V_0) + V_0^2 + A \sin(R) \right) \\
&+ \epsilon^{2\lambda} \left(-\eta_3 V_1 - (1 - \eta_3) T_1 + 2 V_0 V_1 \right) + \ldots \\
T_{0R} + \epsilon^{\lambda+1} T_{0\tau} + \epsilon^{\lambda} T_{1R} + \ldots =& \epsilon^{\lambda} \left(\eta_1 - T_0 (1 - V_0) + B \sin(R) \right) \\
&+ \epsilon^{2\lambda} \left(-T_1 + T_0 V_1 + T_1 V_0 \right) + \ldots
\end{aligned}$$

Here we consider the next order in (2.52) to be $O(\epsilon^{2\lambda})$ as the equations at $O(\epsilon^{\lambda+1})$ and $O(\epsilon^{2\lambda})$ result in the same information, so it does not matter whether we consider a λ value that would cause $O(\epsilon^{2\lambda})$ to come before $O(\epsilon^{\lambda+1})$ or vice-versa. With this in mind, we find the following sets of equations at each order

$$O(1): \quad \begin{cases} V_{0R} = & 0, \\ T_{0R} = & 0, \end{cases} \tag{2.53}$$

$$O(\epsilon^{\lambda}): \quad \begin{cases} V_{1R} = & \eta_1 - \eta_2(\tau) + \eta_3 (T_0 - V_0) - T_0 + V_0^2 + A \sin(R), \\ T_{1R} = & \eta_1 - T_0 (1 - V_0) + B \sin(R), \end{cases} \tag{2.54}$$

$$O(\epsilon^{2\lambda}): \quad \begin{cases} V_{2R} + \epsilon^{1-\lambda} V_{0\tau} = & \eta_3 (T_1 - V_1) - T_1 + 2 V_0 V_1, \\ T_{2R} + \epsilon^{1-\lambda} T_{0\tau} = & -T_1 (1 - V_0) + T_0 V_1, \end{cases} \tag{2.55}$$

From (2.53) the leading order terms in our expansion are purely slow dependent, $V_0 = V_0(\tau)$ and $T_0 = T_0(\tau)$. This allows the solutions of (2.54) and (2.55) to be found, the work for this is found in Appendix B. This results in the following outer solutions

$$\begin{aligned}
V \sim & V_0 + \frac{\epsilon (V_{0\tau}(1 - V_0) + (1 - \eta_3) T_{0\tau})}{(1 - \eta_3) T_0 + (2 V_0 - \eta_3)(1 - V_0)} - \epsilon^{\lambda} A \cos(\Omega t), \\
T \sim & T_0 + \frac{\epsilon T_{0\tau}}{1 - V_0} - \frac{\epsilon T_0 (V_{0\tau}(1 - V_0) + (1 - \eta_3) T_{0\tau})}{(1 - \eta_3) T_0 (1 - V_0) + (2 V_0 - \eta_3)(1 - V_0)^2} - \epsilon^{\lambda} B \cos(\Omega t),
\end{aligned} \tag{2.56}$$

where V_0 and T_0 are the same leading order solutions from the slowly varying Stommel model in section 2.1. Unfortunately the common theme of the two-dimensional model is that these outer solutions are too complex to see directly when an inner scaling is required so we perform a separate scale analysis analogous to that of section 1.4 to find the appropriate inner scaling.

We make the assumption that the inner scaling for both V and T are the same which just makes this calculation slightly easier, but this isn't necessary to arrive at the same conclusion. Hence we chose a general scaling about the bifurcation point $(V, T, \eta_2) = (0, \eta_1, \eta_1\eta_3)$ with

$$V = \epsilon^{\alpha} X, \quad T = \eta_1 + \epsilon^{\alpha} Y, \quad \eta_2(t) = \eta_1\eta_3 + \epsilon^{\beta} n(t), \tag{2.57}$$

where both $\alpha > 0$ and $\beta > 0$ allow for this to be an inner scaling. Applying the scalings in (2.57) to the full two-dimensional model (2.1) gives

$$\begin{aligned} \epsilon^{\alpha}\dot{X} =& -\epsilon^{\beta} n(t) - \epsilon^{\alpha}(X + (1-\eta_3)Y) - \epsilon^{2\alpha} X|X| + A\sin\Big(\epsilon^{-\lambda} t\Big), \\ \epsilon^{\alpha}\dot{Y} =& -\epsilon^{\alpha}(\eta_1|X| + Y) + \epsilon^{2\alpha}|X|Y + B\sin\Big(\epsilon^{-\lambda} t\Big) \\ \dot{n} =& -\epsilon^{1-\beta}. \end{aligned} \tag{2.58}$$

From (2.58) it is apparent that fast behavior is still occurring on different time scales and to truly flesh out the particular choice in α, we then take a multiple scales approach to capture the 'fast' behavior with scales t and $R = \epsilon^{-\lambda} t$. Also note that we choose to have the 'slow' behavior has been moved into regular time with the scalings we applied to the space variables. This choice comes with the ambiguity in β and is discussed further below. Applying the multiple scales in (2.58) results in

$$\begin{aligned} \epsilon^{\alpha-\lambda} X_R + \epsilon^{\alpha} X_t =& -\epsilon^{\beta} n(t) - \epsilon^{\alpha}(X + (1-\eta_3)Y) - \epsilon^{2\alpha} X|X| + A\sin(R), \\ \epsilon^{\alpha-\lambda} Y_R + \epsilon^{\alpha} Y_t =& -\epsilon^{\alpha}(\eta_1|X| + Y) - \epsilon^{2\alpha}|X|Y + B\sin(R) \\ n_t =& -\epsilon^{1-\beta}. \end{aligned} \tag{2.59}$$

Here we balance the leading order terms in each equation of (2.59), $\epsilon^{\alpha-\lambda} X_R$ and $A\sin(R)$ as well as $\epsilon^{\alpha-\lambda} Y_R$ with $B\sin(R)$, which gives us that $\alpha = \lambda$ and confirms that the scales for each variable are the same. The scaling for η_2 has still yet to be determined and could have multiple possibilities depending on λ, but due to this choice in α we expect the oscillatory term to persist in the inner asymptotic expansion of (2.1) regardless of choice in λ and we have an effective means of tracking this behavior with this scaling. We now consider the scales t and $R = \epsilon^{-\lambda} t$ on the canonical system (2.1)

along with the general scaling on η_2 which gives

$$\begin{aligned} V_R + \epsilon^\lambda V_t =& -\epsilon^{\lambda+\beta} n(t) - \epsilon^\lambda(\eta_1 - \eta_1\eta_3 + \eta_3(T-V) - T - V|V| + A\sin(R)), \\ T_R + \epsilon^\lambda T_t =& \epsilon^\lambda(\eta_1 - T(1+|V|) + B\sin(R)), \\ n_t =& -\epsilon^{1-\beta}. \end{aligned} \tag{2.60}$$

We learned in section 1.4 that the analysis from here depends on the relative size of the slow variation with respects to the oscillations. The distinction in these behaviors are when $\lambda \leq 1$ where a mixture between the slow variation and oscillations occur or $\lambda > 1$ where the slow variation dominates the solution. We then consider a separate asymptotic expansion for the following Case I: $\lambda \leq 1$ and Case II: $\lambda > 1$ to find an accurate classification of behavior for the full two-dimensional Stommel model.

2.3.1 Case I: $\lambda \leq 1$

We call this the mixed effects case where there is significant influence from both slow variation and fast oscillations due to the size of λ. Under this range for λ, there are two choices for the scaling on η_2, $\beta = 1$ or $\beta = \lambda$. But we are unsure whether there should be integer powers in an asymptotic expansion due to the uncertainty of the scale β. Thus we choose a rather general expansion with

$$\begin{aligned} V(t,R) \sim& \epsilon^\lambda X_0(t,R) + \epsilon^q X_1(t,R) + \dots \\ T(t,R) \sim& \eta_1 + \epsilon^\lambda Y_0(t,R) + \epsilon^q Y_1(t,R) + \dots \end{aligned} \tag{2.61}$$

with $q > \lambda$ to be consist with our analysis thus far. Substituting (2.61) into (2.60) then gives the governing dynamics for this case

$$\begin{aligned} X_{0R} + \epsilon^\lambda X_{0t} + \epsilon^{q-\lambda} X_{1R} \dots =& -\epsilon^\beta n(t) - \epsilon^\lambda(\eta_3 X_0 + (1-\eta_3)Y_0) \\ & - \epsilon^{2\lambda}(X_0 + \epsilon^{q-\lambda}X_1 + \dots)|X_0 + \epsilon^{q-\lambda}X_1 + \dots| \\ & - \epsilon^q(\eta_3 X_1 + (1-\eta_3)Y_1) + A\sin(R) + \dots \end{aligned}$$

$$\begin{aligned} Y_{0R} + \epsilon^\lambda Y_{0t} + \epsilon^{q-\lambda} Y_{1R} + \dots =& -\epsilon^\lambda(\eta_1|X_0 + \epsilon^{q-\lambda}X_1 + \dots| + Y_0 + \epsilon^{q-\lambda}Y_1 + \dots) \\ & + \epsilon^{2\lambda}|X_0 + \epsilon^{q-\lambda}X_1 + \dots|(Y_0 + \epsilon^{q-\lambda}Y_1 + \dots) \\ & + B\sin(R) + \dots \end{aligned}$$

Where we now separate by the distinct orders of ϵ to find the following equations at each order

$$O(1): \begin{cases} X_{0R} = & A\sin(R), \\ Y_{0R} = & B\sin(R), \end{cases} \tag{2.62}$$

$$O(\epsilon^\lambda): \begin{cases} \epsilon^{q-2\lambda}X_{1R} + X_{0t} = & -\epsilon^{\beta-\lambda}n(t) - \eta_3 X_0 - (1-\eta_3)X_0, \\ \epsilon^{q-2\lambda}Y_{1R} + Y_{0t} = & -\eta_1|X_0| - Y_0. \end{cases} \tag{2.63}$$

We learn from (2.63) that $q = 2\lambda$ prevents terms from being unbalanced, which implies that $\lambda > \frac{1}{2}$ for an expansion to be found, otherwise we would need to include the quadratic terms at $O(\epsilon^\lambda)$ and our equations would be too complicated to solve analytically. This q also suggests that there is no need for integer powers in the expansion (2.61) and all behavior is captures by the interaction between the the slow variation and frequency, ϵ^λ. Since there is a choice in the scaling for η_2 where $\beta = \lambda$ or $\beta = 1$ we must choose here to dictate the future of the analysis. The advantage to choosing $\beta = \lambda$ is that these inner equations are rather simple, but the slow variation is still small. On the other hand, $\beta = 1$ keeps a small coefficient on the parameter but makes the slow variation simple. Both of these choices result in the same equations, so here we choose $\beta = 1$ for simplicity. From (2.62) we find the appropriate form of the leading order terms, $X_0 = P_0(t) - A\cos(R)$ and $Y_0 = Q_0(t) - B\cos(R)$. Using these forms for the leading order term and applying the Fredholm alternative (1.24) to (2.63) we find

$$\begin{aligned} P_{0t} = & -\epsilon^{1-\lambda}n(t) - \eta_3 P_0 - (1-\eta_3)Q_0, \\ Q_{0t} = & -\frac{\eta_1}{2\pi}\int_0^{2\pi} |P_0(t) - A\cos(R)|\, dR - Q_0, \\ n_t = & -1. \end{aligned} \tag{2.64}$$

We learned from **??** that we must approach the integration with the relative size of $P_0(t)$ to the amplitude of oscillation A in mind as these sizes determine the difficulty of integration in (2.64). We consider these sizes of $P_0(t)$ as Sub-case I: $P_0(t) \leq -|A|$ and Sub-Case II:$|P_0(t)| < |A|$ much like in section 2.2. These cases keep the integrand from ever crossing the axis or consider the integrand as its allowed to cross the axis respectively.

Sub-Case I: $P_0(t) \leq -|A|$

We call this the below-axis sub-case where the solution $P_0(t)$ is entirely below the axis $V = 0$ and the full solution X_0 has center of oscillations far

from crossing. Under these conditions we don't expect any tipping behavior as the solution is far from the non-smooth behavior, but we may use this to find the range of η_2 that distinguishes these cases. With $P_0(t) \leq -|A|$, we find (2.64) simplifies to

$$\begin{aligned} P_{0t} =& -\epsilon^{1-\lambda} n(t) - \eta_3 P_0 - (1-\eta_3) Q_0, \\ Q_{0t} =& \eta_1 P_0 - Q_0. \end{aligned} \tag{2.65}$$

We have the means available to solve (2.65) as it takes the form of an equation we have seen in section 2.1, but instead we search for when the pseudo-equilibrium fails the assumption of this sub-case. This results in the parameter range between these sub-cases and taking this approach is more convenient than solving the system. Here the form of the pseudo-equilibria is simple to find as $Q_0(P_0) = \eta_1 P_0$ and thus

$$P_0(t) = -\epsilon^{1-\lambda} \frac{n(t)}{\eta_3 + \eta_1(1-\eta_3)}.$$

But we recall that for this sub-case $P_0(t) \leq -|A|$, which gives the range for n and we rewrite this in the original coordinates of η_2 with

$$\begin{aligned} \epsilon n \geq& \epsilon^{\lambda}(\eta_3 + \eta_1(1-\eta_3))|A|, \\ \eta_2 \geq& \eta_1\eta_3 + \frac{(\eta_3 + \eta_1(1-\eta_3))|A|}{\Omega}. \end{aligned} \tag{2.66}$$

With the parameter range (2.66), we now have an effective region for Sub-Case I and know when the crossings of Sub-Case II begin in terms of the parameter η_2.

Sub-Case II: $|P_0(t)| \leq |A|$

We call this the crossing sub-case and under these conditions we see more complexity arise from the integral in (2.64). As the crossings continue, there is an increasing effect on the system and it is here that we anticipate the tipping to occur. In section 1.4, we found a similar integral to (2.64) that we could evaluate with the assumption that $A \sim O(1)$. We have that the assumptions that allowed for the integration to make sense in the one-dimensional model still hold here with a 'fast' time R that is sufficiently large due to the high frequency. We then follow the approach from the one-dimensional model by integrating with $R_1 = \arccos(P_0/A)$ and $R_2 =$

$2\pi - \arccos(P_0/A)$ and then taking a quadratic Taylor approximation to find the system

$$\begin{aligned} P_{0t} =& -\epsilon^{1-\lambda} n(t) - \eta_3 P_0(s) - (1-\eta_3) Q_0 \\ Q_{0t} =& -\frac{2\eta_1 |A|}{\pi} - \frac{\eta_1}{\pi |A|} P_0^2 - Q_0. \end{aligned} \tag{2.67}$$

Where in it's current form (2.67) is known as a quadratic two-dimensional Riccati-type equation which are notoriously difficult to solve analytically. We recall that allowing for the solution to the equation for T to be in terms of V was realistic to the delayed behavior of the THC, so any behavior that we are interested in lies within the dynamics for V, or it's inner counterpart X. For this reason, we choose to reduce the system (2.67) to a one-dimensional model by assuming our equation for Q_0 is in pseudo-equilibrium with

$$Q_0(P_0) = -\frac{2\eta_1 |A|}{\pi} - \frac{\eta_1}{\pi |A|} P_0^2. \tag{2.68}$$

The resulting reduced one-dimensional system from introducing the equilibrium (2.68) into the leading order inner equation (2.67) is then

$$\begin{aligned} P_{0t} =& -\epsilon^{1-\lambda} n(t) + \frac{2\eta_1 (1-\eta_3)|A|}{\pi} - \eta_3 P_0 + \frac{\eta_1}{\pi |A|} P_0^2, \\ n_t =& -1. \end{aligned} \tag{2.69}$$

To relate the slow variation directly to the solution of (2.69), we swap the differentiation to be with respect to the parameter giving

$$P_{0n} = \epsilon^{1-\lambda} n - \frac{2\eta_1 (1-\eta_3)|A|}{\pi} + \eta_3 P_0 - \frac{\eta_1 (1-\eta_3)}{\pi |A|} P_0^2. \tag{2.70}$$

Now (2.70) is in a form that the result from Zhu & Kuske (4) has the ability to solve. Thus we determine that (2.70) is an Airy-type equation and that it's tipping follows with (4). We promptly write this into original coordinates and notice the relationship to tipping and bifurcating values we've found in previous sections with

$$\begin{aligned} n_{\text{tip}} =& -\epsilon^{(\lambda-1)/3} \left(\frac{\pi |A|}{\eta_1 (1-\eta_3)} \right)^{1/3} (2.33810) + \epsilon^{\lambda-1} \frac{\eta_1 (1-\eta_3)|A|}{\pi} \left(2 - \left(\frac{\pi \eta_3}{2\eta_1 (1-\eta_3)} \right)^2 \right), \\ \eta_{2\text{tip}} =& \epsilon^{(\lambda-1)/3} \left(\frac{\pi |A|}{\eta_1 (1-\eta_3)} \right)^{1/3} \mu_{\text{Airy}} + \eta_{2\text{osc}} \end{aligned} \tag{2.71}$$

We conclude that our tipping in (2.71) follows closely to the tipping found with (1.66) in section 1.4 where we found a weighted average between the smooth tipping and the oscillatory bifurcation for this range of λ. We also discovered along the way that any $\lambda \leq \frac{1}{2}$ causes fundamentally different inner equations which lead to unsolvable and incoherent asymptotics under this approach. This heuristically makes sense as for $\lambda \leq \frac{1}{2}$ we have low frequency oscillations with our polynomial relationship and the contributions to the dynamics from this behavior require a different approach than presented in this paper. For more, see Zhu & Kuske [**?**] for an example of a low-frequency method.

2.3.2 Case II: $\lambda > 1$

We call this case the slow dominate case; here we expect integer powers of ϵ to appear due to the $O(\epsilon^\lambda)$ being quite small for this range of λ and thus we choose the expansion

$$\begin{aligned} V(t,R) \sim& \epsilon X_0(t,R) + \epsilon^\lambda X_1(t,R) + \epsilon^q X_2(t,R) + \dots \\ T(t,R) \sim& \epsilon Y_0(s,R) + \epsilon^\lambda Y_1(t,R) + \epsilon^q Y_2(t,R) + \dots \end{aligned} \tag{2.72}$$

Substituting (2.72) into (2.60) then gives the full dynamics of this system with their respective orders of ϵ

$$\begin{aligned} \epsilon X_{0R} + \epsilon^{\lambda+1} X_{0t} + \epsilon^\lambda X_{1R} + \dots = & -\epsilon^{\lambda+\beta} n(t) - \epsilon^{\lambda+1}(\eta_3 X_0 + (1-\eta_3) Y_0) \\ & - \epsilon^{\lambda+2}(X_0 + \epsilon^{q-\lambda} X_1 + \dots)|X_0 + \epsilon^{q-\lambda} X_1 + \dots| \\ & - \epsilon^{2\lambda}(\eta_3 X_1 + (1-\eta_3) Y_1) + \epsilon^\lambda A \sin(R), \end{aligned}$$

$$\begin{aligned} \epsilon Y_{0R} + \epsilon^{\lambda+1} Y_{0t} + \epsilon^\lambda Y_{1R} + \dots = & -\epsilon^{\lambda+1}(\eta_1 |X_0 + \epsilon^{\lambda-1} X_1 + \epsilon^{q-1} X_2 + \dots| - Y_0 - \epsilon^{\lambda-1} Y_1 + \dots) \\ & + \epsilon^2 |X_0 + \epsilon^{\lambda-1} X_1 + \epsilon^{q-1} X_2 + \dots|(Y_0 + \epsilon^{\lambda-1} Y_1 + \dots) \\ & + \epsilon^\lambda B \sin(R). \end{aligned}$$

Where we separate by each distinct order of ϵ to find the following equations at each order

$$O(\epsilon): \begin{cases} X_{0R} = & 0, \\ Y_{0R} = & 0, \end{cases} \tag{2.73}$$

$$O(\epsilon^{\lambda}): \begin{cases} X_{1R} = & A\sin(R), \\ Y_{1R} = & B\sin(R), \end{cases} \tag{2.74}$$

$$O(\epsilon^{\lambda+1}): \begin{cases} \epsilon^{q-\lambda-1}X_{2R} + X_{0t} = & -\epsilon^{\beta-1}n(t) - \eta_3 X_0 - (1-\eta_3)Y_0, \\ \epsilon^{q-\lambda-1}Y_{2R} + Y_{0t} = & -\eta_1|\epsilon^{\lambda}|X_0 + \epsilon^{\lambda-1}X_1| - Y_0, \end{cases} \tag{2.75}$$

We learn in (2.75) that $q = \lambda + 1$ prevents terms from becoming trivial or unbalanced and thus we choose this. We also find $\beta = 1$ that prevents triviality contrary to Case I where we chose the value of β for convenience. In (2.73) we find that the leading order behavior for this case is purely slow, $X_0 = X_0(t)$ and $Y_0 = Y_0(t)$, thus giving the slow domination of this case. We are able to extract the oscillatory forcing into X_1 and Y_1 with (2.74) and since the slow behavior in X_1 and Y_1 are just next order corrections to the purely slow X_0 and Y_0, without loss of generality we allow the slow behavior to be expressed by X_0 and Y_0; thus we have purely oscillatory corrections, $X_1 = -A\cos(R)$ and $Y_1 = -B\cos(R)$. Applying Fredholm (1.24) to (2.75) then gives

$$\begin{aligned} X_{0t} =& -n(t) - \eta_3 X_0 - (1-\eta_3)Y_0, \\ Y_{0t} =& -\frac{\eta_1}{2\pi}\int_0^{2\pi} |X_0(t) - \epsilon^{\lambda-1}A\cos(R)|\, dR - Y_0, \\ n_t =& -1. \end{aligned} \tag{2.76}$$

From Case I, we used the pseudo-equilibrium of Q_0 for an integral of this type regardless of the size of the oscillations to find a solvable equation. Here we expect (2.76) to have some kind of quadratic form like in Case I, so we choose a priori to reduce this into a one-dimensional problem by assuming the equation for Y_0 is in it's pseudo-equilibrium with

$$Y_0(X_0) = -\frac{\eta_1}{2\pi}\int_0^{2\pi} |X_0 - \epsilon^{\lambda-1}A\cos(R)|\, dR. \tag{2.77}$$

We find the resulting reduced one-dimensional equation by introducing (2.77) into the full inner equation (2.76) with

$$X_{0t} = -n(t) - \eta_3 X_0 + \frac{\eta_1(1-\eta_3)}{2\pi}\int_0^{2\pi} |X_0(t) - \epsilon^{\lambda-1}A\cos(R)|\, dR. \tag{2.78}$$

Where in (2.78) the behavior is very similar to Case I as long as the amplitude of oscillations inside the integral are still manageable with our assumptions from that case (i.e $\epsilon^{\lambda-1}A \sim O(1)$). This indicates that $\lambda \approx 1$ to see mixed behavior of Case I and to see this similarity, we once more follow the method of section 1.4. Our assumption on the size of the oscillations allow us to integrate (2.78) with $R_1 = \arccos\big(x_0/\epsilon^{\lambda-1}A\big)$ and $R_2 = 2\pi - \arccos\big(x_0/\epsilon^{\lambda-1}A\big)$. Another application of a quadratic Taylor approximation then yields

$$X_{0t} = -n(t) + \epsilon^{\lambda-1}\frac{2\eta_1(1-\eta_3)|A|}{\pi} - \eta_3 X_0 + \epsilon^{1-\lambda}\frac{\eta_1(1-\eta_3)}{\pi|A|}X_0^2. \tag{2.79}$$

Where we again find a form that we apply the result from Zhu & Kuske in (4) to. Thus we find the tipping for the scaled parameter n and then transform back into the original coordinates for tipping in η_2 with

$$\begin{aligned} n_{\text{mixed}} =& -\epsilon^{(\lambda-1)/3}\left(\frac{\pi|A|}{\eta_1(1-\eta_3)}\right)^{1/3}(2.33810) + \epsilon^{\lambda-1}\frac{\eta_1(1-\eta_3)|A|}{\pi}\left(2-\left(\frac{\pi\eta_3}{2\eta_1(1-\eta_3)}\right)^2\right), \\ \eta_{2\text{mixed}} =& \epsilon^{(\lambda-1)/3}\left(\frac{\pi|A|}{\eta_1(1-\eta_3)}\right)^{1/3}\mu_{\text{smooth}} + \eta_{2\text{osc}}. \end{aligned} \tag{2.80}$$

On the other hand, when λ becomes large, these oscillations become more insignificant, and inside the integral in (2.59) their contribution gets weaker. For sufficiently large λ, here these values range from approximately $2 \le \lambda \le 4$ depending on other model parameters, (2.76) begins to act like

$$\begin{aligned} X_{0t} =& -n(t) - \eta_3 X_0 - (1-\eta_3)Y_0, \\ Y_{0t} =& -\eta_3|X_0| - Y_0, \\ n_t =& -1. \end{aligned} \tag{2.81}$$

Where (2.81) is the same system as the purely slow model in section 2.1. Since this is the same inner behavior and we still have slow variation, we are able to use the approximation found there for the tipping (2.19). This indicates that the oscillations decay to a point where only the slow variation effects the tipping of the Stommel model.

With both Case I and Case II, we have the tipping behavior for any choice in λ. For $\lambda \le 1$, we found similar averaging between the oscillatory bifurcation and the smooth tipping as in section 1.4. This behavior continued even past $\lambda = 1$ but the oscillatory contribution begins to contribute less to the over

all tipping. Once λ was sufficiently large, the oscillations all but die off in their contribution and we recover the purely slow tipping. This gives us an effective description of the tipping for the most general version of the Stommel model and we recap this in the following table.

Two-Dimensional Tipping	
Slow:	$\eta_{2\text{slow}} = \min(\eta_1\eta_3 - \epsilon\log(\epsilon)/\lambda_i)$ for $i \in \{1,2\}$
High Freq. Osc:	$\eta_{2\text{osc}} = \eta_1\eta_3 + \frac{\eta_1(1-\eta_3)\lvert A\rvert}{\pi\Omega}\left(2 - \left(\frac{\pi\eta_3}{2\eta_1(1-\eta_3)}\right)^2\right)$
Slowly Oscillatory $\lambda \leq 1$:	$\eta_{2\text{mixed}} = \epsilon^{(\lambda-1)/3}\left(\frac{\pi\lvert A\rvert}{\eta_1(1-\eta_3)}\right)^{1/3}\mu_{\text{smooth}} + \eta_{2\text{osc}}$
Slowly Oscillatory $\lambda > 1$ and $\lambda \approx 1$:	$\eta_{2\text{mixed}} = \epsilon^{(\lambda-1)/3}\left(\frac{\pi\lvert A\rvert}{\eta_1(1-\eta_3)}\right)^{1/3}\mu_{\text{smooth}} + \eta_{2\text{osc}}$
Slowly Oscillatory $\lambda > 1$:	$\eta_{2\text{slow}} = \min(\eta_1\eta_3 - \epsilon\log(\epsilon)/\lambda_i)$ for $i \in \{1,2\}$

Table 2.1: The tipping of the two-dimensional model for each mechanism and case.

In figure 2.8, we see an example of the numerical solution of V to the canonical system (2.1) with slow variation and oscillatory forcing. This example has tipping occurring in Case I due to $\lambda \in (\frac{1}{2}, 1]$ producing a mixed effect from both the slow variation and oscillations on the tipping. The vertical lines are the tipping, black solid for the numerical and blue dotted for the approximation for this case (2.71). Although there is a mixture of effects, the tipping still is occurring in the region near the oscillatory bifurcation. This tells us that for these choices in the model parameters that the strongest effect is the oscillatory forcing. This also is shown in figure (2.9) which has the numerical solution of T plotted against V. Here we see that due to the early tipping in V, the solution for T also never achieves it's maximum and there is early tipping here as well, which agrees with the assumptions we had made of considering T responding to V. We also see that there are areas of the stable branch that is skipped over from the early tipping, and even the oscillations cross the unstable branch frequently near the tipping, which is consistent with the crossing behavior in the numerical solution for V.

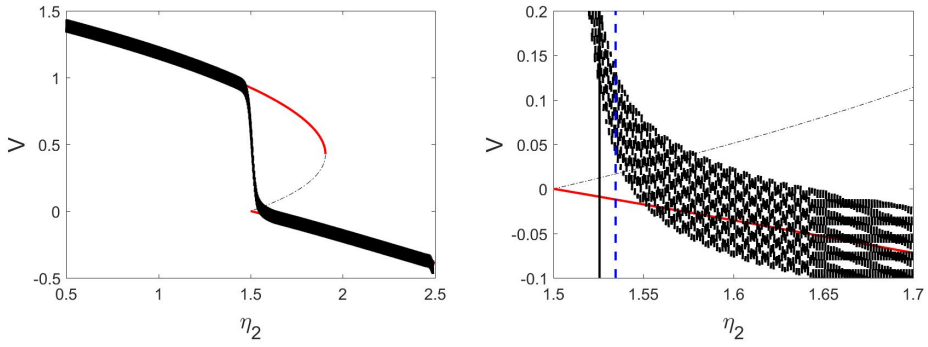

(a) (b)

Figure 2.8: Model values are $\lambda = .8$, $\epsilon = .01$ with $A = B = 2$. In (a) the numerical solution (black dotted line) to (2.1) is given with $\eta_1 = 4$, $\eta_3 = .375$. In (b) a zoom in closer to the non-smooth bifurcation region where the blue vertical line is the tipping prediction against the black dotted vertical line which is the numerical bifurcation.

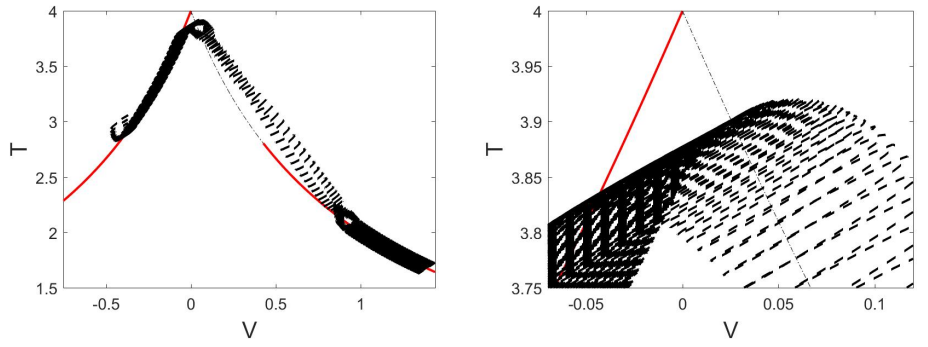

(a) (b)

Figure 2.9: Model values are $\lambda = .8$, $\epsilon = .01$ with $A = B = 2$. In (a) we have the numerical solution (black dotted) over the standard equilibrium plot for V vs. T. In (b) a zoom of the bifurcation area.

In figure 2.10 we have chosen a value of λ that causes the tipping to fall into Case II as $\lambda > 1$ but this choice is close to the boundary and thus we see comparable behavior to Case I with the addition that the slow variation is now dominant as in section 2.1. Upon a zoom in, it is apparent that oscillations are still present and this is where we see the mixture of effects

that cause a similar tipping to take place. We've plotted the purely slow tipping as the green vertical dotted line for comparison. As the tipping occurs near the purely slow tipping this confirms that the slow variation is indeed dominating the tipping. In figure 2.11 we again see very similar behavior to the purely slow model in section 2.1 but the zoom in further reveals the oscillations are present and have minor influence by forcing the solution to cross the unstable branch near the tipping.

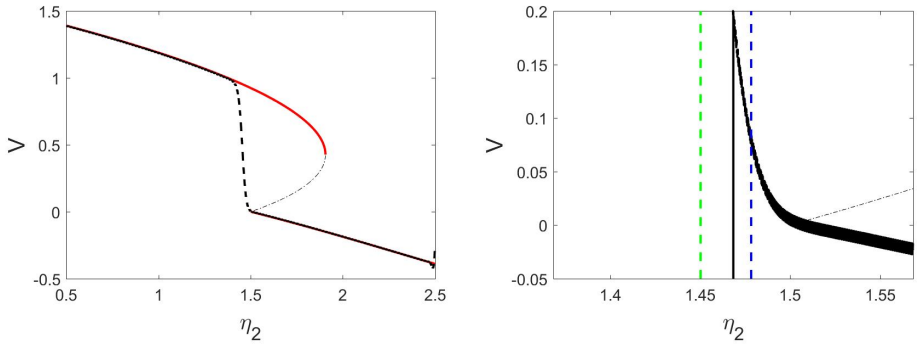

(a) (b)

Figure 2.10: Model values are $\lambda = 1.3$, $\epsilon = .01$ with $A = B = 2$. In (a) the numerical solution (black dotted line) to (2.1) is given with $\eta_1 = 4$ and $\eta_3 = .375$. In (b) a zoom in closer to the non-smooth bifurcation region where the blue dotted vertical line is the prediction against the black solid vertical line which is the numerical bifurcation.

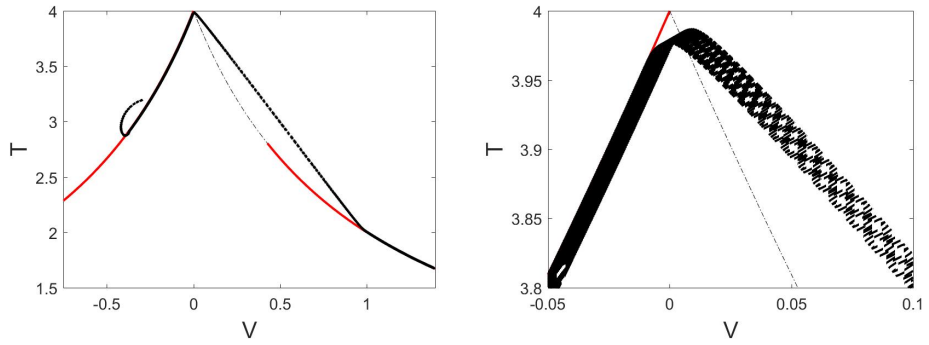

(a) (b)

Figure 2.11: Model values are $\lambda = 1.3$, $\epsilon = .01$ with $A = B = 2$. In (a) we have the numerical solution (black dotted) over the standard equilibrium plot for V vs. T. In (b) a zoom of the bifurcation area.

In figure 2.12 we see the numerics for a λ that is large enough to force the problem to behave like the purely slow model like in section 2.1. Even upon a zoom it is almost impossible to notice that oscillations are occurring in this solution. The green dotted vertical line is our purely slow tipping estimate (2.19) where the blue dotted is the same mixed approximation (2.71). Further evidence is seen in figure 2.13 where this compares very similar to (2.2).

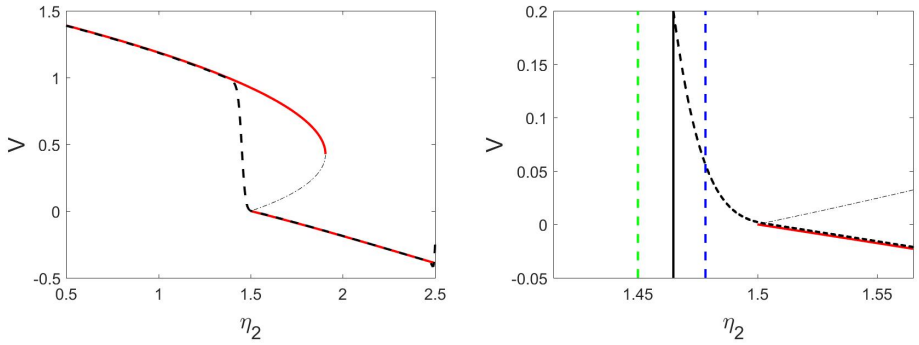

(a) (b)

Figure 2.12: Model values are $\lambda = 2$, $\epsilon = .01$ with $A = B = 2$. In (a) the numerical solution (black dotted line) to (2.1) is given with $\eta_1 = 4$ and $\eta_3 = .375$. In (b) a zoom in closer to the non-smooth bifurcation region where the blue vertical line is the prediction against the black dotted vertical line which is the numerical bifurcation.

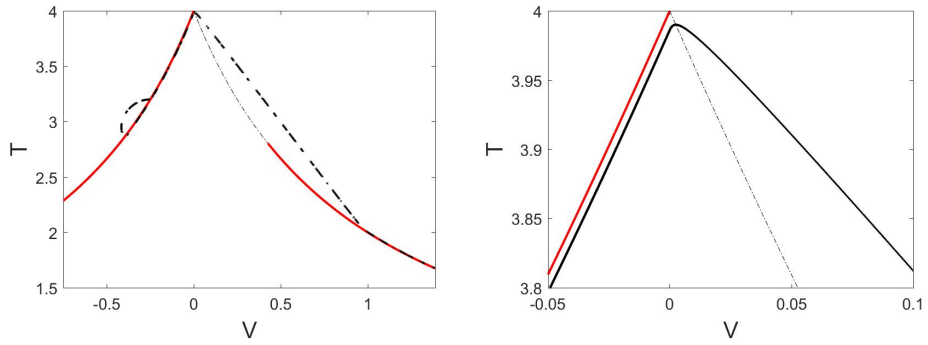

(a) (b)

Figure 2.13: Model values are $\lambda = 2$, $\epsilon = .01$ with $A = B = 2$. In (a) we have the numerical solution (black dotted) over the standard equilibrium plot for V vs. T. In (b) a zoom of the bifurcation area.

Although the figures above show that we have classified the behavior appropriately for the various cases in λ and relative solution sized, performance of our approximate tipping needs to be evaluated to verify our analysis had good results. In figure 2.14 we compare the tipping between Case I and Case II with the numerical tipping across λ with a fixed ϵ. For smaller λ,

the frequency Ω gets smaller and the Case I tipping becomes more predominant. But for the analysis performed in this section, $\Omega \gg 1$ and for $\lambda < \frac{1}{2}$ we have $\Omega \sim O(1)$. We will not consider low frequency corresponding to $\lambda < \frac{1}{2}$ in this section. The larger λ becomes, the less effect we see from the oscillatory forcing until it is negligible for some $\lambda > 1$. We notice that our one-dimensional reduction tipping approximation, there is some bias due to this being a reduced approach, there is likely a slightly bigger coefficient and this becomes apparent for $\lambda > 1$. Although we use a one-dimensional reduced equation to get these approximations, they seem to be performing quite well across all λ hence validating the method developed for tipping with varying λ.

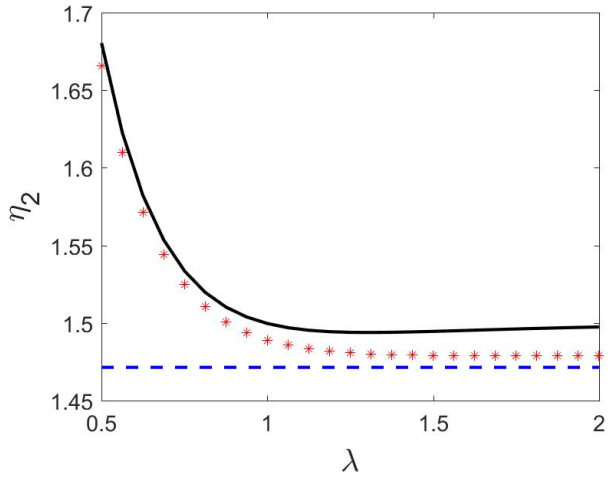

Figure 2.14: An example of numerical tipping (red stars) as the numerical solution to (1.1) passes $x = .2$ for the last time. Parameter values are $\epsilon = .01$ and $A = 1$. The lines are the Case I tipping estimate (black solid line) and the Case II tipping estimate (blue dotted line).

We also are interested in the performance of the tipping approximations across values of ϵ while leaving λ fixed. The performance of each estimate is seen in figure 2.15. For Case I tipping, the range of appropriate ϵ is highly dependent on the choice in λ. Often, the range is very small to get accurate estimates. Once this range is left, there are interesting phase effects for the tipping which causes oscillations in the numeric tipping points. For Case II tipping, we that there is a transition happening towards the purely slow tipping, similarly to section 2.1

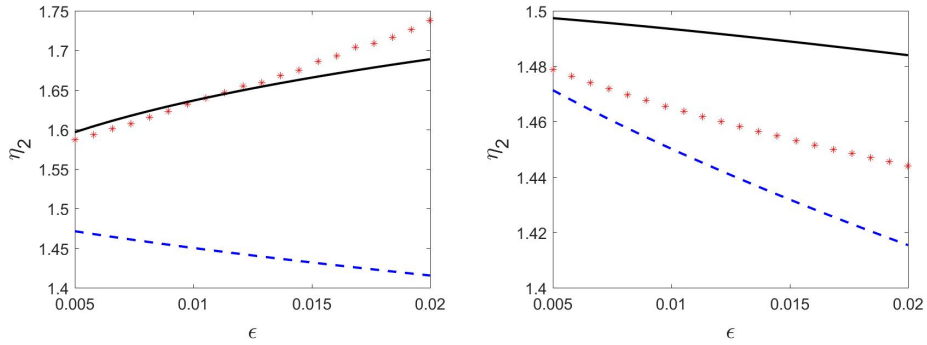

(a) $\lambda = .8$ (b) $\lambda = 1.3$

Figure 2.15: The numerical tipping (red stars) follows the appropriate case depending on λ for $\epsilon = 0.005$. The Case I tipping estimate (black solid line) and purely slow tipping estimate (blue dotted line) are shown.

With the numerical results agreeing with our results, we may finally conclude that this method is both useful for analyzing the non-smooth behavior in the Stommel model but also results in an approximation that is more accurate in the extremes of the model (i.e $\Omega \gg 1$ or $\epsilon \ll 1$). This gives us a very accessible means of extracting the tipping in the full two-dimensional without needing to solve difficult Riccati equations or other complex systems that appear from the full problem. All that is needed to verify is our solutions remain stable until we arrive at the region of tipping.

2.3.3 Stability

Case I: $\lambda \leq 1$

From the analysis, we had discovered the inner equations that govern the behavior of the solution for this range of λ are

$$\begin{aligned} P_{0t} &= -\epsilon^{1-\lambda} n(t) - \eta_2 P_0 - (1-\eta_3) Q_0, \\ Q_{0t} &= -\frac{\eta_1}{2\pi} \int_0^{2\pi} |P_0 - A\cos(R)|\, dR - Q_0. \end{aligned} \tag{2.82}$$

But we also found that the relative size of $P_0(t)$ dictates the difficulty of (2.82). In the analysis we treat these as Sub-Case I: $P_0(t) \leq -|A|$ and Sub-Case II: $|P_0(t)| < |A|$ which each require a separate analysis due to their differing behavior.

Sub-Case I: $P_0(t) \leq -|A|$

We called this the entirely below-axis sub-case due to the solution remaining below the axis and hence predictable under these conditions thus we anticipate this sub-case to remain stable. The equation (2.82) simplifies for this sub-case to

$$\begin{aligned} P_{0t} =& -\epsilon^{1-\lambda} n(t) - \eta_2 P_0 - (1-\eta_3) Q_0, \\ Q_{0t} =& \eta_1 P_0 - Q_0. \end{aligned} \tag{2.83}$$

Which from the analysis we choose to reduce (2.83) with the pseudo-equilibria $Q_0(P_0) = \eta_1 P_0$. This gives the following one-dimensional equation with it's pseudo-equilibria as

$$\begin{aligned} P_{0t} =& -\epsilon^{1-\lambda} n(t) - (\eta_3 + \eta_1(1-\eta_3)) P_0 = f(t, P_0), \\ Z^0(t) =& -\epsilon^{1-\lambda} \frac{n(t)}{\eta_3 + \eta_1(1-\eta_3)}. \end{aligned} \tag{2.84}$$

We adopt a similar strategy for analyzing the stability from the one-dimensional model in section 1.4 due to (2.84) being a one-dimensional equation. Hence we take a simple linear perturbation about the pseudo-equilibrium with $P_0(t) = Z^0(t) + U(t)$ and $\|U(t)\| \ll 1$. Taking special care to note that $Z^0(t)$ also varies in time, we find the Taylor approximation

$$\begin{aligned} P_{0t} =& f(t, Z^0) + f_{P_0}(t, Z^0)(P_0(t) - Z^0(t)) + O(\|(P_0(t) - Z^0(t))^2\|^2), \\ U_t + Z_t^0 =& -(\eta_3 + \eta_1(1-\eta_3)) U, \\ U_t =& -\epsilon^{1-\lambda} \frac{1}{\eta_3 + \eta_1(1-\eta_3)} - (\eta_3 + \eta_1(1-\eta_3)) U. \end{aligned} \tag{2.85}$$

With (2.85) we find that the perturbations decay exponentially to a nearby equilibrium. This indicates the solution for this sub-case is hyperbolically stable and further agrees that no tipping will happen for this size of the solution.

Sub-Case II: $|P_0(t)| < -|A|$

We called this the crossing case and from the analysis we anticipate the tipping to occur as the solution is gradually becoming uncontrollable with the crossing. Under the conditions of this sub-case, we integrate (2.82) with

the R_1 and R_2 from the analysis and take the same Taylor approximation to find

$$\begin{aligned} P_{0t} =& - n(t) - \eta_3 P_0 - (1-\eta_3)Q_0, \\ Q_{0t} =& - \epsilon^{\lambda-1}\frac{2\eta_1|A|}{\pi} - \epsilon^{1-\lambda}\frac{\eta_1(1-\eta_3)}{\pi|A|}P_0^2 - Q_0. \end{aligned} \tag{2.86}$$

Once more, we assume that the equation for Q_0 is in pseudo-equilibrium to reduce to the following one-dimensional inner equation with equilibrium where here we let $a = \frac{\eta_1(1-\eta_3)}{\pi|A|}$ for simplicity

$$\begin{aligned} P_{0t} =& - \epsilon^{1-\lambda}n(t) + \frac{2\eta_1(1-\eta_3)|A|}{\pi} - \eta_3 P_0 + aP_0^2 = f(t, P_0), \\ Z^0(t) =& \frac{1}{2a}\left(\eta_3 - \sqrt{4a(\epsilon^{1-\lambda}n(t) - n_{\text{osc}})}\right). \end{aligned} \tag{2.87}$$

Where we choose to write the argument of the square root in terms of the bifurcation found in (2.42). We then consider the linear perturbation about the pseudo-equilibrium $P_0(t) = Z^0(t) + U(t)$ with $\|U\| \ll 1$. We take a Taylor expansion here to find the dynamics of the perturbation, but recall that we have contributions to the derivative from both the perturbation as well as the pseudo-equilibrium. This is seen with

$$\begin{aligned} P_{0t} =& Z_t^0 + U_t, \\ Z_t^0 =& \begin{cases} \frac{\epsilon^{1-\lambda}}{\sqrt{4a(\epsilon^{1-\lambda}n(t) - n_{\text{osc}})}} & \epsilon^{1-\lambda}n(t) > n_{\text{osc}}, \\ 0 & \epsilon^{1-\lambda}n(t) = n_{\text{osc}}. \end{cases} \end{aligned} \tag{2.88}$$

Thus we find the following Taylor expansion for the perturbations

$$\begin{aligned} P_{0t} =& f(t, Z^0) + f_{P_0}(t, Z^0)(P_0 - Z^0) + O(\|P_0 - Z^0\|^2), \\ U_t + Z_t^0 =& - \sqrt{4a(\epsilon^{1-\lambda}n(t) - n_{\text{osc}})}U, \\ U_t =& \begin{cases} \frac{\epsilon^{1-\lambda}}{\sqrt{4a(\epsilon^{1-\lambda}n(t) - n_{\text{osc}})}} - \left(\sqrt{4a(\epsilon^{1-\lambda}n(t) - n_{\text{osc}})}\right)U & \epsilon^{1-\lambda}n(t) > n_{\text{osc}}, \\ 0 & \epsilon^{1-\lambda}n(t) = n_{\text{osc}}. \end{cases} \end{aligned} \tag{2.89}$$

From (2.89) we find exponentially decaying perturbations that give asymptotic stability until we get to the oscillatory bifurcation. The oscillatory bifurcation corresponds to non-hyperbolic behavior and we lose stability shortly after which indicates of the tipping to occur after the bifurcation.

Case II: $\lambda > 1$

From the analysis we determined this to be the slowly dominant case and we had discovered the inner equations that govern the behavior of the solution for this range of λ to be

$$\begin{aligned} P_{0t} =& - n(t) - \eta_2 P_0 - (1-\eta_3)Q_0, \\ Q_{0t} =& - \frac{\eta_1}{2\pi}\int_0^{2\pi} |P_0 - \epsilon^{\lambda-1} A\cos(R)|\, dR - Q_0. \end{aligned} \tag{2.90}$$

The behavior of this case when $\lambda \sim 1$ is very similar to Case I, thus we anticipate the stability to behave similarly as well. Hence we consider the behavior when $|P_0(t)| < \epsilon^{\lambda-1}|A|$ which is where we found tipping to occur in the analysis. As long as we have $\epsilon^{\lambda-1}A \sim O(1)$, we are follow the same approach as Case I where we integrate (2.90) with a similar R_1 and R_2 and use a Taylor approximation to get

$$\begin{aligned} P_{0t} =& - n(t) - \eta_2 P_0 - (1-\eta_3)Q_0, \\ Q_{0t} =& - \epsilon^{\lambda-1}\frac{2\eta_1(1-\eta_3)|A|}{\pi} - \epsilon^{1-\lambda}\frac{\eta_1}{\pi|A|}P_0^2 - Q_0. \end{aligned}$$

The analysis gave sufficient reason to reduce the inner equations to a one-dimensional model and thus like in Case I w find the inner equation with pseudo-equilibrium where here we let $a = \frac{\eta_1(1-\eta_3)}{\pi|A|}$ for simplicity

$$\begin{aligned} P_{0t} =& - n(t) + \epsilon^{\lambda-1}\frac{2\eta_1(1-\eta_3)|A|}{\pi} - \eta_3 P_0 + \epsilon^{1-\lambda} a P_0^2, \\ Z^0(t) =& \frac{1}{2a}\left(\epsilon^{\lambda-1}\eta_3 - \sqrt{\epsilon^{\lambda-1}4a(n(t) - \epsilon^{\lambda-1}n_{\text{osc}})}\right) \end{aligned}$$

Where we consider the linear perturbation about the pseudo-equilibrium $P_0(t) = Z^0(t)_U(t)$ with $\|U\| \ll 1$. We take a Taylor expansion here to find the dynamics of the perturbation, but recall that we have contributions to the derivative from both the perturbation as well as the pseudo-equilibrium. This is seen with

$$\begin{aligned} P_{0t} =& Z_t^0 + U_t, \\ Z_t^0 =& \begin{cases} \frac{\epsilon^{(\lambda-1)/2}}{\sqrt{4a(n(t)-\epsilon^{\lambda-1}n_{\text{osc}})}} & n(t) > \epsilon^{\lambda-1}n_{\text{osc}}, \\ 0 & n(t) = \epsilon^{\lambda-1}n_{\text{osc}}. \end{cases} \end{aligned} \tag{2.91}$$

Thus we find the following Taylor expansion for the perturbations

$$\begin{aligned} P_{0t} =& f(t, Z^0) + f_{P_0}(t, Z^0)(P_0 - Z^0) + O(\|P_0 - Z^0\|^2), \\ U_t + Z_t^0 =& -\left(\sqrt{\epsilon^{1-\lambda} 4a(n(t) - \epsilon^{\lambda-1} n_{\text{osc}})}\right) U, \\ U_t =& \begin{cases} \frac{\epsilon^{(\lambda-1)/2}}{\sqrt{4a(n(t) - \epsilon^{\lambda-1} n_{\text{osc}})}} - \left(\sqrt{\epsilon^{1-\lambda} 4a(n(t) - n_{\text{osc}})}\right) U & n(t) > \epsilon^{\lambda-1} n_{\text{osc}}, \\ 0 & n(t) = \epsilon^{\lambda-1} n_{\text{osc}}. \end{cases} \end{aligned} \tag{2.92}$$

From (2.92) we find that the perturbations decay exponentially and we have asymptotic stability until we get to the oscillatory bifurcation. The bifurcation found in (2.42) corresponds to non-hyperbolic behavior and we then lose the stability which indicates of the tipping to occur after the bifurcation. Comparing this to Case I, we see there is small nuances between these perturbations, although the overall stability remains the same. As for when λ grows, we already established this behaves like the purely slow model and hence we can use the stability from that section to conclude that our solution is still stable until the slow tipping point, at which we lose stability as anticipated.

Thus the stability for both Case I and Case II agrees with the results found in the analysis. We have that the behavior of the solution is stable from the outer solution, stability holds before the solution begins to cross the axis $V = 0$ and once the crossing begins to happen we lose stability at the location of the oscillatory bifurcation. Because there is slow variation in this model, there is still delayed behavior and thus the tipping happens shorty after the oscillatory bifurcation. In both cases we discovered that the pseudo-equilibrium has a contribution to the derivative and this in turn causes the perturbations to decay towards a small constant. This means that there is a small region around the pseudo-equilibrium that attracts the solution and this is seen in the numerical results.

Chapter 3

Summary and Future Work

With the results found in this paper, we have accurately described what kind of behavior is present about the non-smooth bifurcation when new mechanisms are introduced in both the one-dimensional model (1.1) and two-dimensional Stommel model (2.1). We had considered the mixture of early bifurcation due to high oscillatory forcing $\Omega \gg 1$ with amplitude $A \sim O(1)$ and the delayed tipping due to slow variation in the bifurcating parameter at rate ϵ where $\epsilon \ll 1$. The main result being that these mechanisms have opposite effects on the tipping/bifurcation and do mix with a kind of weighted average to produce an effective tipping approximation. These results give insight into the hysteresis behavior of the Stommel model and the understudied realm of non-smooth dynamics. The work presented here used asymptotic expansions as well as the methods of multiple scales to identify reduced equations and find asymptotic solutions to the systems of differential equations. We found that depending on the region and mechanism, the reduced equations have differing expressions depending on the size of the solution. We also discover that linking the slow variation ϵ and the frequency Ω gives important insight into how the system will behave.

The method developed in the one-dimensional model was to form an outer asymptotic expansion by separating the order of dynamics by a common small value, typically in terms of ϵ. With the outer dynamics found, we scaled the model to find the inner equations to typically be a simpler problem. From the inner equations, we solve and determine when the solution is no longer controllable. This results in the tipping/bifurcations in the one-dimensional system (1.1) which had good agreement with the numerical results from a simple differential equation solver. Due to the many similarities to the two-dimensional system (2.1) we were able to modify the same analysis to find the tipping/bifurcations here as well.

Although the work here is not entirely finished as an analysis would need to be done on cases where $\Omega \sim O(1)$ or smaller. This mechanism functions qualitatively different as slow oscillations have more contribution to the dynamics. This is also seen from the analysis where low frequency oscillations no longer allow for asymptotic expansions in terms of Ω^{-1} and no longer

fall under our assumptions to integrate with T_1 and T_2. Thus this case behaves fundamentally different and can influence tipping in a way we hadn't explored here. Also, large amplitude behavior $A \gg 1$ can force an additional rescaling before any familiar approaches hold. In figure **??** we show an example of these mechanisms which shows their different influence on the system. These cases were mentioned but have yet to be performed on this model, although both have been studied around the smooth case in [**?**]. It is possible that they could have some surprising results in the non-smooth case. These cases would help further classify the tipping behavior for the variety of cases in real world ocean dynamics.

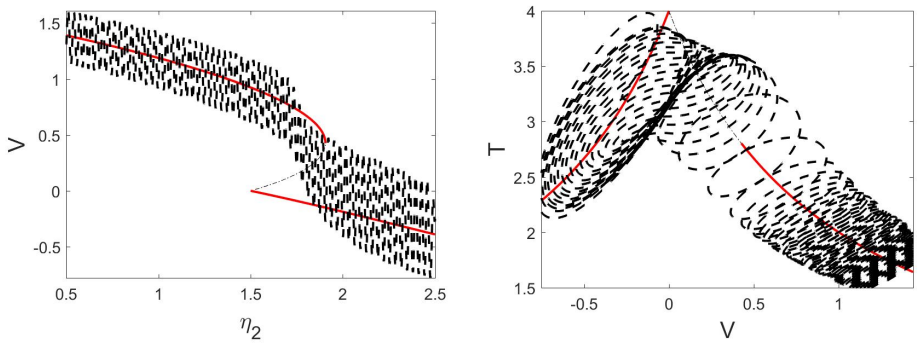

(a) (b)

Figure 3.1: Model parameters are $\epsilon = .01$ and $\Omega = 3$.

Appendix A

One-Dimensional

High Frequency Oscillatory Forcing

Here we continue the analysis to explicitly find the solution to the outer equation for the purely oscillatory model. Recall we found $x_1 = v_1(t) - A\cos(T)$, we then apply the Fredholm alternative (1.24) to the $O(\Omega^{-2})$ equation in (1.23) to get

$$\begin{aligned} 0 =& \frac{1}{2\pi}\int_0^{2\pi} -x_{1t} - 2x_1 + 2x_0x_1\, dT, \\ v_{1t} =& -2v_1 + 2(1-\sqrt{1+\mu})v_1, \\ v_{1t} =& -2\sqrt{1+\mu}v_1 \end{aligned} \tag{A.1}$$

We search for the equilibrium to find stable behavior on this order but since (A.1) has a very simple form, the equilibrium is $v_1(t) \equiv 0$ and thus we find the correction term to only have oscillatory behavior, $x_1 = -A\cos(T)$.

Slow Variation and Oscillatory Forcing

Here we continue to find the terms of the outer solution for the slow varying and oscillatory forcing model. We have thus far found $x_0 = x_0(\tau)$ and we have equations at $O(\epsilon^{\lambda})$ and $O(\epsilon^{2\lambda})$ that give information about x_0 and x_1 respectively. From the $O(\epsilon^{\lambda})$ equation (1.49), we apply the Fredholm alternative (1.24) to find

$$\begin{aligned} 0 =& \frac{1}{2\pi}\int_0^{2\pi} -\mu(\tau) - 2x_0(\tau) + x_0(\tau)^2 + A\sin(T)\, dT, \\ 0 =& -\mu(\tau) - 2x_0(\tau) + x_0(\tau)^2, \\ x_0(\tau) =& 1 - \sqrt{1+\mu(\tau)}, \\ x_{1T} =& A\sin(T) \end{aligned} \tag{A.2}$$

From (A.2) we find that $x_1 = v_1(\tau) - A\cos(T)$, which gives us access to solving the next order equation. Thus we now do the same for the $O(\epsilon^{2\lambda})$

equation (1.50) to find

$$\begin{aligned} 0 =& \frac{1}{2\pi}\int_0^{2\pi} -\epsilon^{1-\lambda}x_{0\tau} - 2x_1 + 2x_0x_1\, dT, \\ \epsilon^{1-\lambda}x_{0\tau} =& -2v_1 + 2(1-\sqrt{1+\mu(\tau)})v_1, \\ v_1(\tau) =& -\epsilon^{1-\lambda}\frac{x_{0\tau}}{2\sqrt{1+\mu(\tau)}}. \end{aligned} \tag{A.3}$$

Where we recall that $\mu_\tau = -1$ and that $x_{0\tau} = -\frac{\mu_\tau}{2\sqrt{1+\mu(\tau)}} = \frac{1}{2\sqrt{1+\mu(\tau)}}$ thus we have the form of the next order term in the expansion as

$$x_1(\tau, T) = -\epsilon^{1-\lambda}\frac{1}{4(1+\mu(\tau))} - A\cos(T). \tag{A.4}$$

Appendix B

Two-Dimensional

High Frequency Oscillatory Forcing

Here we show that the correction term for the outer solution is purely oscillatory. From the analysis, we found both leading order terms to be purely slow dependent $V_0 = V_0(\tau)$ and $T_0 = T_0(\tau)$. To find the explicit form for these, we apply Fredholm (1.24) to the $O(\Omega^{-1})$ equations in (2.24) to find

$$\begin{aligned}
&\begin{cases} 0 = & \frac{1}{2\pi}\int_0^{2\pi} -V_{0t} + \eta_1 - \eta_2 + \eta_3(T_0 - V_0) - T_0 + V_0^2 + A\sin(R)\,dR, \\ 0 = & \frac{1}{2\pi}\int_0^{2\pi} -T_{0t} + \eta_1 - T_0(1 - V_0) + B\sin(R)\,dR, \end{cases} \\
&\begin{cases} V_{0t} = & \eta_1 - \eta_2 + \eta_3(T_0 - V_0) - T_0 + V_0^2, \\ T_{0t} = & \eta_1 - T_0(1 - V_0), \end{cases} \\
&V_{1R} = A\sin(R), \quad T_{1R} = B\cos(R).
\end{aligned} \tag{B.1}$$

Since we have a fixed parameter η_2, we find the following equilibria both V_0 and T_0 as well as the form of the correction terms

$$\begin{aligned}
T_0(V_0) &= \frac{\eta_1}{1 - V_0}, \\
0 &= \eta_1 - \eta_2 + \eta_3(T_0(V_0) - V_0) - T_0(V_0) + V_0^2, \\
V_1 &= X_1(t) - A\cos(R), \quad T_1 = Y_1(t) - B\cos(R).
\end{aligned}$$

Where we note these equilibria to be the same as the static problem with no forcing from the introduction. But with the form of the correction terms, we now solve the equation at $O(\Omega^{-2})$ (2.25) by applying Fredholm (1.24) again. This results in

$$\begin{aligned}
&\begin{cases} 0 = & \frac{1}{2\pi}\int_0^{2\pi} -V_{1t} + \eta_3(T_1 - V_1) - T_1 + 2V_0V_1\,dR, \\ 0 = & \frac{1}{2\pi}\int_0^{2\pi} -T_{1t} + T_1(1 - V_0) + T_0V_1\,dR, \end{cases} \\
&\begin{cases} X_{1t} = & \eta_3(Y_1 - X_1) - Y_1 + 2X_0X_1, \\ Y_{1t} = & Y_1(1 - X_0) + Y_0X_1, \end{cases}
\end{aligned} \tag{B.2}$$

We then search for the equilibria of (B.2) to find

$$\begin{aligned} Y_1(X_1) &= -\frac{Y_0 X_1}{1-X_0}, \\ 0 &= \left(\eta_3\left(\frac{Y_0}{1-X_0}-1\right) - \frac{Y_0}{1-X_0} + 2X_0\right) X_1. \end{aligned}$$

Thus we find that the correction terms are purely oscillatory since $X_1 \equiv 0$ and $Y_1 \equiv 0$. Thus we have $V_1 = -A\cos(R)$ and $T_1 = -B\cos(R)$.

Slow Variation and Oscillatory Forcing

Here we continue to find terms of the outer solution by working through the equations (2.54)-(2.55). From the analysis, we had already determined that the leading order terms are purely slow, $V_0 = V_0(\tau)$ and $T_0 = T_0(\tau)$. To find their exact form, we apply Fredholm (1.24) to the $O(\epsilon^\lambda)$ equation (2.54) to find

$$\begin{aligned} &\begin{cases} 0 = & \frac{1}{2\pi}\int_0^{2\pi} \eta_1 - \eta_2(\tau) + \eta_3(T_0 - V_0) - T_0 + V_0^2 + A\sin(R)\, dR, \\ 0 = & \frac{1}{2\pi}\int_0^{2\pi} \eta_1 - T_0(1-V_0) + B\sin(R)\, dR, \end{cases} \\ &\begin{cases} 0 = & \eta_1 - \eta_2(\tau) + \eta_3(T_0 - V_0) - T_0 + V_0^2, \\ 0 = & \eta_1 - T_0(1-V_0), \end{cases} \\ &V_{1R} = A\sin(R), \quad T_{1R} = B\cos(R). \end{aligned} \tag{B.3}$$

The leading order solution to (B.3) is the same as the purely slow problem in section 2.1 with

$$\begin{aligned} T_0(V_0) &= \frac{\eta_3}{1-V_0}, \\ 0 &= \eta_1 - \eta_2(\tau) + \eta_3(T_0(V_0) - V_0) - T_0(V_0) + V_0^2. \end{aligned}$$

But we also find the form of the correction terms, $V_1 = X_1(\tau) - A\cos(R)$ and $T_1 = Y_1(\tau) - B\cos(R)$, which allow us to solve the $O(\epsilon^{2\lambda})$ equation

(2.55). Applying Fredholm (1.24) here results in

$$\begin{cases} 0 = & \frac{1}{2\pi}\int_0^{2\pi} -\epsilon^{1-\lambda}V_{0\tau} + \eta_3(T_1 - V_1) - T_1 + 2V_0V_1 + A\sin(R)\,dR, \\ 0 = & \frac{1}{2\pi}\int_0^{2\pi} \epsilon^{1-\lambda}T_{0\tau} - T_1(1-V_0) + T_0V_1\,dR, \end{cases}$$
$$\begin{cases} \epsilon^{1-\lambda}V_{0\tau} = & \eta_3(Y_1 - X_1) - Y_1 + 2V_0X_1, \\ \epsilon^{1-\lambda}T_{0\tau} = & Y_1(1-V_0) + T_0X_1, \end{cases} \tag{B.4}$$

We recall that $\eta_{2\tau} = -1$ and solving (B.4) requires the derivatives of V_0 and T_0 which are solvable explicitly as

$$\begin{aligned} T_{0\tau}(V_{0\tau}) &= -\frac{\eta_1 V_{0\tau}}{1-V_0}, \\ V_{0\tau} &= \frac{(1-V_0)}{\eta_1 + \eta_3(\eta_1 + 1 - V_0) - 2V_0(1-V_0)}. \end{aligned}$$

With everything put together, we find the solution to (B.4) as

$$\begin{aligned} Y_1(X_1) =& \frac{\epsilon^{1-\lambda}T_{0\tau} - T_0X_1}{1-V_0}, \\ X_1 =& \frac{\epsilon^{1-\lambda}(V_{0\tau}(1-V_0) + (1-\eta_3)T_{0\tau})}{(1-\eta_3)T_0 + (2V_0 - \eta_3)(1-V_0)}. \end{aligned}$$

Where we now have the first correction term as

$$\begin{aligned} V_1(\tau, R) =& \frac{\epsilon^{1-\lambda}(V_{0\tau}(1-V_0) + (1-\eta_3)T_{0\tau})}{(1-\eta_3)T_0 + ((2V_0 - \eta_3)(1-V_0)} - A\cos(R), \\ T_1(\tau, R) =& \frac{\epsilon^{1-\lambda}T_{0\tau}}{1-V_0} - \frac{\epsilon^{1-\lambda}T_0(V_{0\tau}(1-V_0) + (1-\eta_3)T_{0\tau})}{(1-\eta_3)T_0(1-V_0) + (2V_0 - \eta_3)(1-V_0)^2} - B\cos(R). \end{aligned}$$

Additional Information

This chapter shows you how to include additional information in your thesis, the removal of which will not affect the submission. Such material should be removed before the thesis is actually submitted.
First, the chapter is unnumbered and not included in the Table of Contents. Second, it is the last section of the thesis, so its removal will not alter any of the page numbering etc. for the previous sections. Do not include any floats, however, as these will appear in the initial lists.
The `ubcthesis` LaTeX class has been designed to aid you in producing a thesis that conforms to the requirements of The University of British Columbia Faculty of Graduate Studies (FoGS).
Proper use of this class and sample is highly recommended—and should produce a well formatted document that meets the FoGS requirement. Notwithstanding, complex theses may require additional formatting that may conflict with some of the requirements. We therefore *highly recommend* that you consult one of the FoGS staff for assistance and an assessment of potential problems *before* starting final draft.
While we have attemped to address most of the thesis formatting requirements in these files, they do not constitute an official set of thesis requirements. The official requirements are available at the following section of the FoGS web site:

`http://www.grad.ubc.ca/current-students/dissertation-thesis-preparation`

We recommend that you review these instructions carefully.